ERDC/SL TR-00-6

US Army Corps
of Engineers®
Engineer Research and
Development Center

Ultimate Deflection Response of Lightly Reinforced Concrete Intake Towers

Richard C. Dove

August 2000

Structures Laboratory

The contents of this report are not to be used for advertising, publication, or promotional purposes. Citation of trade names does not constitute an official endorsement or approval of the use of such commercial products.

The findings of this report are not to be construed as an official Department of the Army position, unless so designated by other authorized documents.

PRINTED ON RECYCLED PAPER

ERDC/SL TR-00-6
August 2000

Ultimate Deflection Response of Lightly Reinforced Concrete Intake Towers

by Richard C. Dove

Waterways Experiment Station
U.S. Army Engineer Research and Development Center
3909 Halls Ferry Road
Vicksburg, MS 39180-6199

Final report

Prepared for U.S. Army Corps of Engineers
Washington, DC 20314-1000

Under Work Unit 32911

Engineer Research and Development Center Cataloging-in-Publication Data

Dove, Richard C.

Ultimate deflection response of lightly reinforced concrete intake towers / by Richard C. Dove ; prepared for U.S. Army Corps of Engineers.

125 p. : ill. ; 28 cm. -- (ERDC/SL ; TR-00-6)

Includes bibliographic references.

1. Intakes (Hydraulic engineering) 2. Reinforced concrete. 3. Earthquakes and hydraulic structures. I. United States. Army. Corps of Engineers. II. Engineer Research and Development Center (U.S.) III. Structures Laboratory (U.S.) IV. Title. V. Series: ERDC/SL TR ; 00-6.

TA7 E8 no.ERDC/SL TR-00-6

Contents

List of Figures

List of Tables

Preface

The research reported herein was sponsored by Headquarters, U.S. Army Corps of Engineers, under Research Program 387 – Earthquake Engineering – Structures, Work Unit 32911, Nonlinear Response and Failure Mechanisms of Intake Towers.

The principal investigator was Dr. Richard C. Dove, U.S. Army Engineer Research and Development Center (ERDC), Waterways Experiment Station, Structures Laboratory (SL), Vicksburg, MS. This project was conducted during October 1998 through December 1999 under the general supervision of Dr. Michael J. O'Connor, Acting Director, SL, and Dr. Bryant Mather, Director Emeritus, SL, ERDC, and under the direct supervision of Dr. Reed Mosher, Chief, Structural Mechanics Division, SL.

At the time of publication of this report, Dr. James R. Houston was Director of ERDC, and COL James S. Weller, EN, was Commander.

Conversion Factors, Non-SI to SI Units of Measurement

Non-SI units of measurement used in this report can be converted to SI units as follows:

Multiply	By	To Obtain
cubic feet	0.02831685	cubic meters
Fahrenheit degrees	5/9	Celsius degrees or kelvins[1]
feet	0.3048	meters
inches	2.54	centimeters
pounds	0.4535	kilograms
pounds per cubic foot	16.01846	kilograms per cubic meter
pounds per square inch	0.006894757	megapascals

[1] To obtain Celsius (C) temperature readings from Fahrenheit (F) readings, use the following formula: C = (5/9) (F - 32). To obtain kelvin readings, use: K = (5/9) (F - 32) + 273.15.

1 Introduction

In the event of an earthquake, it is vitally important that the catastrophic failure of a dam and subsequent sudden release of the reservoir be prevented. An important part of the prevention of such a failure is maintaining the ability to control the release of water after the earthquake. If a dam is damaged, the prompt and controlled lowering of the water level will remove hydrostatic pressure and help to prevent the propagation of the damage into a catastrophic failure. For most earthen dams, and some concrete dams, the release of water is controlled through a reinforced concrete intake tower (Figure 1). The functional survival of such towers is the main concern of this research effort.

The success of the tower in resisting failure is dependent upon the magnitude of the earthquake loads and the structural details controlling the nonlinear dynamic response and failure mechanisms of the specific tower. Currently, available analysis techniques and engineering guidance for intake towers may not properly include these factors. The evaluation and/or development of better design and analysis procedures and guidance is the primary goal of the research reported here.

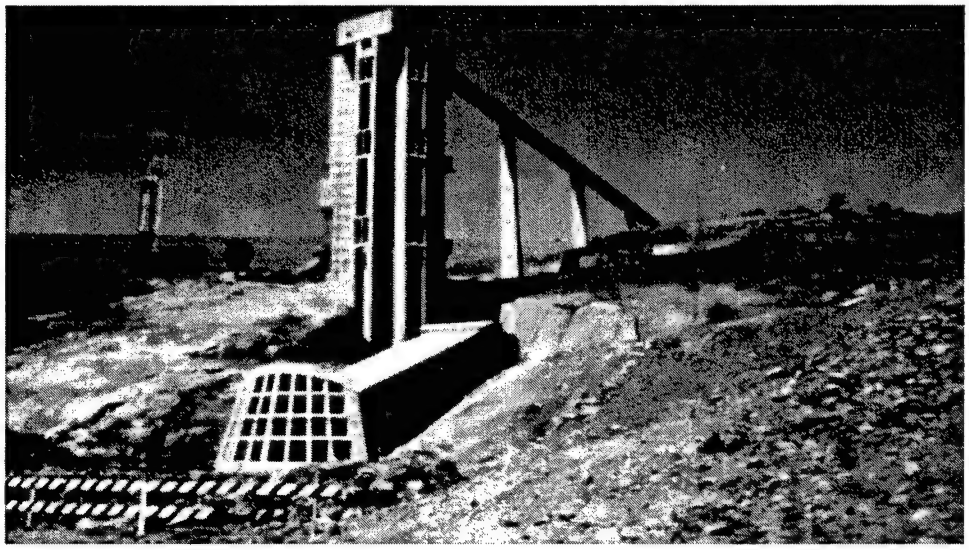

Figure 1. Lost Creek Intake Tower during construction

Objective

The overall objective of this research is to understand the nonlinear response of existing, lightly reinforced intake towers. The ultimate objective is the evaluation and/or development of approximate or simplified analysis procedures for the evaluation of the ductility of existing intake towers.

There were three phases in the fulfillment of this ultimate objective. The first phase was a statistical analysis of the inventory of existing intake towers (Dove 1996). The specific objective of this tower inventory analysis was to quantify the distribution and variation of the structural characteristics of the U.S. Army Corps of Engineers' inventory of existing intake towers as relating to their earthquake location hazard. This analysis was used to assist in the identification of possible failure mechanisms and to help quantify the extent of the problem of the seismic response of existing towers. The information generated was used in planning the second phase of this research effort, the Intake Tower Substructure (ITS) experimentation series conducted in 1996 and 1997 (Dove 1998). The objectives of these experiments were to observe the response of scale models of typical intake towers, quantify the ductility available, and use the information generated for the development of approximate and/or simplified analysis procedures for the evaluation of the ductility of existing intake towers.

The results of the ITS experiments showed that more information was required for the application of the simplified analysis procedures under development. Specifically, a method is needed to properly estimate the ultimate deflection capacity of existing intake towers. Calculation of this deflection capacity requires knowledge of the rotational capacity of the critical section at the base of the tower. This, in turn, requires a method of estimating the strain penetration/failure deflection characteristics of the reinforcing steel in the failure zone. Developing an empirical equation for the estimation of these parameters is the objective of the research reported here.

Approach

This research is a continuation of work conducted under the Earthquake Engineering Research Program, Work Unit 32911, "Nonlinear Dynamic Response and Failure Mechanisms of Intake Towers." The research began with the determination of the structural characteristics of intake towers that might have problems with earthquakes (Dove 1996). Structural drawings of 77 existing towers were systematically analyzed to determine the geometric and material properties of the towers. The results of the analysis were used to design experiments consisting of the one-way and cyclic static loading to failure of three 1/8-scale models of a typical intake tower configurations (Dove 1998). The current experimentation, discussed in this report, was conducted to provide additional information needed to properly model the strain penetration/failure deflection characteristics of the reinforcing steel in the failure zone of existing intake towers. Ten, half-scale experiments (Figure 2) were conducted to provide a statistically significant basis for the development of an empirical estimation of

the parameters needed. Specifically, conducting 10 experiments allowed for an experimental design that included a modified full-factorial variation of the three main variables of interest. The three variables were: concrete strength, reinforcing steel strength, and reinforcing steel diameter. More detail about the design of the experiments is presented in the next chapter of this report.

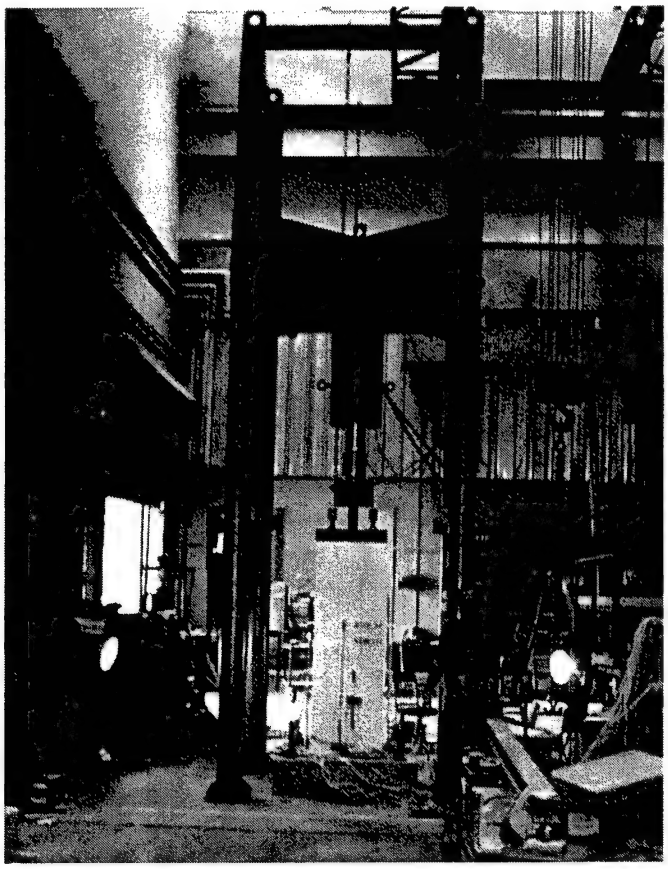

Figure 2. Load frame containing typical strain penetration experiment specimen

2 Experimental Description

Experiment Design

Ten, half-scale experiments were conducted to provide a statistically significant basis for the development of an empirical estimation of the parameters needed. A commercial statistical analysis program STAGRAPHICS was used to design the experimental program. Specifically, the experimental design was based on a modified full-factorial variation of the three main variables of interest, concrete strength, reinforcing steel strength, and reinforcing steel diameter. A full-factorial design is a simple concept in that the design includes all the combinations of the extremes on each variable. With three variables, the number of combinations is two raised to the third power, or eight. In addition to the eight combinations, proper experimental design includes an experiment consisting of the combination of the middle values of the variables. This allows for a check of the linearity of the model. Inclusion of the middle values assumes that the variables are continuous. In this specific design, the reinforcing steel strength variable of yield strength was only available in 60,000 psi and 40,000 psi. Thus, two middle experiments were designed consisting of the middle values of the concrete strength and reinforcing steel diameter and the high and low values of the steel strength, for a total of 10 experiments. The test matrix is shown in Table 1. Note that the name of each experiment consists of the reinforcing bar diameter in eighths, followed by the relative steel strength (H for high, M for medium, L for low), and then by the relative concrete strength (H for high, M for medium, L for low). For example, the designation of 3SLCH is for a model with 3/8-in. reinforcing bars, low-strength steel, and high-strength concrete.

Model Configuration

The primary concern of this experiment design was the proper modeling of the response of an individual reinforcing bar found in an existing intake tower during an earthquake. In prior experimentation it was shown that the response of these lightly reinforced structures was dominated by the localized failure of the reinforcing in a single crack. The dimensions, configuration, and structural parameters of the experimental components in the current effort were selected to model this failure mode for typical prototype structures in the existing inventory rectangular intake towers. Appendix A contains construction drawings, A1 through A14, of the model. The experimental specimen consists of a 6-ft-tall, 2-ft by 2-ft concrete monolith reinforced with six vertical reinforcing bars. This

Table 1
Experimental Design with Nominal Variable Values

Experiment	Diameter, in.	Steel Yield Strength psi	Concrete Strength psi
3SLCL	3/8	40,000	2,500
3SLCH	3/8	40,000	5,500
3SHCL	3/8	60,000	2,500
3SHCH	3/8	60,000	5,500
4SLCM	1/2	40,000	4,000
4SHCM	1/2	60,000	4,000
5SLCL	5/8	40,000	2,500
5SLCH	5/8	40,000	5,500
5SHCL	5/8	60,000	2,500
5SHCH	5/8	60,000	5,500

represents a section of one wall of a prototype tower (Figure A1). The full-scale prototype would be a 4-ft-thick wall with No. 6, 8, and 10 reinforcing bars placed horizontally and vertically at spacings of 12 in. Only the center bar at each face was instrumented, since it was expected that these bars would be least influenced by edge effects. Each model included a construction joint with a typical lap slice detail. This construction joint was painted with a joint release compound to assure failure at that location. Another construction joint existed between each monolith and the heavily reinforced base slab used to bolt the specimen to the load floor. Eight concrete anchors were cast in the top of each model. These anchors were used to attach the loading system to the specimen. Figure A3 shows the overall layout for the model.

Instrumentation Configuration

At the time of the experiments, the data acquisition system used was capable of acquiring a total of 80 channels of data. The same basic instrumentation layout was used in all experiments. Two of the channels were allocated to the measurement of load and deflection in the vertical hydraulic loader, deflection was measured at 8 positions, and strain was measured at 26 to 60 positions, depending on the bar size in each experiment.

Detailed locations of the strain gages can be seen in Appendix A. The strain gages were mounted above and below the construction joint on the center bar of each face of the specimen. The intention was to capture the spread of the plastic zone within these bars. Gages were mounted on both sides of the No. 4 and 5 bars to enable the averaging out of bending strains. Gages were only mounted on one side of the No. 3 bars because of size constraints. In all cases, the gages were

mounted on flat areas machined into the longitudinal ribs on each bar, minimizing the removal of material (Figure 3).

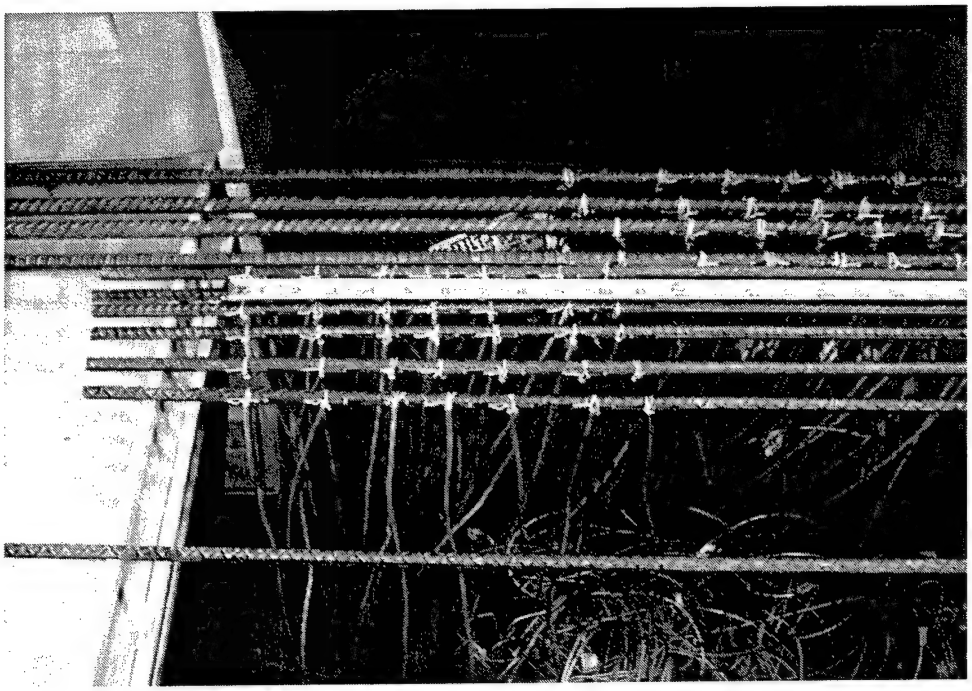

Figure 3. Strain gaged reinforcement

The deflection gages were mounted directly on the specimen spanning the construction joint. The probes of these 8-in. linearly varying deflection transducer (LVDT) gages were attached to rigid links via flexible couplings. The couplings allowed for limited lateral displacement while measuring vertical displacement. These gages were expected to give a direct measurement of the crack width up to failure at this critical section.

Test Article Construction

Construction of all 10 of the models was completed simultaneously. The 12-in.-thick bases were constructed first. The base reinforcing consisted of one layer of No. 8 bars laid out in a 6-in. by 6-in. grid. Figure 4 shows the base slab rebar placed in the base concrete forms. Figure 5 shows the base slab concrete placement. The vertical model vertical reinforcement was placed in the base slab and the concrete forms constructed for the lower section of the model (Figure 6). Concrete was placed (Figure 7) and the construction joint at the top of the lower section was painted with a release compound to promote failure at location (Figure 8). The reinforcement of the top half of models was placed (Figure 9) and the upper forms were constructed. At this point the load anchors were

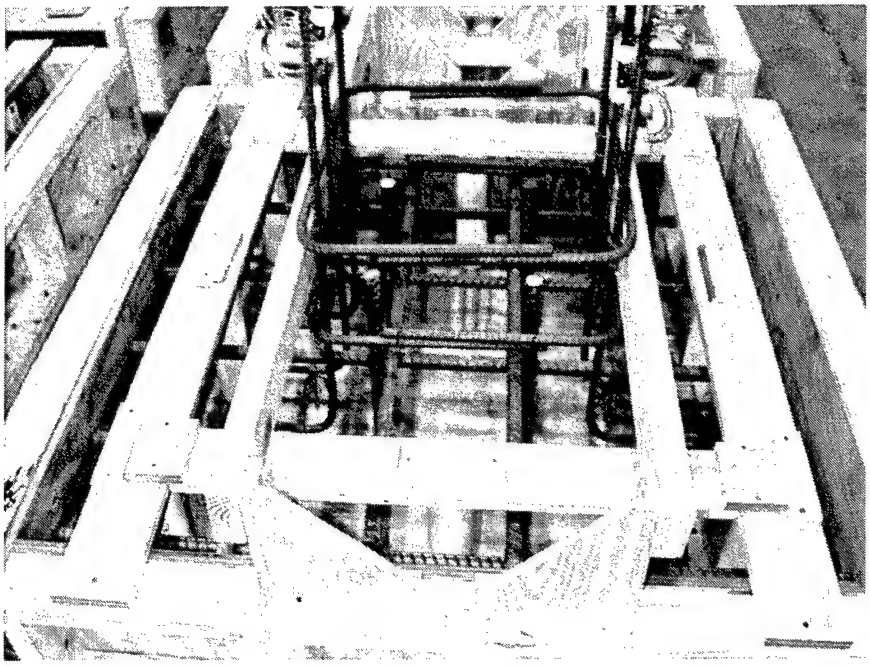

Figure 4. Typical base slab reinforcement

Figure 5. Base slab concrete placement

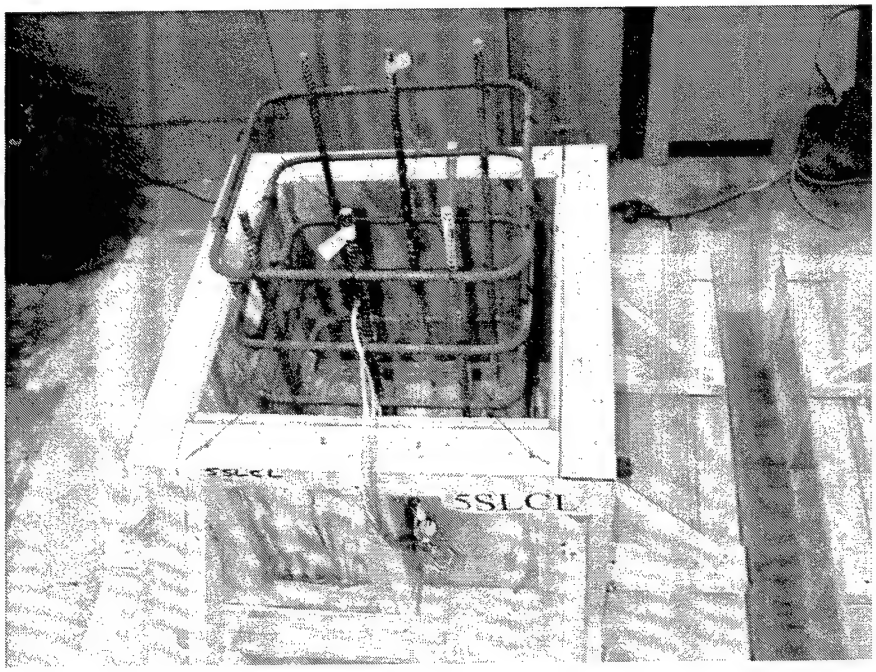

Figure 6. Typical reinforcement in lower half of monolith

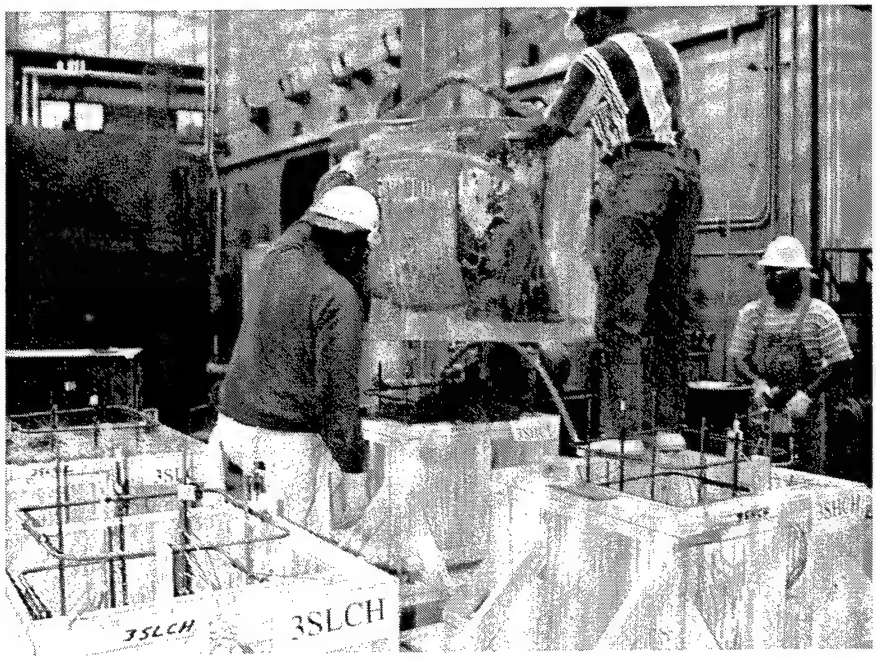

Figure 7. Concrete placement in lower half of monoliths

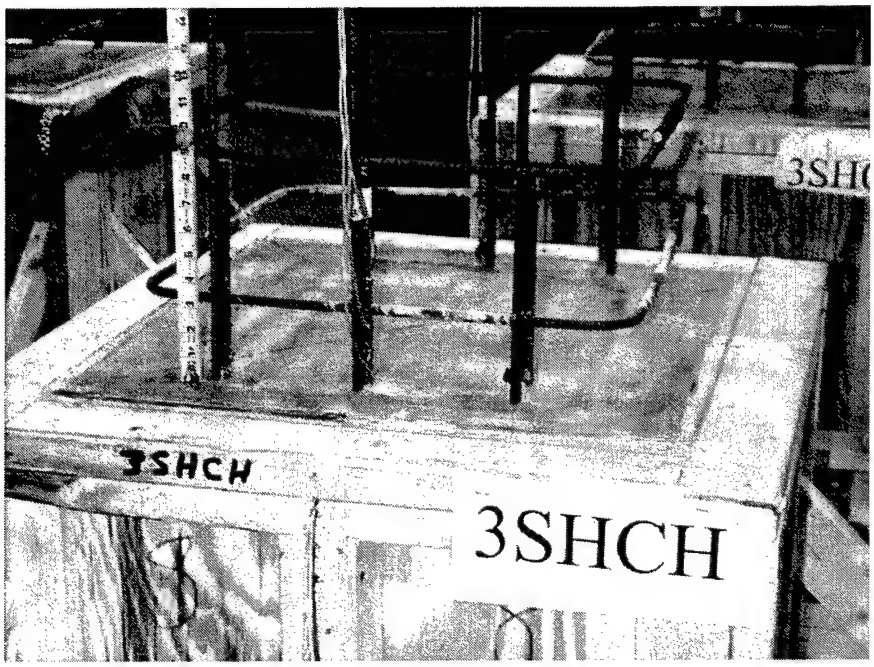

Figure 8. Typical construction joint at intended failure plane

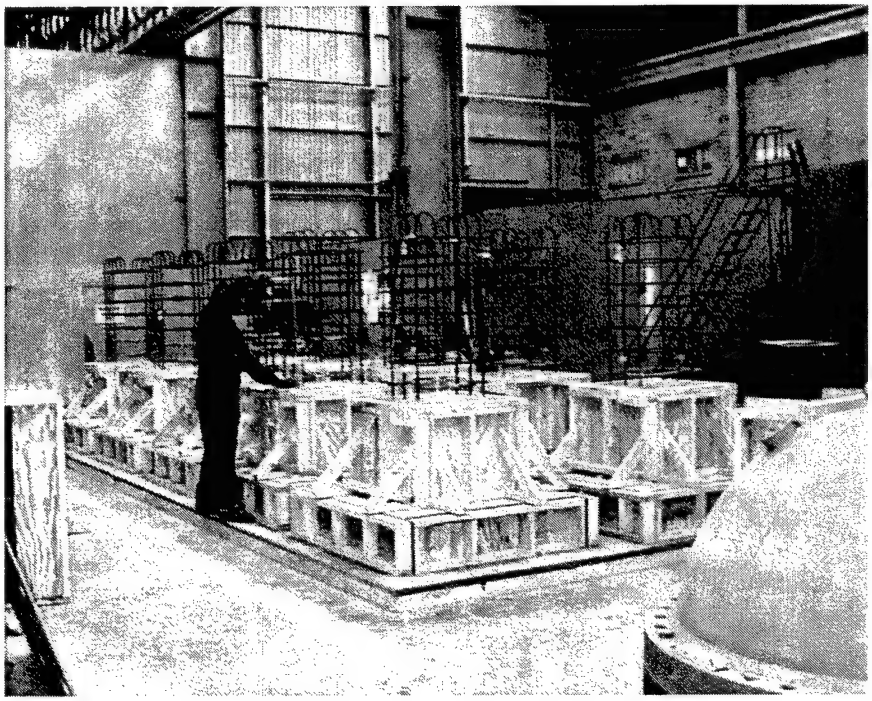

Figure 9. Reinforcement of top half of models

inserted, and the final concrete was placed (Figure 10). Proper alignment of the anchors with the hold-down boltholes in the base slab was critical and was maintained by use of a template and plumb bobs. Every attempt was made to maintain consistent concrete properties across the various models by placing each type concrete in all models containing that type at the same time. Forms were stripped after about 2 weeks of curing (Figure 11). Steel and concrete material properties are presented in Appendix B.

Experimental Procedure

As mentioned above, each specimen was mounted in a load frame (Figure 12). Vertical force was applied to the each model with a servocontrolled 200-kip hydraulic loader. An initial vertical compression load of 50 kips was applied to the structure. This vertical was applied in each experiment to simulate the dead load of an 83-ft-tall half-scale or 166-ft-tall full-scale tower. After application of the initial dead load, all strain gages and deflection gages were reset to zero. Thus, the initial condition of the model included dead load effects as in a prototype structure. The load measurement was not reset to zero. From this compressed condition, the experiment proceeded with the application the deflection controlled vertical tension load. The load head was moved upward at a rate of 0.01 in./sec to a deflection of 0.1 in. as measured by the ram's internal deflection gage. At this point, the load head was returned to zero. This was repeated for a total of three repetitions. After the three repetitions, the next load cycle began and the total deflection applied was increased by 0.1 in. to a total of 0.2 in. Again, three cycles were applied. This process of the application of increasing deflections, repeated three times, was continued until failure occurred. As longer deflections were applied, the load rate was increased to complete the experiment in a reasonable time. Photographic support included video cameras, as well as digital and still photography in color. Photographic coverage included before, during, and after experimentation.

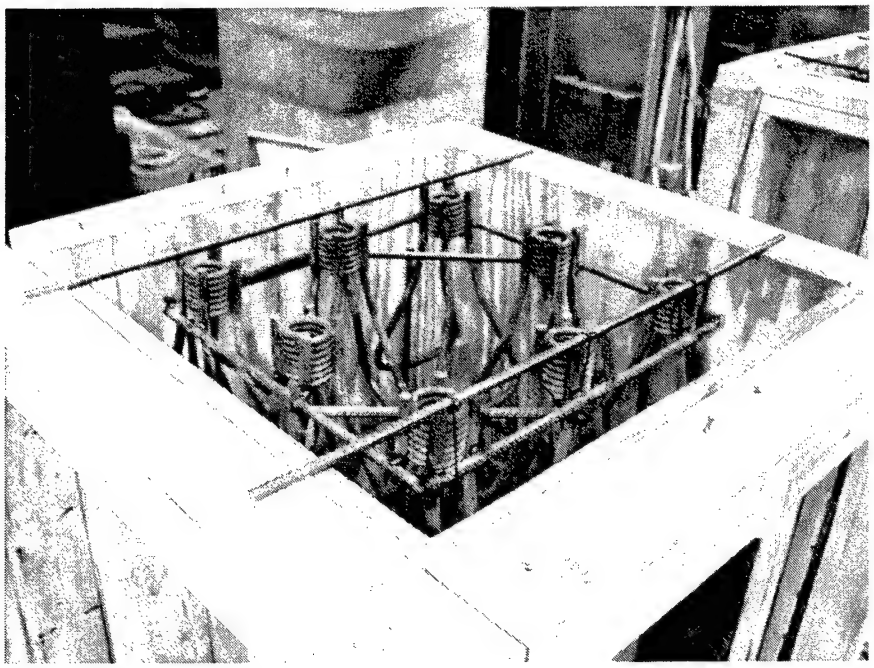

Figure 10. Typical group of load anchors in top of upper half of model

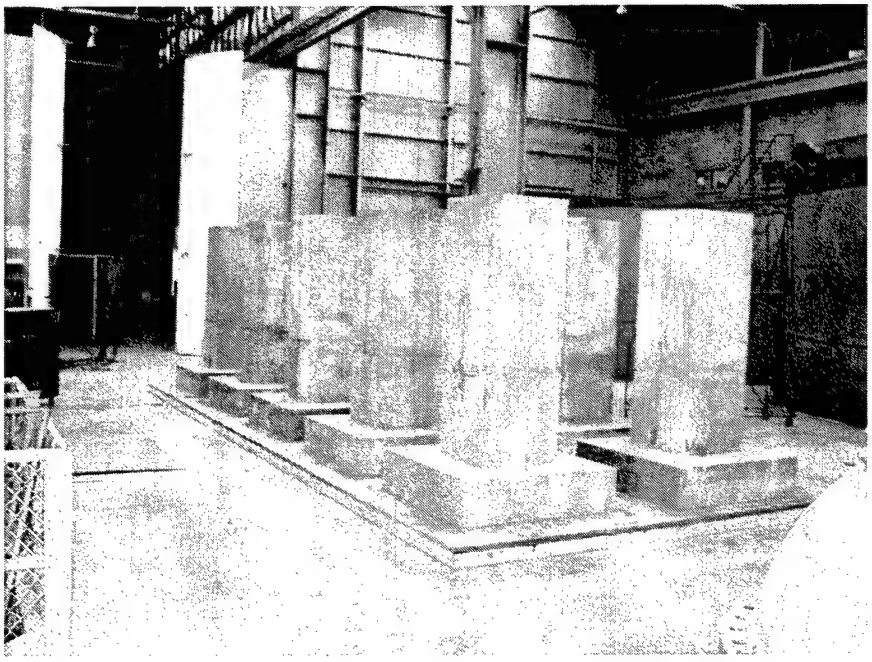

Figure 11. Completed models

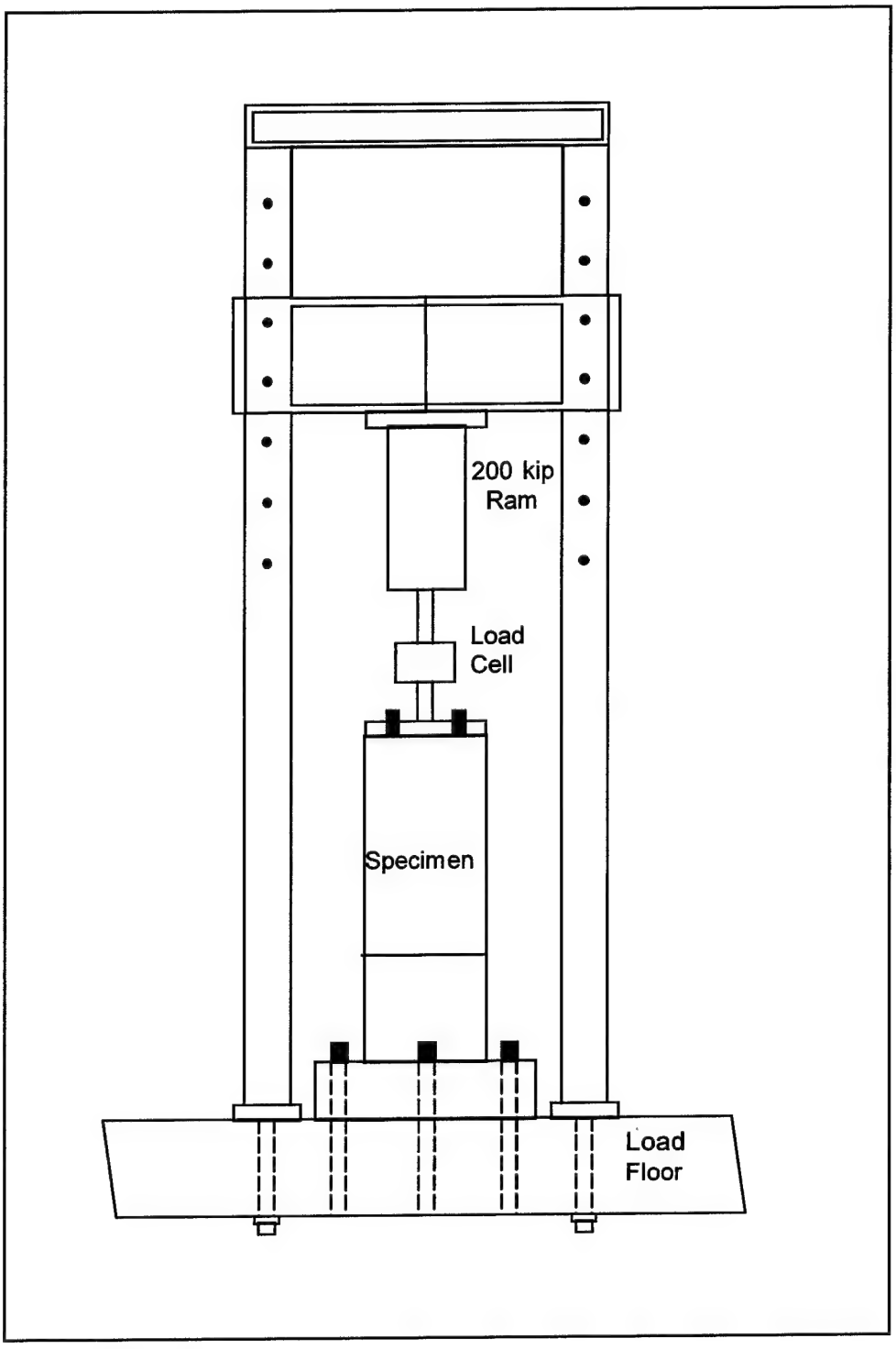

Figure 12. Schematic of load frame with specimen

3 Experimental Results

The 10 strain penetration experiments were conducted from September 1998 to February 1999. For the most part, the experimental method proved very successful and 9 of the 10 experiments returned good to excellent results. A massive amount of data was generated, including load, strain, and deflection measurements. Strain data plots are presented in Appendix C. Extensive photographic and video records were also obtained. This chapter contains a short description of the results observed in each experiment with some selected photos and data plots. The next chapter contains an analysis these experimental results.

Experiment 3SLCL Results

The experiment 3SLCL was conducted on 27 December 1998. Figure 13 shows the model during loading. A single crack formed at the cold joint and failure occurred within the crack (Figure 14). The cyclic application of the vertical deflection loads proceeded through 18 cycles to initial failure during the third application of the 0.6-in. cycle. The total deflection at failure was 0.345 in., as measured by the average of four 40-in. and four 8-in. LVDT gages. The load-deflection curve is shown in Figure 15. Loading was continued until complete failure was reached. The apparent failure mode was a localized response of the rebar with no concrete degradation. There was only a small degree of very localized crushing of the concrete immediately around the rebar failure zone. This conical zone of crushed concrete extended about one bar diameter into the model above and below the cold joint. The reinforcing bar appeared to fail in tension. Some bending of the rebar was evident, caused by the compression of the rebar during the reverse loading cycles.

Experiment 3SLCH Results

The experiment 3SLCH was conducted on 22 October 1998. Figure 16 shows the model during loading. A single crack formed at the cold joint and failure occurred within the crack (Figure 17). The cyclic application of the vertical deflection loads proceeded through 16 cycles to apparent failure during the first application of the 0.6-in. cycle. For analysis purposes, the failure was taken as occurring during the last application of the 0.5-in. cycle. The total

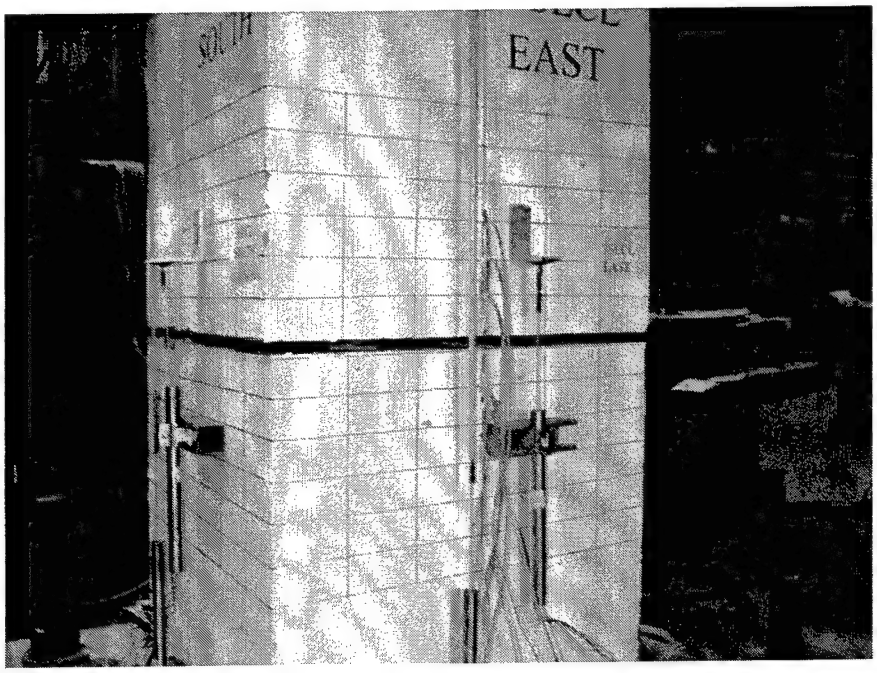

Figure 13. View of south and east sides of 3SLCL failure plane

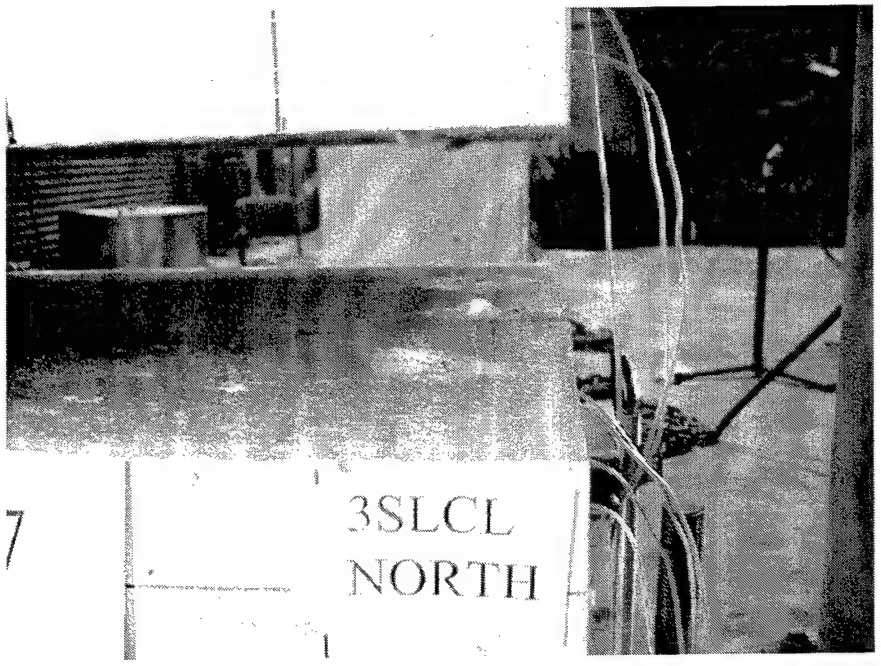

Figure 14. Closeup view of 3SLCL failure plane

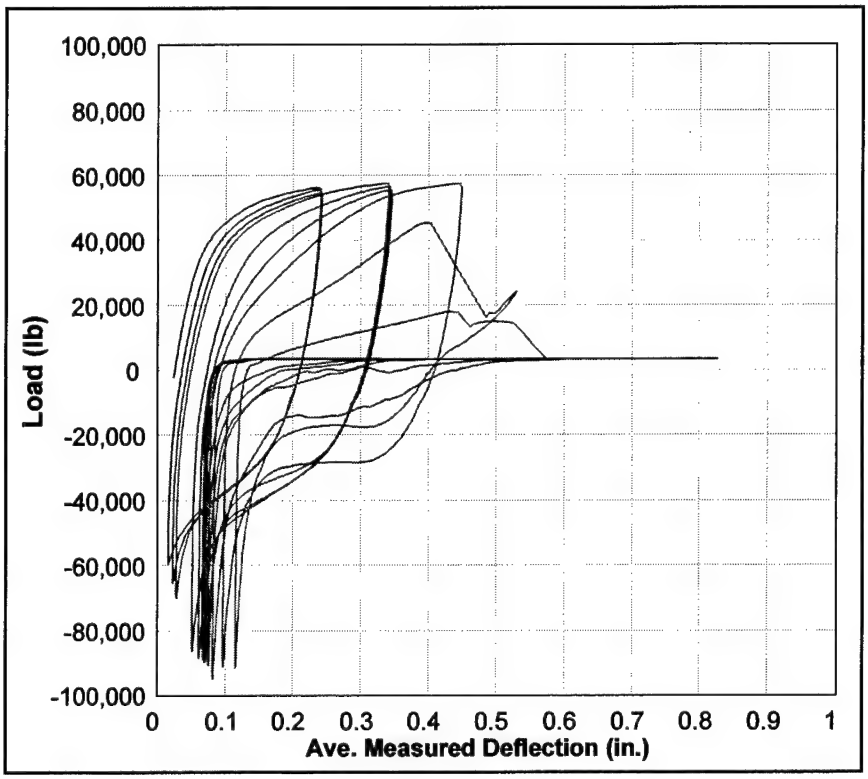

Figure 15. Load-deflection curve for experiment 3SLCL

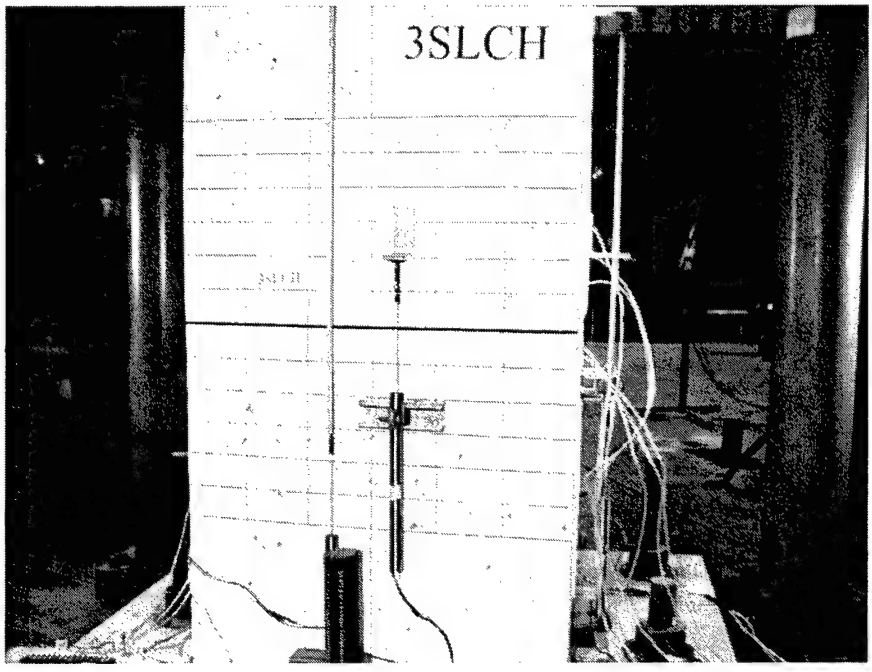

Figure 16. West view of 3SLCH failure plane

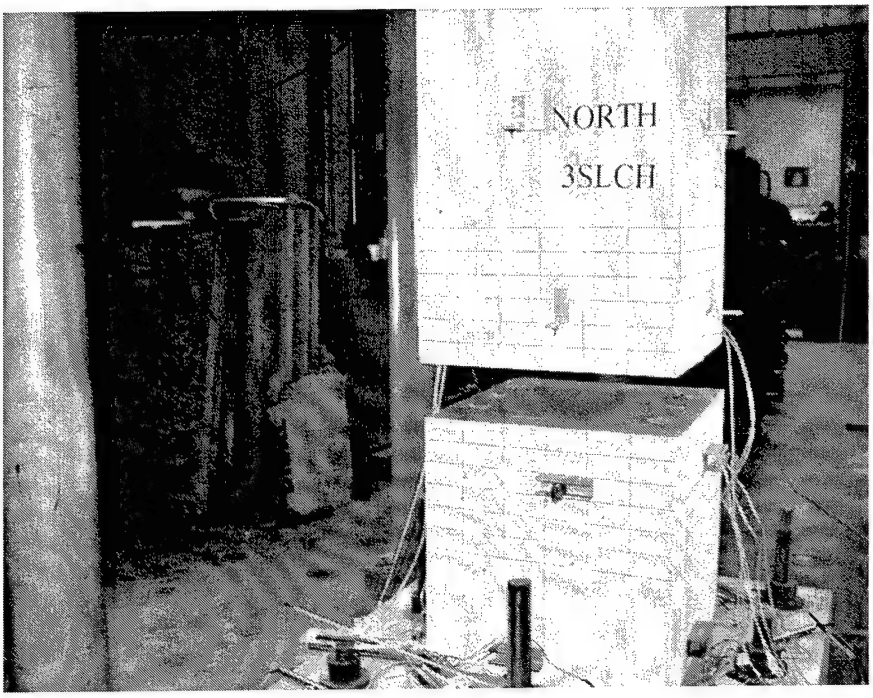

Figure 17. Postexperiment view of 3SLCH failure plane

deflection at failure was 0.382 in., as measured by the average of four 40-in. and four 8-in. LVDT gages. The load-deflection curve is shown in Figure 18. Loading was continued until complete failure was reached. The apparent failure mode was a localized response of the rebar with no concrete degradation. There was only a small degree of very localized crushing of the concrete immediately around the rebar failure zone. This conical zone of crushed concrete extended about one bar diameter into the model above and below the cold joint. The reinforcing bar appeared to fail in tension. Some bending of the rebar was evident, caused by the compression of the rebar during the reverse loading cycles.

Experiment 3SHCL Results

The experiment 3SHCL was conducted on 14 December 1998. Figure 19 shows the model during loading. A single crack formed at the cold joint and failure occurred within the crack (Figure 20). The cyclic application of the vertical deflection loads proceeded through 16 cycles to apparent failure during the first application of the 0.7-in. cycle. For analysis purposes, the failure was taken as occurring during the last application of the 0.6-in. cycle. The total deflection at failure was 0.338 in., as measured by the average of four 40-in. and four 8-in. LVDT gages. The load-deflection curve is shown in Figure 21. Loading was continued until complete failure was reached. As in the other experiments, the apparent failure mode was a localized response of the rebar with no concrete degradation. However, the failure mode was complicated by the

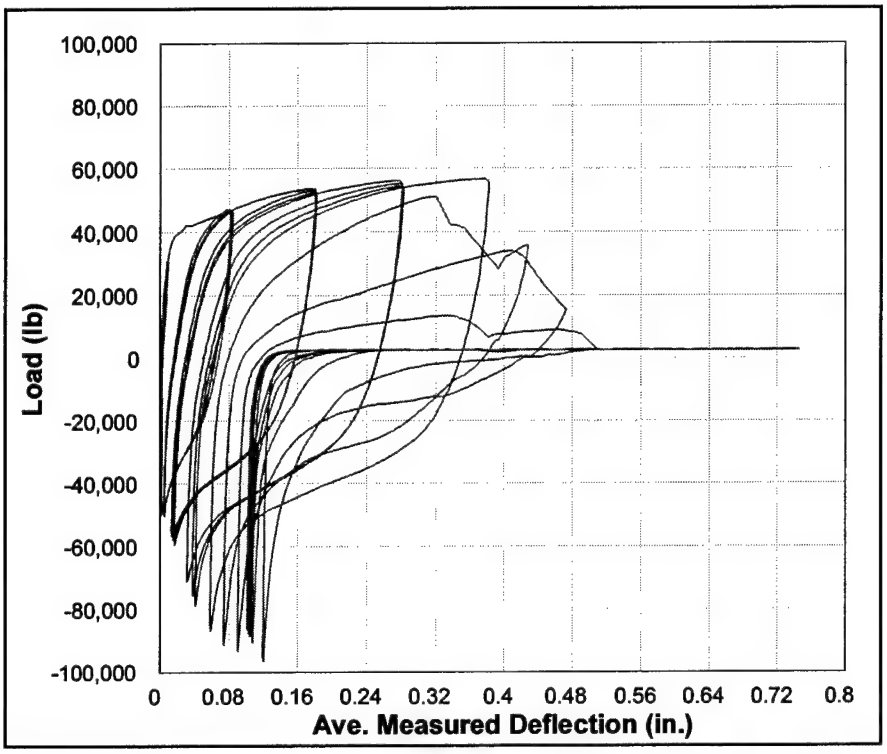

Figure 18. Load-deflection curve for experiment 3SLCH

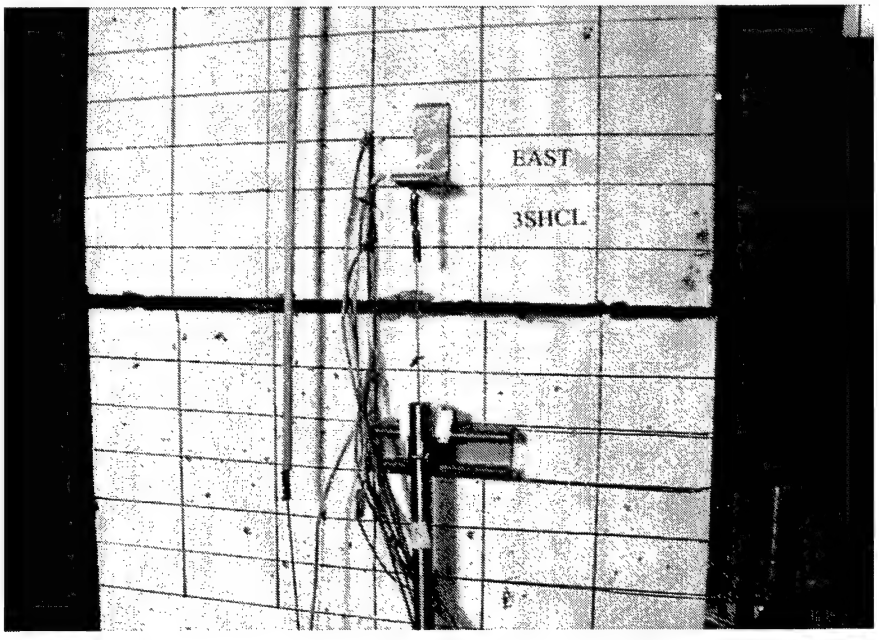

Figure 19. East view of 3SHCL failure plane

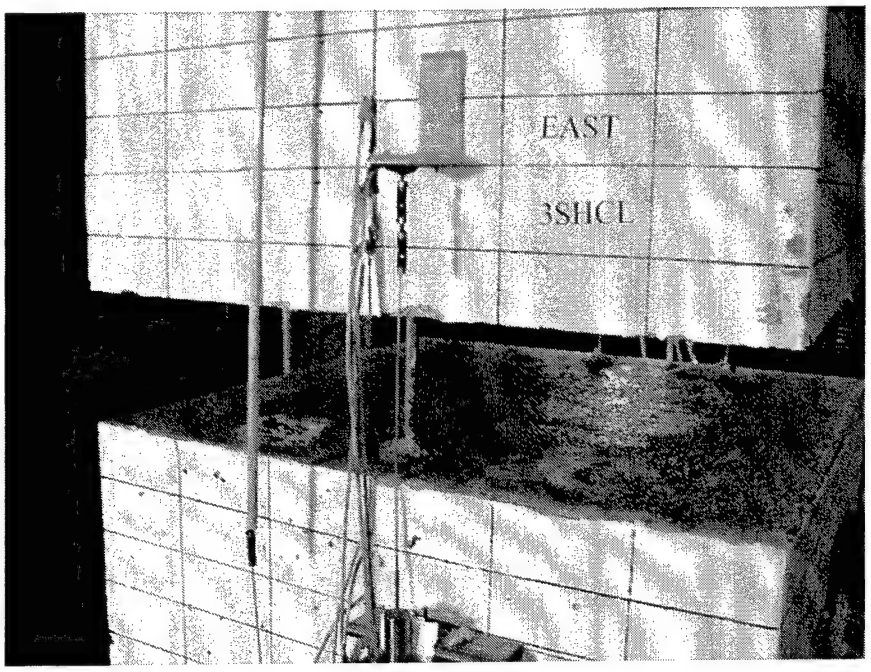

Figure 20. Postexperiment view of 3SHCL failure plane showing lap splice failure

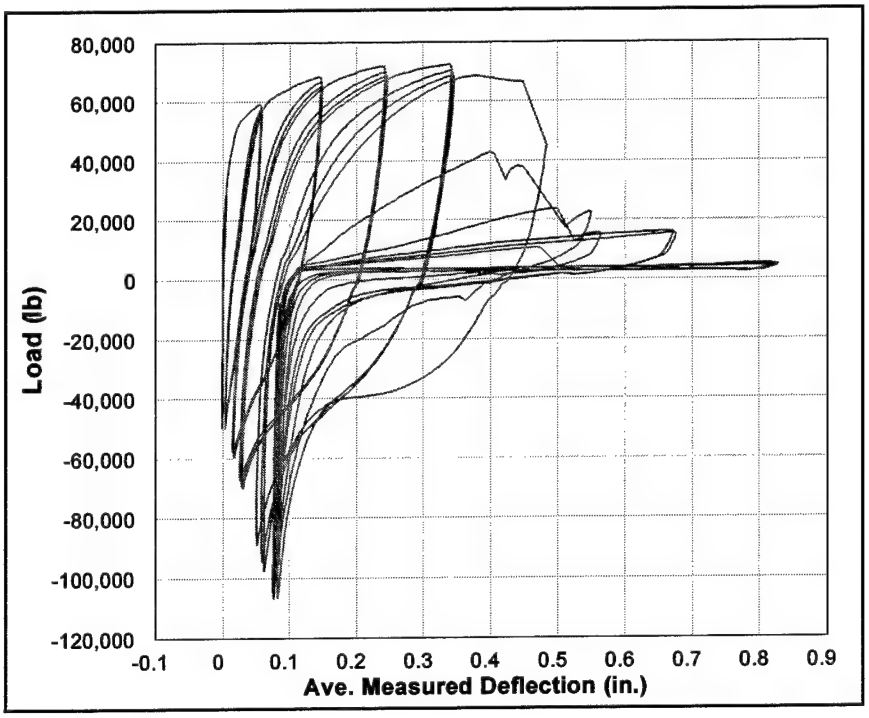

Figure 21. Load-deflection curve for experiment 3SHCH

failure of the 9-in.-long lap splice of one bar. The center bar in the east face of the model pulled out of the upper section of the model. Lap failure was quite possibly caused by the seven strain gages located on this bar. The protective coating applied to the gages may have acted to break the rebar/concrete bond. The lap failure of this one bar did not appear to influence the overall failure mode of the model. In all the remaining bars, there was only a small degree of very localized crushing of the concrete immediately around the rebar failure zone. This conical zone of crushed concrete extended about one bar diameter into model above and below the cold joint. The reinforcing bar appeared to fail in tension. There was evidence of some bending of the rebar, caused by the compression of the rebar during the reverse loading cycles.

Experiment 3SHCH Results

The experiment 3SHCH was conducted on 29 December 1998. Figure 22 shows the model during loading. A single crack formed at the cold joint and failure occurred within the crack (Figure 23). The cyclic application of the vertical deflection loads proceeded through 19 cycles to apparent failure during the first application of the 0.7-in. cycle. For analysis purposes, the failure was taken as occurring during the last application of the 0.6-in. cycle. The total deflection at failure was 0.294 in., as measured by the average of four 40-in. and four 8-in. LVDT gages. The load-deflection curve is shown in Figure 24. Loading was continued until complete failure was reached. The apparent failure mode was a localized response of the rebar with no concrete degradation. There was only a small degree of very localized crushing of the concrete immediately around the rebar failure zone. This conical zone of crushed concrete extended about one bar diameter into model above and below the cold joint. The reinforcing bar appeared to fail in tension. Some bending of the rebar was evident, caused by the compression of the rebar during the reverse loading cycles.

Experiment 4SLCM Results

The experiment 4SLCM was conducted on 4 February 1999. Figure 25 shows the model during loading. A single crack formed at the cold joint and failure occurred within the crack (Figure 26). The cyclic application of the vertical deflection loads proceeded through 23 cycles to apparent failure during the second application of the 0.8-in. cycle. For analysis purposes, the failure was taken as occurring during the last application of the 0.7-in. cycle, cycle 21. The total deflection at failure was 0.402 in., as measured by the average of four 40-in. and four 8-in. LVDT gages. The load-deflection curve is shown in Figure 27. Loading was continued until complete failure was reached. The apparent failure mode was a localized response of the rebar with no concrete degradation. There was only a small degree of very localized crushing of the concrete immediately around the rebar failure zone. This conical zone of crushed concrete extended about one bar diameter into model above and below the cold joint. The reinforcing bar appeared to fail in tension. Some bending of the rebar was

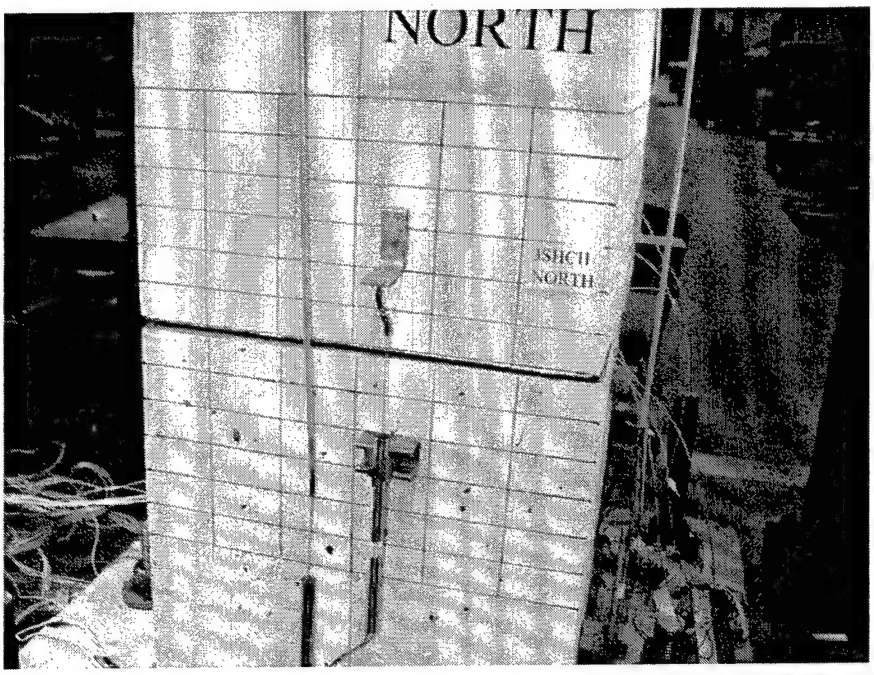

Figure 22. North view of 3SHCH failure plane

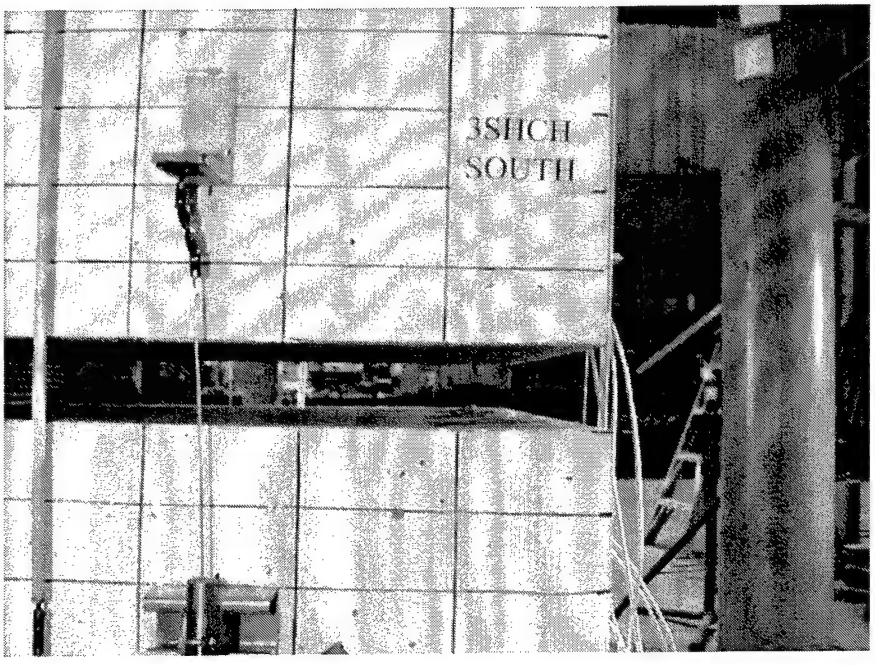

Figure 23. Postexperiment view of 3SHCH failure plane

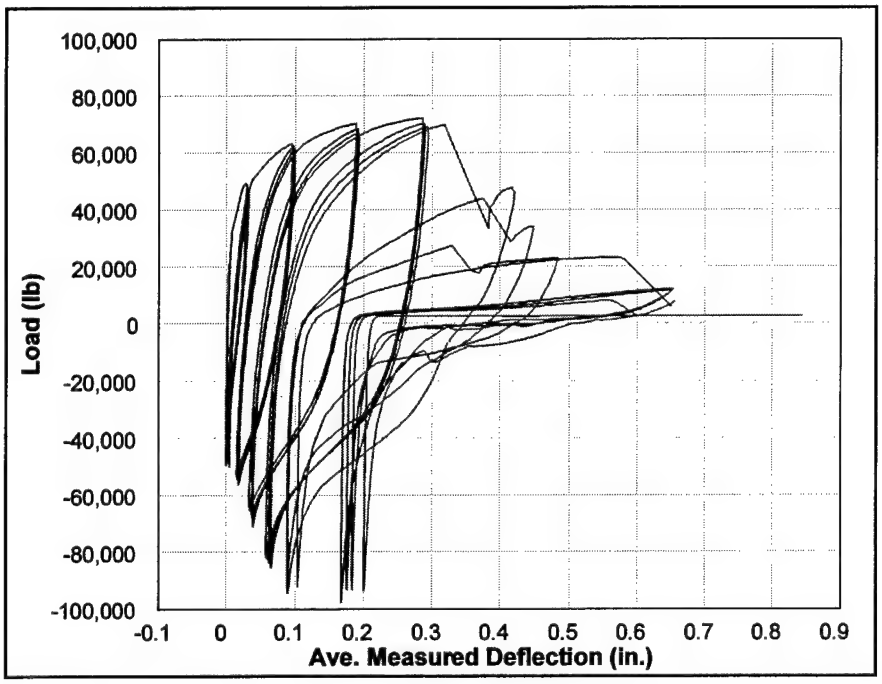

Figure 24. Load-deflection curve for experiment 3SHCH

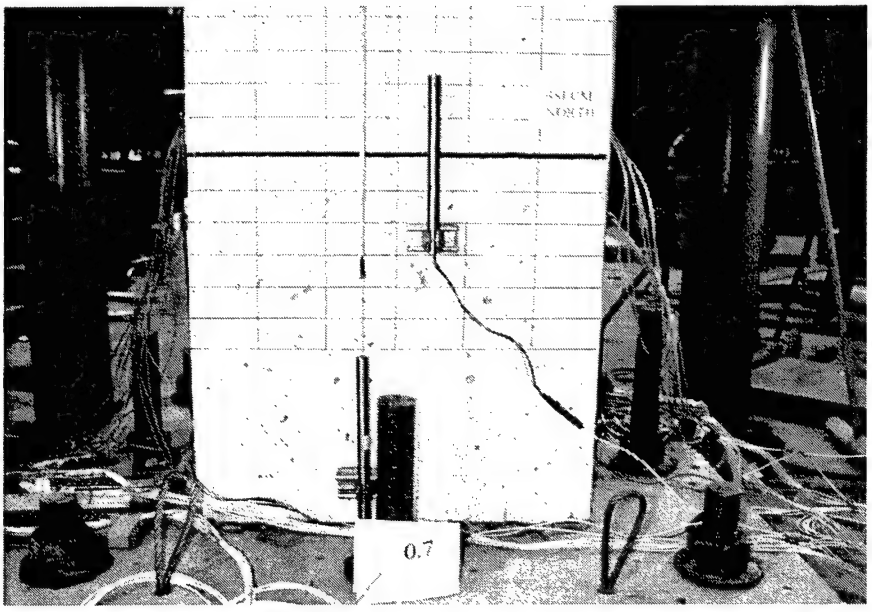

Figure 25. North view of 4SLCM failure plane

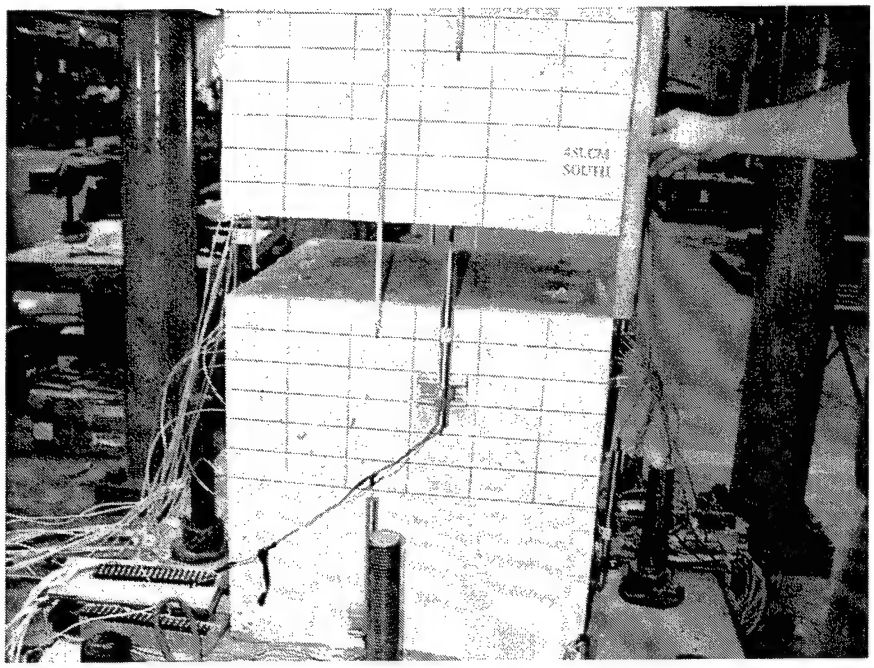

Figure 26. Postexperiment view of 4SLCM failure plane

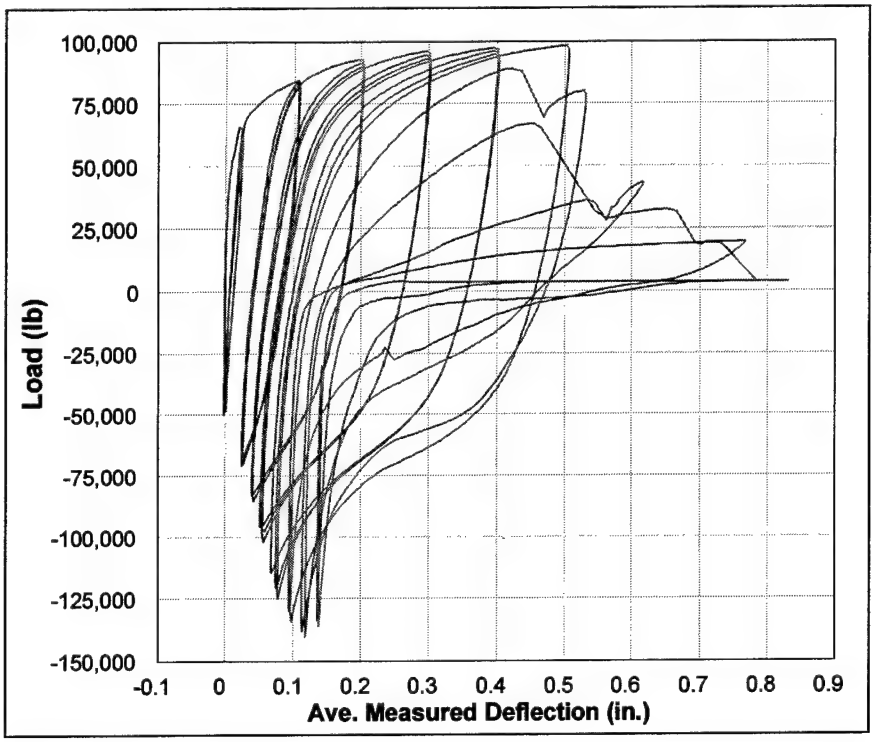

Figure 27. Load-deflection curve for experiment 4SLCM

evident, caused by the compression of the rebar during the reverse loading cycles.

Experiment 4SHCM Results

The experiment 4SHCM was conducted on 9 December 1998. Figure 28 shows the model during loading. A single crack formed at the cold joint and failure occurred within the crack (Figure 29). The cyclic application of the vertical deflection loads proceeded through 23 cycles to apparent failure during the second application of the 0.8-in. cycle. For analysis purposes, the failure was taken as occurring during the last application of the 0.7-in. cycle, cycle 21. The total deflection at failure was 0.402 in., as measured by the average of four 40-in. and four 8-in. LVDT gages. The load-deflection curve is shown in Figure 30. Loading was continued until complete failure was reached. The apparent failure mode was a localized response of the rebar with no concrete degradation. There was only a small degree of very localized crushing of the concrete immediately around the rebar failure zone. This conical zone of crushed concrete extended about one bar diameter into the model above and below the cold joint. The reinforcing bar appeared to fail in tension. Some bending of the rebar was evident, caused by the compression of the rebar during the reverse loading cycles.

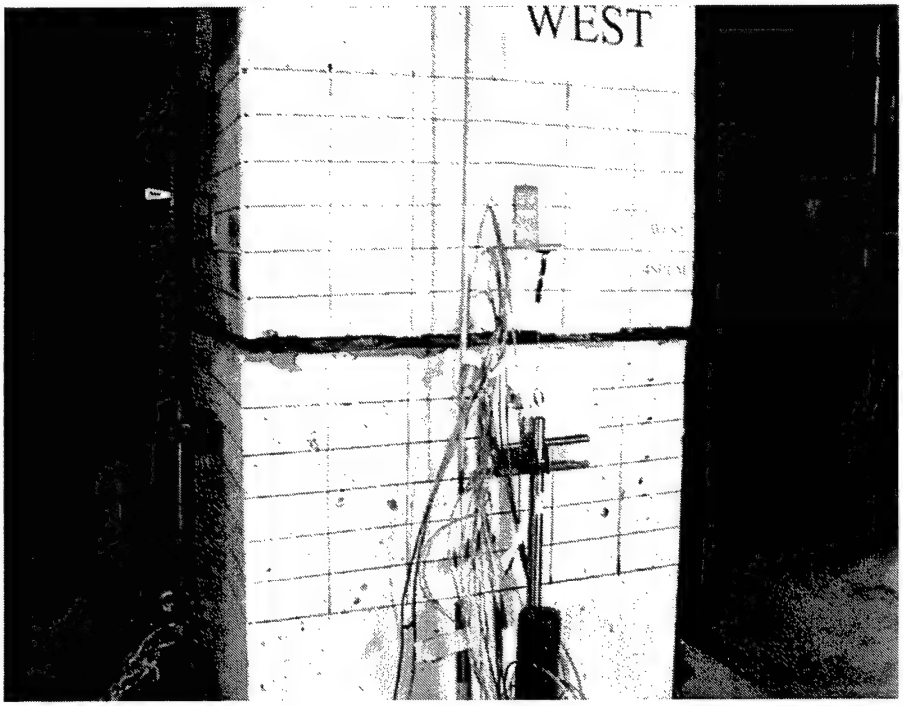

Figure 28. West view of 4SHCM failure plane

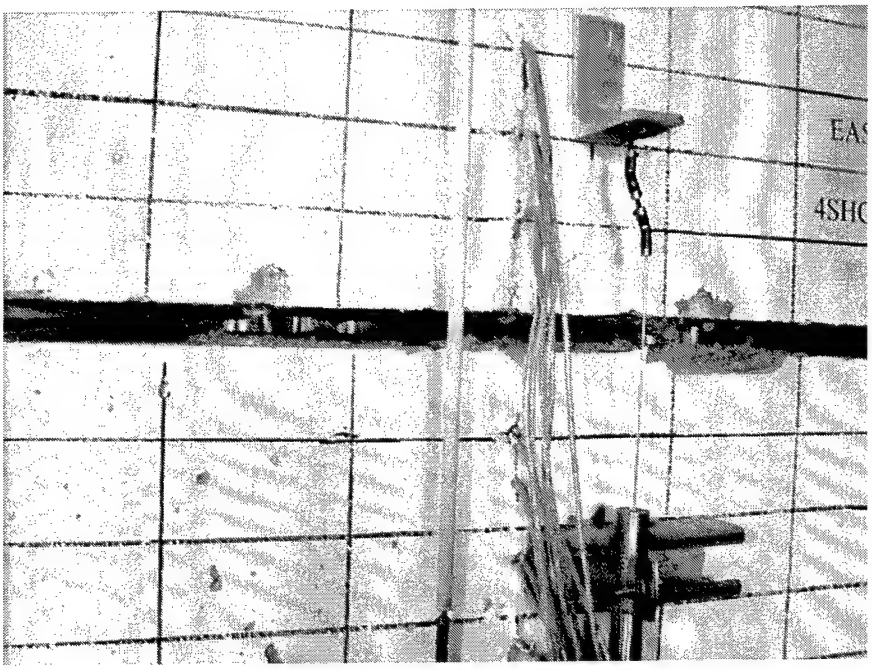

Figure 29. Postexperiment view of 4SHCM failure plane

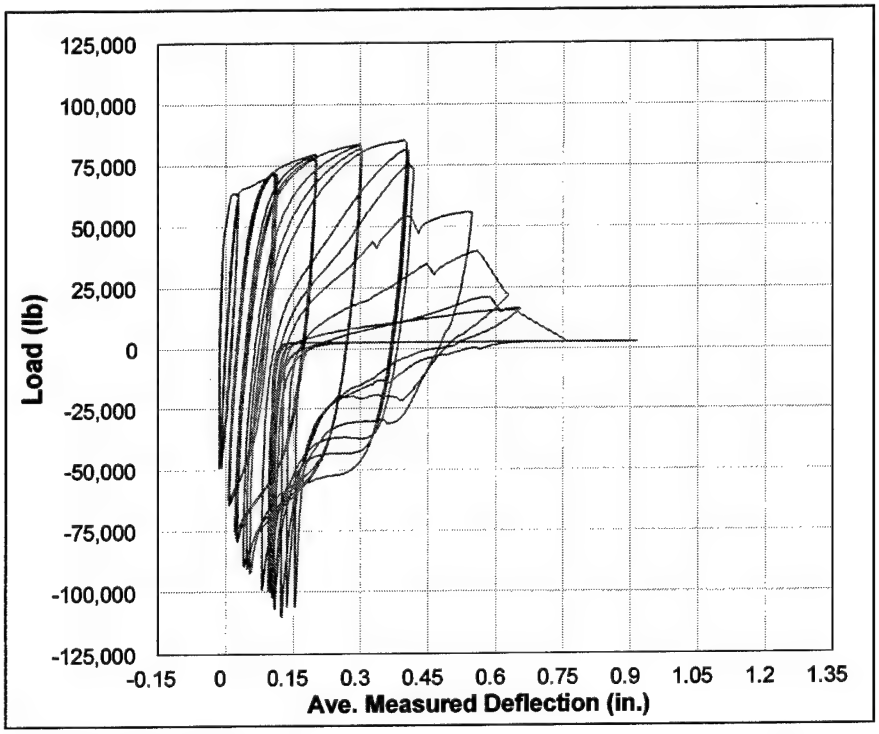

Figure 30. Load-deflection curve for experiment 4SHCM

Experiment 5SLCL Results

The experiment 5SLCL was conducted on February 9, 1999. Figure 31 shows the model during loading. This is the first experiment discussed in which more than a single crack formed. The second crack formed approximately 20 in. above the cold joint. Failure eventually occurred within the crack at the cold joint (Figure 32). Careful observation of the cracks showed them to be almost exactly the same width during loading. This could be expected, as the load was the same throughout the length of the model. The cyclic application of the vertical deflection loads proceeded through 34 cycles to apparent failure during the first application of the 1.3-in. cycle. For analysis purposes, the failure was

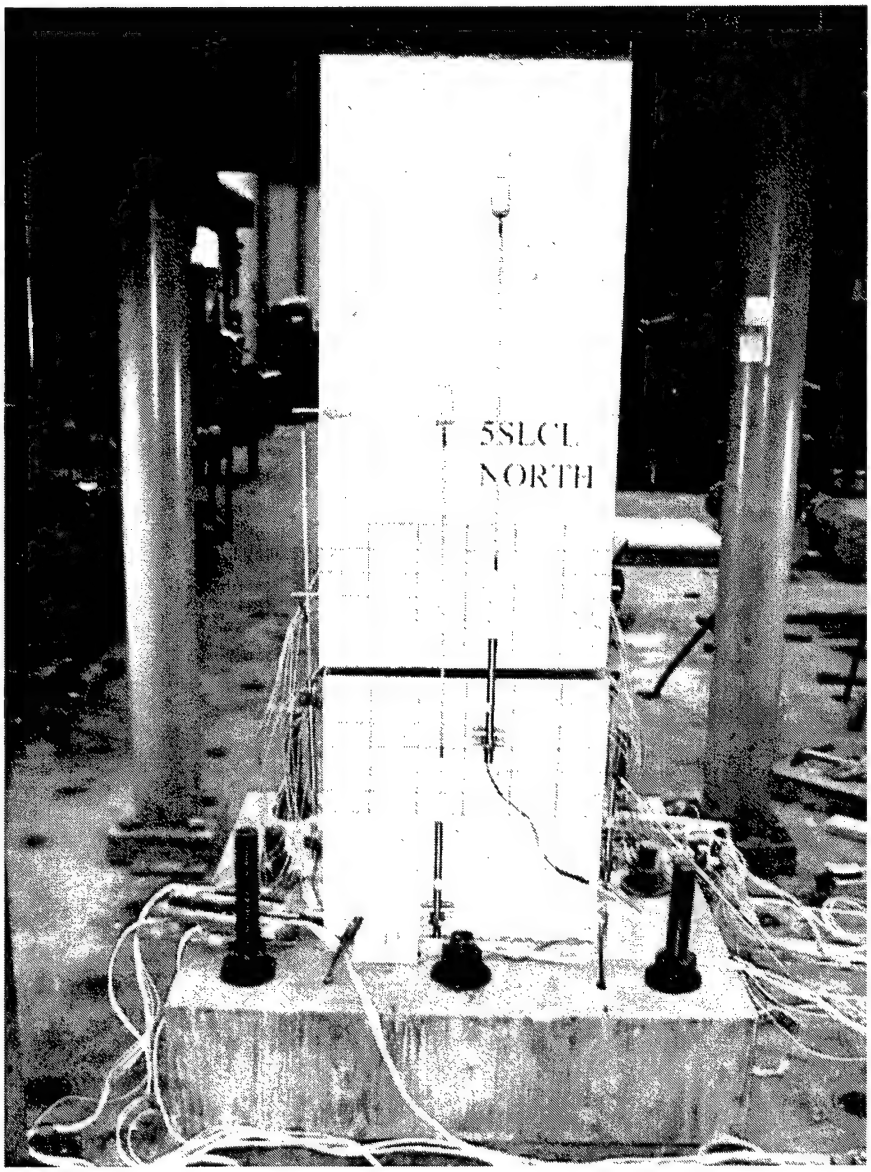

Figure 31. North view of 5SLCL failure plane

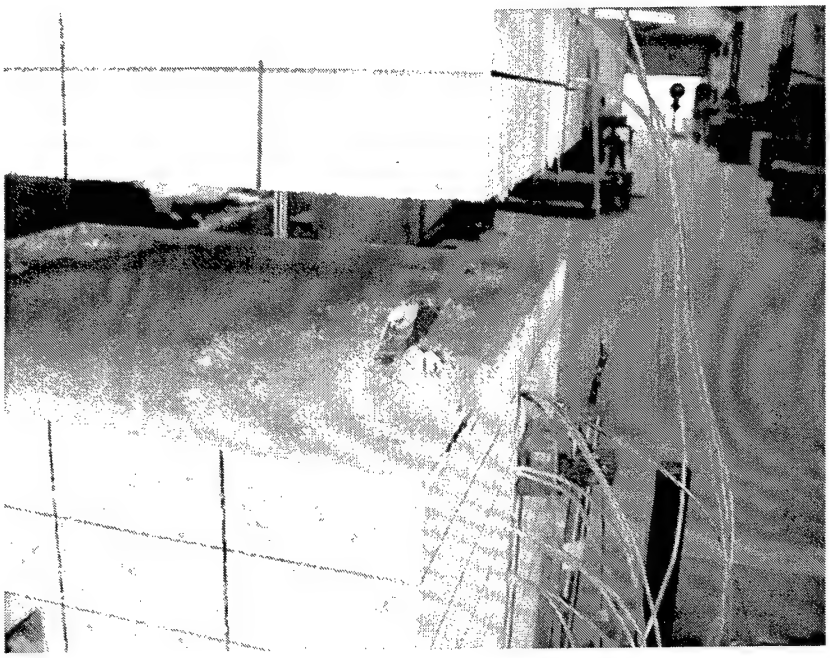

Figure 32. Postexperiment view of 5SLCL failure plane

taken as occurring during the last application of the 1.2-in. cycle 33. Note that the increase in the number of cycles from prior experiments was partly as a result of the mechanics of the loading procedure. A deflection-controlled ram input the load. Hence, having two cracks effectively halved the loading rate of each crack. This increased the number of cycles required for failure. Fortunately, increasing the number of cycles should give a conservative estimate of capacity. The number of cracks also needed to be accounted for in examining the deflection measurements. Given that the cracks were apparently the same width up to failure, the measured deflections were divided by the number of cracks spanned by each gage. The crack normalized total deflection at failure was 0.424 in., as measured by the average of six 40-in. and two 8-in. LVDT gages. Note that both 8-in. gages spanned one crack and both measured 0.420 in. This confirms the normalization process. The load-deflection curve is shown in Figure 33. Loading was continued until complete failure was reached. The apparent failure mode was a localized response of the rebar with no concrete degradation. There was only a small degree of very localized crushing of the concrete immediately around the rebar failure zone. This conical zone of crushed concrete extended about one bar diameter into model above and below the cold joint. The reinforcing bar appeared to fail in tension. Some bending of the rebar was evident, caused by the compression of the rebar during the reverse loading cycles.

Experiment 5SLCH Results

The experiment 5SLCH was conducted on 29 September 1998. Figure 34 shows the model during loading. As in all the experiments with No. 5 rebar,

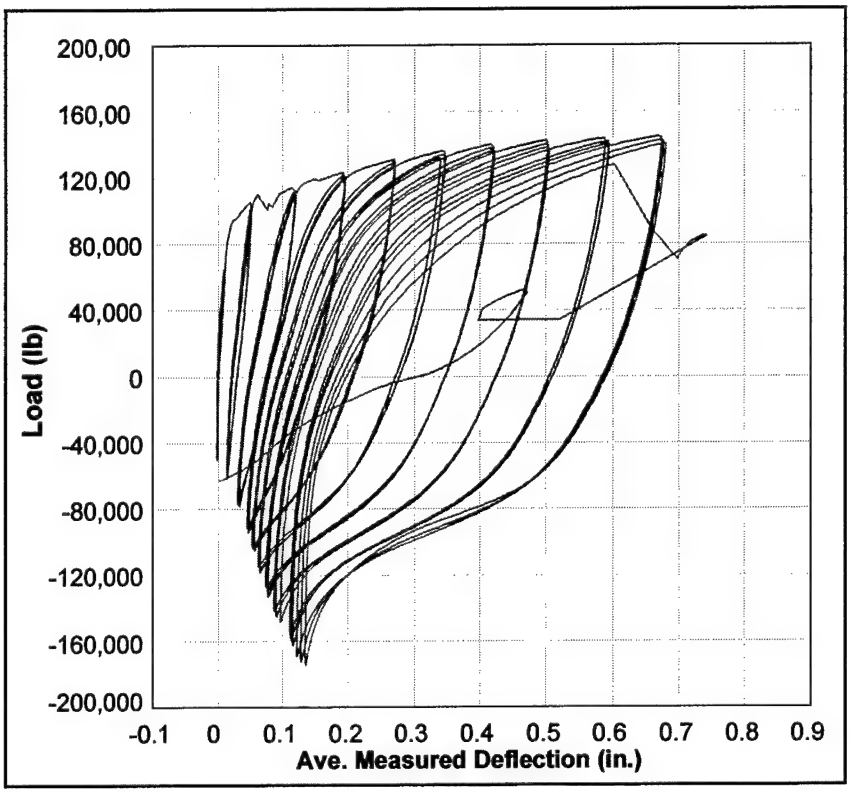

Figure 33. Load-deflection curve for experiment 5SLCL (not crack normalized)

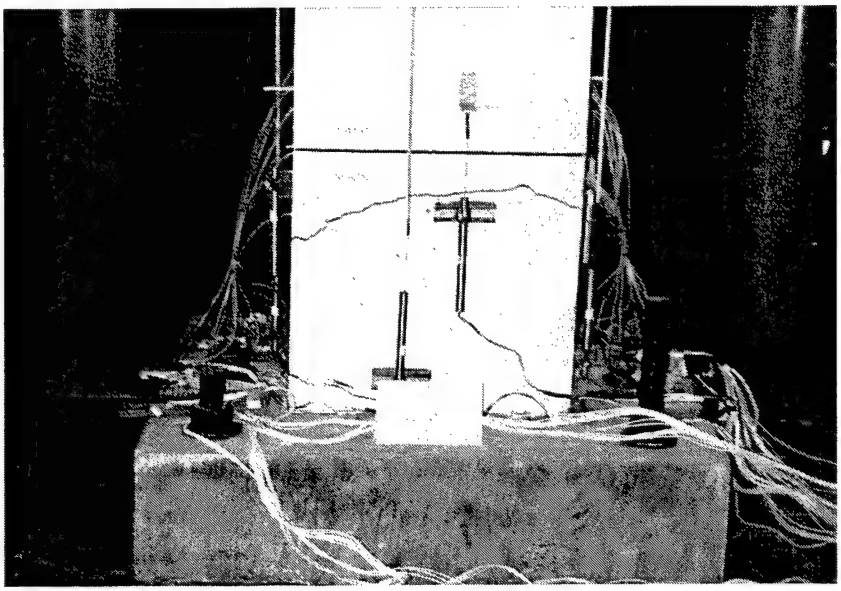

Figure 34. North view of 5SLCH failure plane showing multiple cracks

more than a single crack formed. In this case, a second crack formed approximately 4 to 9 in. below the cold joint. Failure eventually occurred within the crack at the cold joint (Figures 35 through 37). Careful observation of the cracks showed them to be almost exactly the same width during loading. A small minor crack also formed near the base of the model but did not seem to influence failure. The apparent failure mode was a localized response of the rebar; however, in this case, there was substantial concrete response. The concrete response consisted of spalling of cover concrete between the cold joint and the second crack on the west face of the model. This loss of cover concrete did not change the failure mode of the rebar. The reinforcing bar appeared to fail in tension with some of the typical bending of the rebar, caused by the compression of the rebar during the reverse loading cycles. The cyclic application of the vertical deflection loads proceeded through 30 cycles to apparent failure during the third application of the 1.1-in. cycle. Note that the cycle number was increased because of the mechanics of the loading procedure and the multicrack response as discussed in the prior section. Fortunately, increasing the number of cycles should give a conservative estimate of capacity. The number of cracks was accounted for in examining the deflection measurements. Given that the cracks were apparently the same width up to failure, the measured deflections were divided by the number of cracks spanned each gage. The crack normalized total deflection at failure was 0.362 in., as measured by the average of the surviving three 40-in. and two 8-in. LVDT gages. Note that one 8-in. gage spanned one crack and measured 0.355 in. This confirms the normalization process. The load-deflection curve is shown in Figure 38. The deflections in this curve are not crack normalized, accounting for unusual shape of the curve. Loading was continued until complete failure was reached.

Experiment 5SHCL Results

The experiment 5SHCL was conducted on 12 December 1999. Figure 39 shows the model during loading. As in all the experiments with No. 5 rebar, more than a single crack formed. In this case, a total of four cracks formed. Failure eventually occurred within the crack at the cold joint (Figure 40). Careful observation of the cracks showed them to be almost exactly the same width during loading. It is interesting to note that the distance between all the cracks was relatively uniform at about 20-in. or 32 bar diameters. This is not a bad estimation of the development length of the rebar. The cyclic application of the vertical deflection loads proceeded through 45 cycles to apparent failure during the third application of the 1.6-in. cycle. Note that the cycle number increased further due to the increased number of cracks in the response. The large number of cycles should still give a conservative estimate of capacity. The number of cracks was accounted for in examining the deflection measurements. Given that the cracks were apparently the same width up to failure, the measured deflections were divided by the number of cracks spanned by each gage. The crack normalized total deflection at failure was 0.293 in., as measured by the average of the surviving six 40-in. LVDT gages. Note that one 40-in. gage spanned two cracks and the remaining five spanned three cracks, yet the crack normalized widths were very uniform. This again confirms the normalization process, even

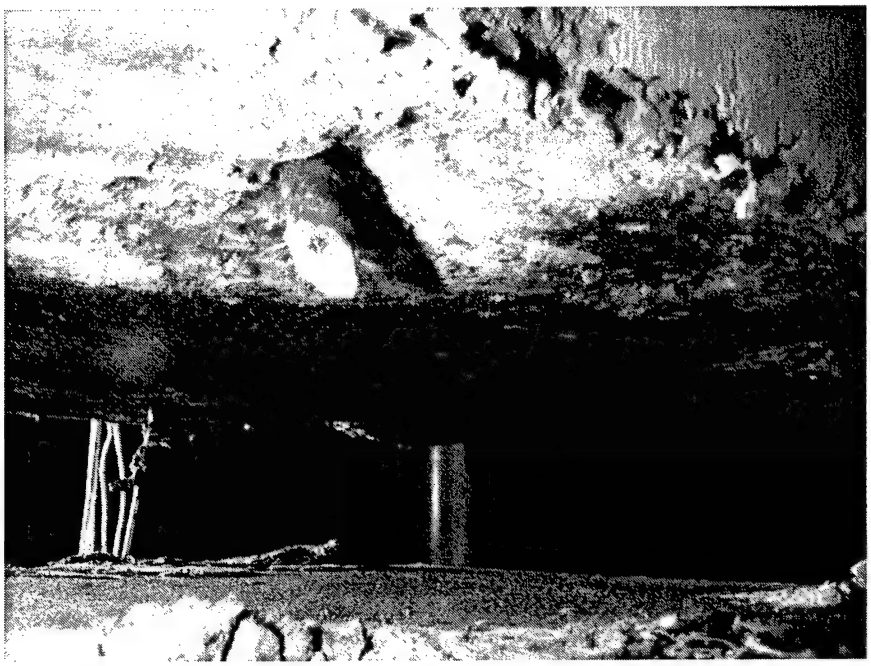

Figure 35. Closeup view of 5SLCH failure plane and rebar

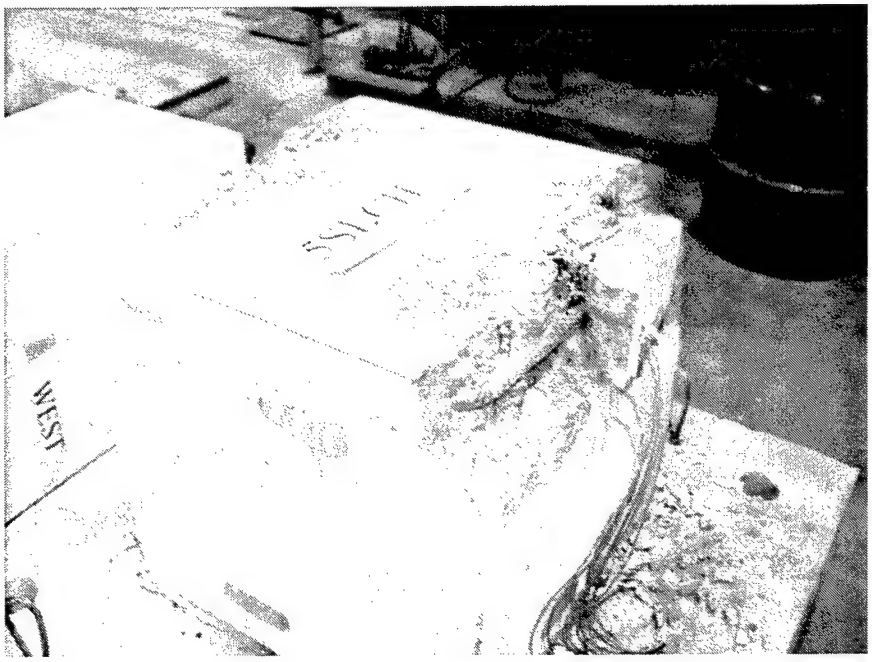

Figure 36. View of 5SLCH lower portion of failure plane with upper half removed

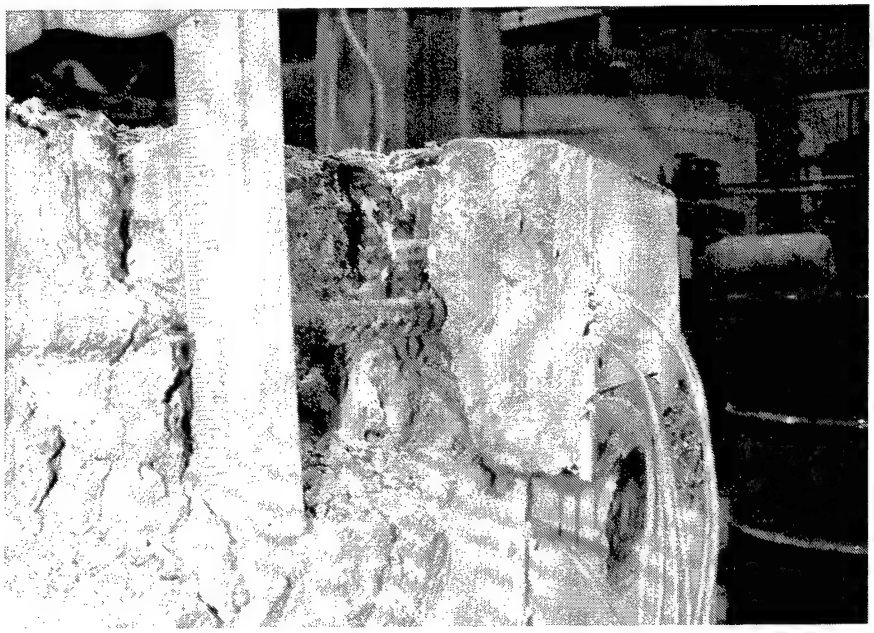

Figure 37. View of 5SLCH failure plane cover concrete spall

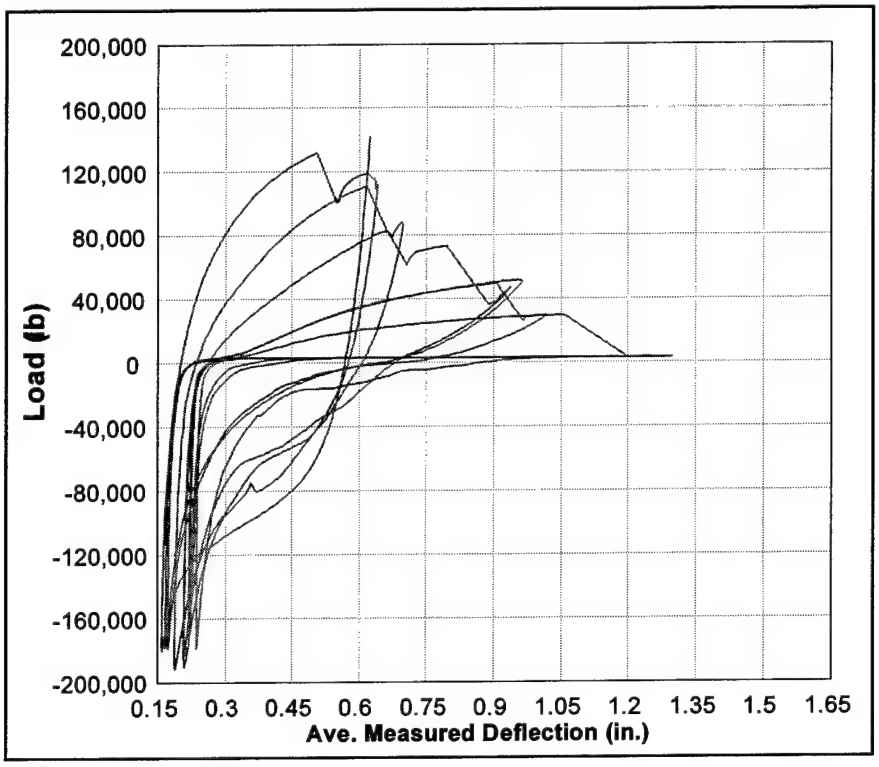

Figure 38. Load-deflection curve for experiment 5SLCH (not crack normalized)

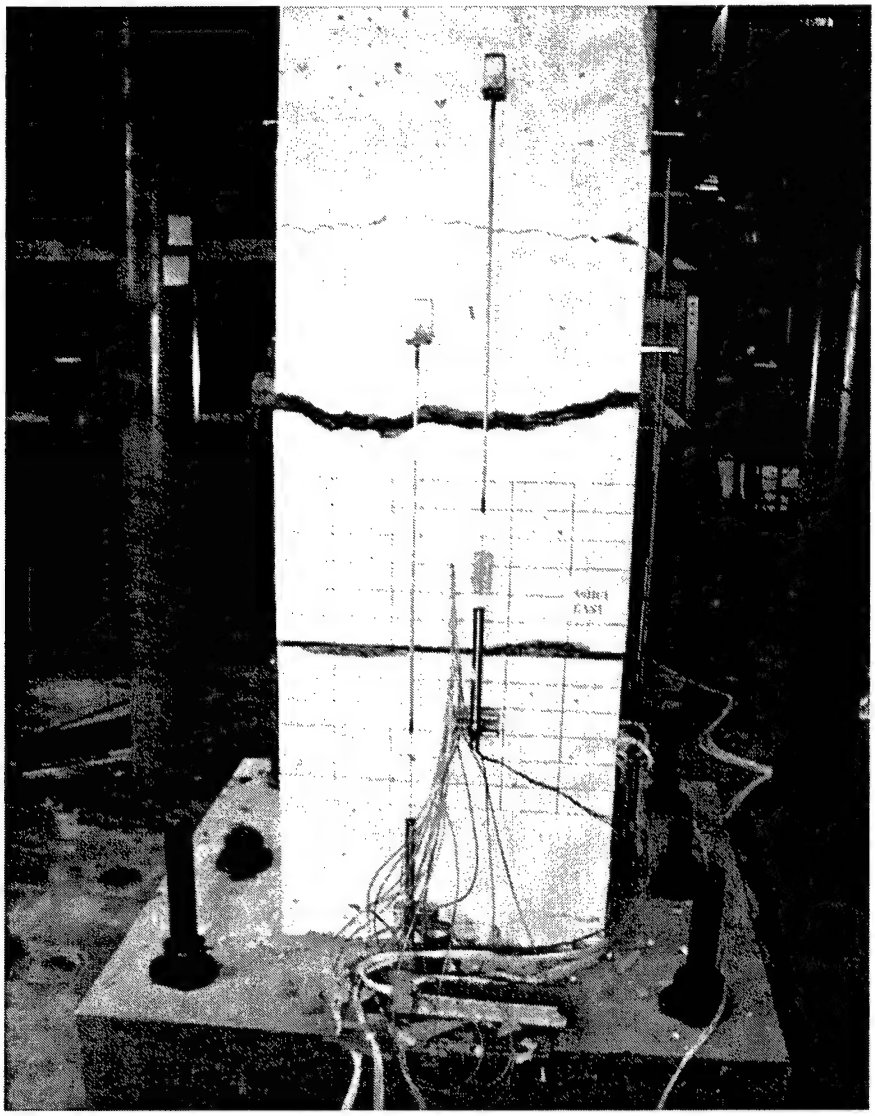

Figure 39. East view of 5SHCL failure plane showing multiple cracks

with this many cracks. The load-deflection curve is shown in Figure 41. Loading was continued until complete failure was reached. The apparent failure mode was a localized response of the rebar. In this case, there was not substantial concrete response other than the formation of the multiple cracks. The reinforcing bar appeared to fail in tension with some of the typical bending of the rebar, caused by the compression of the rebar during the reverse loading cycles.

Experiment 5SHCH Results

The experiment 5SHCL was initially scheduled to be conducted on 22 January 1999. Unfortunately, there was a mishap during the initial attachment of the vertical ram to the model. The hydraulic system began to severely vibrate

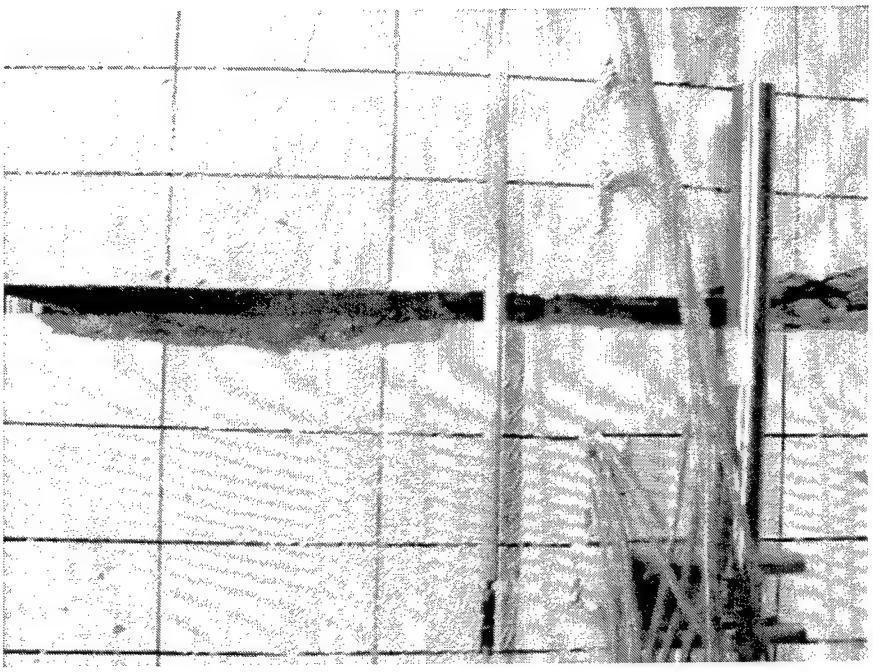

Figure 40. Closeup view of 5SHCL failure plane and rebar

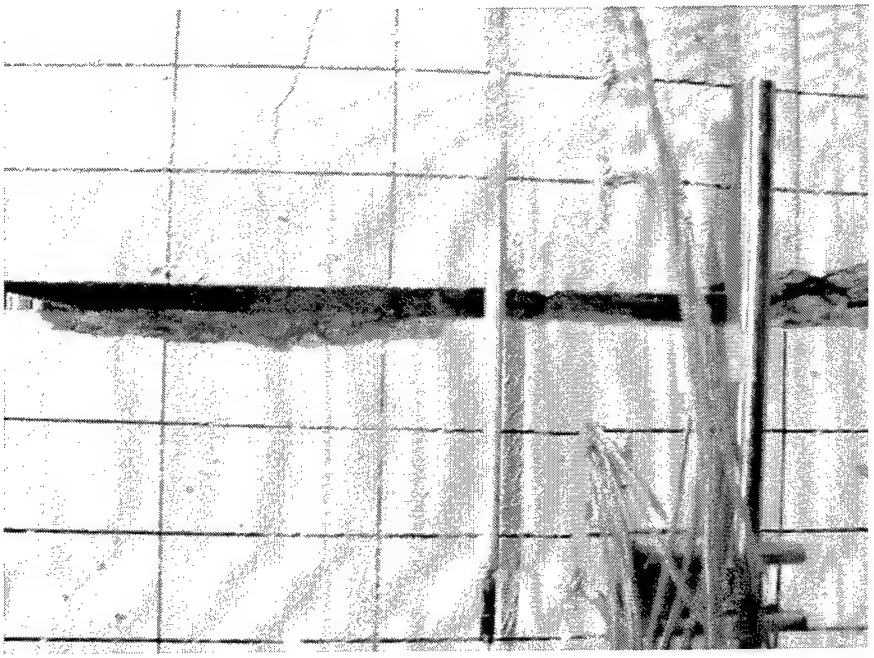

Figure 41. Load-deflection curve for experiment 5SHCL (not crack normalized)

upon application of the dead load to the model. As a result of this oscillation, one of the load plate bolt nuts vibrated down to contact the load plate. When the hydraulic system was shut down and then restarted, the ram violently rebounded upward about 2 in. pulling upward on the single bolt and failing one corner of the model (Figure 42). Fortunately no one was injured. An attempt was made to salvage the model by removing the damaged portion, replacing the lifting bolts, providing additional anchoring and replacing the concrete with very high strength grout (Figures 43 and 45). When an attempt was made to load the repaired model, failure occurred at the interface of the new and old concrete (Figure 46). This failure mode was obviously an artifact of the repairs made and the experiment was abandoned.

Figure 42. Damage to 5SHCH model due to accidental loading

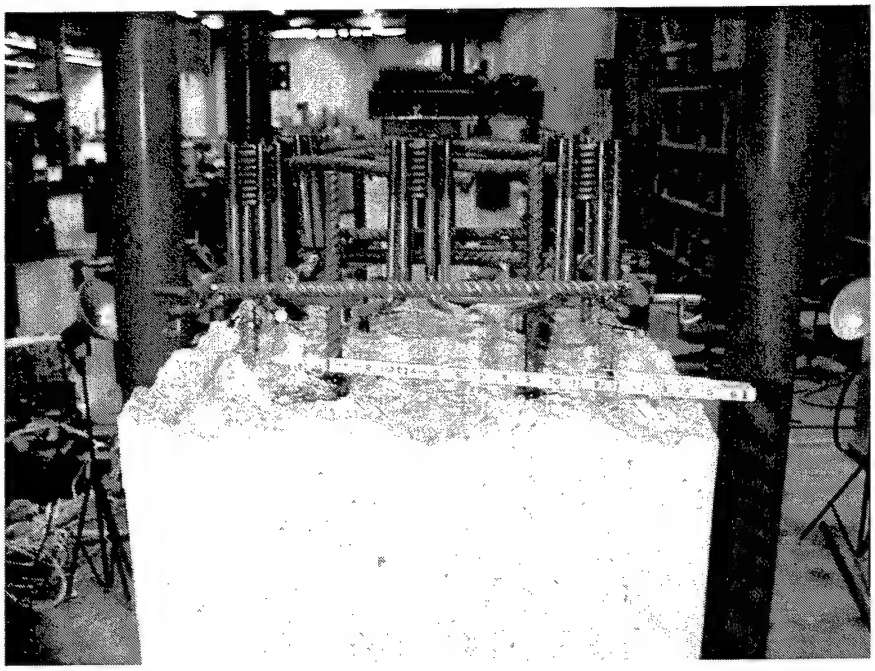

Figure 43. Repair of 5SHCH model

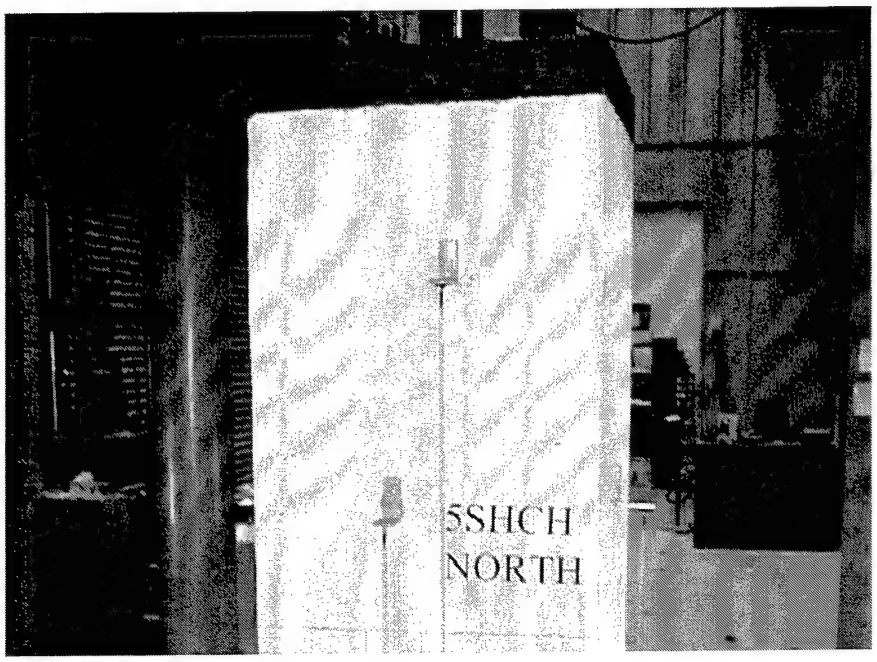

Figure 44. Repair of 5SHCH model

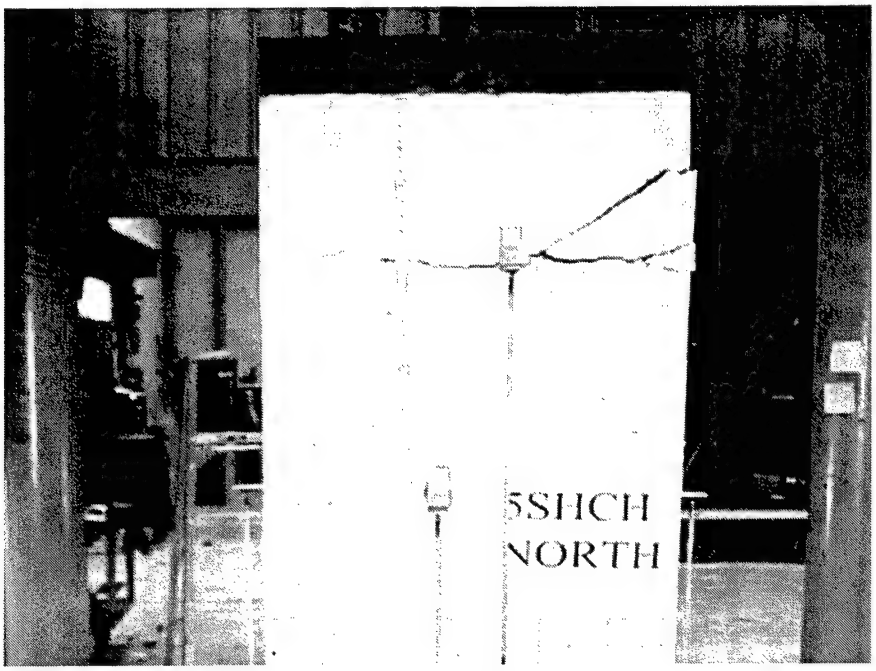

Figure 45. Failure of 5SHCH model at repair

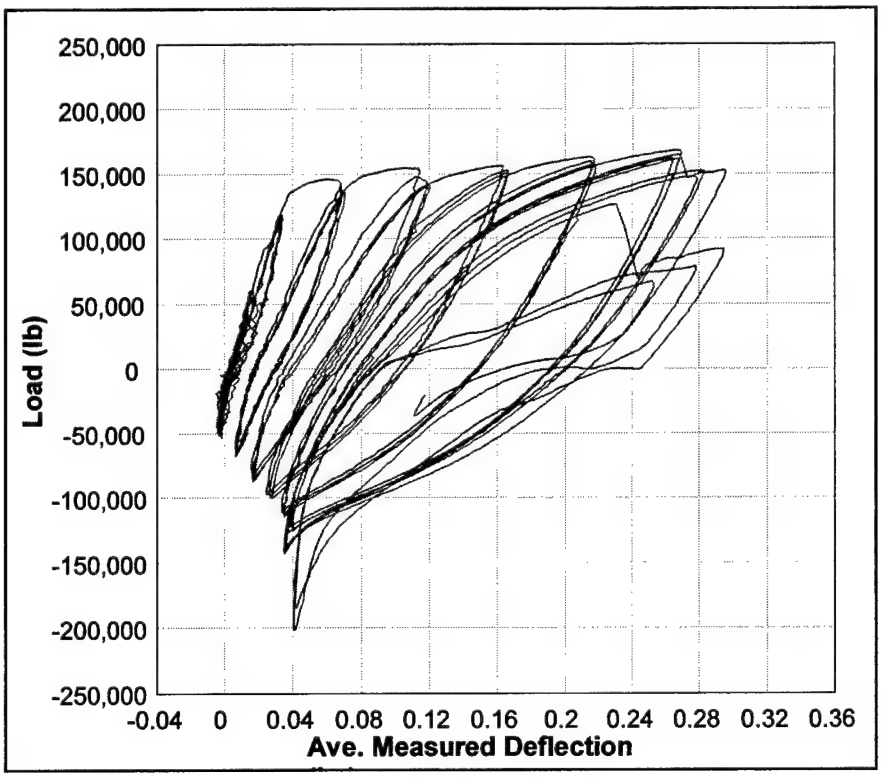

Figure 46. Load-deflection curve for repaired model in experiment 5SHCH

4 Analysis

Postexperimental analysis was conducted on the nine models that returned usable data. In examining the results, it soon became apparent that the crack width at failure was the most useful data obtained. The major objective of the experimental effort was to obtain the information needed to conduct the deflection-based analysis of lightly reinforced intake towers. Crack width was identified as the best parameter for input into such a deflection analysis. A statistical analysis was conducted to generate an empirical relationship for crack width.

Deflection-Based Analysis Technique

The nonlinear response and ductility of lightly reinforced intake towers has been the focus of an analytical and experimental effort at the U.S. Army Engineer Research and Development Center (ERDC) for some time (Truman 1996). It has been shown that lightly reinforced intake towers can exhibit ductility but with a very localized failure. When a lightly reinforced intake tower is excited by a seismic event, a single crack forms at the base of the tower or at the location of a major stiffness change. Experimentation has shown that ultimate failure is dependent on the response of the rebar within the crack. A deflection-based analysis technique is being developed that reflects this localized failure mode. This technique is a modification of a response spectrum analysis and includes explicit consideration of the earthquake-induced displacements of a structure. It also attempts to account for the shift of the structure fundamental frequencies with formation of plastic regions in the structure. This method is presented in EC 1110-2-285, "Structural Analysis and Design of Intake Structures for Outlet Works" (Headquarters, Department of the Army 1995), as an alternative method applicable to towers with vertical steel percentages of 1 percent or less. Most existing Corps intake towers have less than 1 percent vertical steel.

The assumed model consists of a simple cantilever beam attached to a rotational spring. The spring models the response of the cracked region. The beam models the response of the uncracked tower above the crack. The definition of the rotational spring stiffness requires the calculation of the moment-curvature (M-Phi) relationship. This can be accomplished with various computer programs. With the M-Phi relationship in hand, one can calculate the moment-rotation (M-Theta) relationship by multiplying the curvature by an

assumed plastic hinge length. The M-Theta relationship is the stiffness of the rotational spring. One further simplification is required. If a response spectrum analysis is to be conducted, the spring must be linear. The M-Theta relationship is often strongly bilinear. A proposed method of getting around this problem is to approximate a linear relationship. First, the area under the bilinear curve up to a maximum allowable rotation is calculated. Then an artificial, linear, M-Theta curve is generated that has the same area and the same maximum rotation. This has the advantage of maintaining the same total energy required to reach the same maximum rotation. The main disadvantage is that the rotational stiffness and, hence, the frequency of response of the spring are somewhere between the elastic and inelastic values. This approximation is still under evaluation.

The next step in the deflection-based analysis is to calculate the expected deflection under the given earthquake loads. Given the linear spring stiffness, the beam element properties, and any added mass due to water, a response spectrum analysis can be conducted using a commercial structural analysis program. The maximum deflection calculated is the deflection demand of the tower under the input earthquake. To complete the analysis, we now need the deflection capacity of the tower. The deflection capacity is closely modeled by the following:

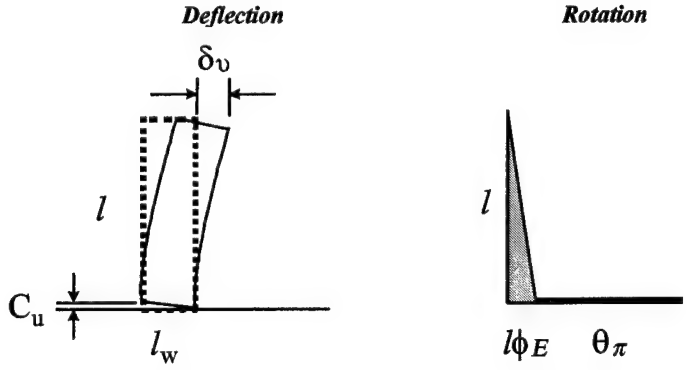

(1)

$$\delta_u = \frac{\phi_E l^2}{3} + \theta_p l \qquad \theta_p = \frac{Cu}{l_w}$$

$$\phi_E = \frac{M}{EI_g} \qquad \delta_u = \frac{\phi_E l^2}{3} + \frac{Cu}{l_w} l$$

where

δ_u = the ultimate deflection capacity

ϕ_E = the ultimate elastic curvature at the base of the tower

θ_p = the plastic rotation at ultimate

l_w = the depth of the section

l = the height of the tower above the crack

C_u = the ultimate crack width at failure

This model assumes that the ultimate lateral deflection consists of the sum of two parts. The first part is the elastic response of the body of the intake tower above the cracked section. The second part is a rigid body rotation of the tower as the crack opens at the base of the elastic section, and the tower rotates about the neutral axis of the cracked section. It is conservative to assume that the neutral axis is coincident with the edge of the tower. Hence, the lateral rigid-body deflection at the top of the tower varies directly with the crack width, and its maximum value is as a ratio of the tower height and the tower width times the ultimate crack width.

Statistical Analysis

The current experimental effort was conducted to determine the proper model for the response of the intake tower. As part of this effort, a statistical analysis was conducted of the results of the experiment. The analysis was conducted using the STAGRAPHICS program. The values of parameters included in statistical model are shown in Table 2. These parameters included those associated with the steel (bar diameter, bar area, yield strength, yield strain, hardening strain, ultimate strength, ultimate rupture strain) as well as the concrete (density, compressive strength, modulus of elasticity) and finally the response (number of cracks, ultimate crack width, cycles to failure). An analysis of variance was conducted and the results were somewhat surprising (Table 3). The only input parameters that showed significant correlation to the crack width were those associated with the steel material properties of strength and strain. It is especially interesting to note that there was not a significant correlation to bar diameter. This may complicate scaling assumptions, since the crack width of a full-scale bar will not be twice that of a half-scale bar (Figure 47). However, if the crack width is only significantly dependent on the steel material properties, the generation of an estimate of the ultimate crack width is greatly simplified. Again utilizing the STAGRAPICS program, a linear model was generated to describe the relationship between the various parameters and the ultimate crack width. The best model developed was between the ultimate rupture strain and the crack width. Numerous other parameter combinations and permutations did not significantly improve the model. The equation generated is:

$$\text{Ultimate crack width } (C_u) = 0.175913 + 1.03506 * \text{Ultimate rupture strain } (\varepsilon_u) \quad (2)$$

where

C_u = ultimate crack width resulting from cyclic loading to failure of the lightly reinforced section

ε_u = ultimate rupture strain of the rebar as measured in a standard one-way tensile test (Figure 48)

This strain was obtained by measuring the posttest elongation over an 8-in. gage length and dividing by the gage length for three samples of each bar type. The STAGRAPICS results stated that, since the P-value in the ANOVA table is less than 0.01, there is a statistically significant relationship between C_u and ε_u at the 99-percent confidence level. The R-Squared statistic indicates that the model as fitted explains 64.371 percent of the variability in C_u. The correlation coefficient equals 0.802315, indicating a moderately strong relationship between the variables. A plot of the model generated is shown in comparison to the measured values in Figure 49. Figure 50 shows a comparison between the ultimate crack widths calculated by the model and the measured values.

Table 2
Values of Parameters Included in Statistical Model

Name	Bar Diam	Bar Area	Fy	Yield Strain	HrdStrain	Fult	RuptStrain	ConDens	fsubc	ConcE	Cracks	Width	Cycles
3 SLCL	3	0.11	58655	0.0023	0.0214	85194	0.2021	143	3297	4573333	1.00	0.345	18
3 SHCL	3	0.11	76297	0.0030	0.0134	110232	0.1354	143	3475	4541667	1.00	0.338	18
3 SLCH	3	0.11	58655	0.0023	0.0214	85194	0.2021	142	5383	5391667	1.00	0.382	16
3 SHCH	3	0.11	76297	0.0030	0.0134	110232	0.1354		5977		1.00	0.294	18
4 SLCM	4	0.20	50516	0.0018	0.0192	71086	0.2333	143	3724		1.00	0.402	21
4 SHCM	4	0.20	57112	0.0023	0.0182	84021	0.2000	141	3967	4670000	1.00	0.417	21
5 SLCL	5	0.31	55511	0.0023	0.0166	84783	0.1917	144	3577	4800000	1.63	0.424	33
5 SHCL	5	0.31	65773	0.0030	0.0049	107428	0.1250	143	3360	4540000	2.83	0.293	45
5 SLCH	5	0.31	55511	0.0023	0.0166	84783	0.1917	142	5318	5400000	1.75	0.360	30

where

BarDiam= nominal bar diameter (1/8 in.)

BarArea = nominal bar area ($in.^2$)

Fy = average steel yield strength as determined by three standard tensile tests ($lb/ in.^2$)

YieldStrain = average steel yield strain, as determined by three standard tensile tests (in./in.)

HrdStrain = average steel strain at onset of hardening, as determined by three standard tensile tests (in./in.)

Fult = average steel ultimate strength as determined by three standard tensile tests ($lb/ in.^2$)

RuptStrain = average ultimate steel strain, as determined by three standard tensile tests (in./in.)

ConDens = average concrete density from all available concrete cylinders (lb/ft^3)

fsubc = average concrete compressive strength ($lb/in.^2$)

ConcE = concrete modulus of elasticity

Cracks = average number of cracks formed within deflection gage span

Width = average, crack normalized, ultimate model deflection (in.)

Cycles = number of load cycles required to cause failure

Table 3
Variable Pairs with Statistically Significant Analysis of Variance Correlation

BarDiam and BarArea	YieldStrain and RuptStrain
BarDiam and Cracks	**YieldStrain and Width**
BarDiam and Cycles	HrdStrain and Fult
BarArea and Cracks	HrdStrain and RuptStrain
BarArea and Cycles	HrdStrain and Cracks
Fy and YieldStrain	HrdStrain and Cycles
Fy and Fult	Fult and RuptStrain
Fy and RuptStrain	**Fult and Width**
Fy and Width	**RuptStrain and Width**
YieldStrain and HrdStrain	fsubc and ConcE
YieldStrain and Fult	Cracks and Cycles

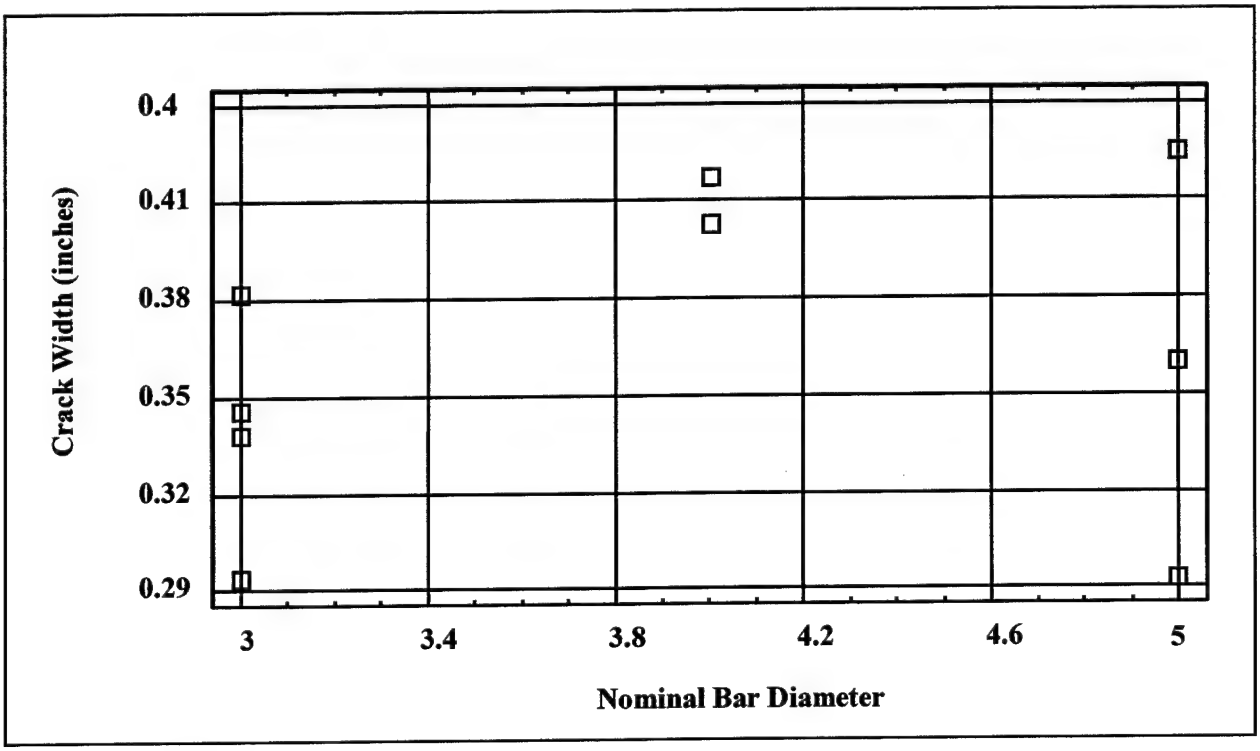

Figure 47. Measured ultimate crack width versus nominal bar diameter for all nine experiments

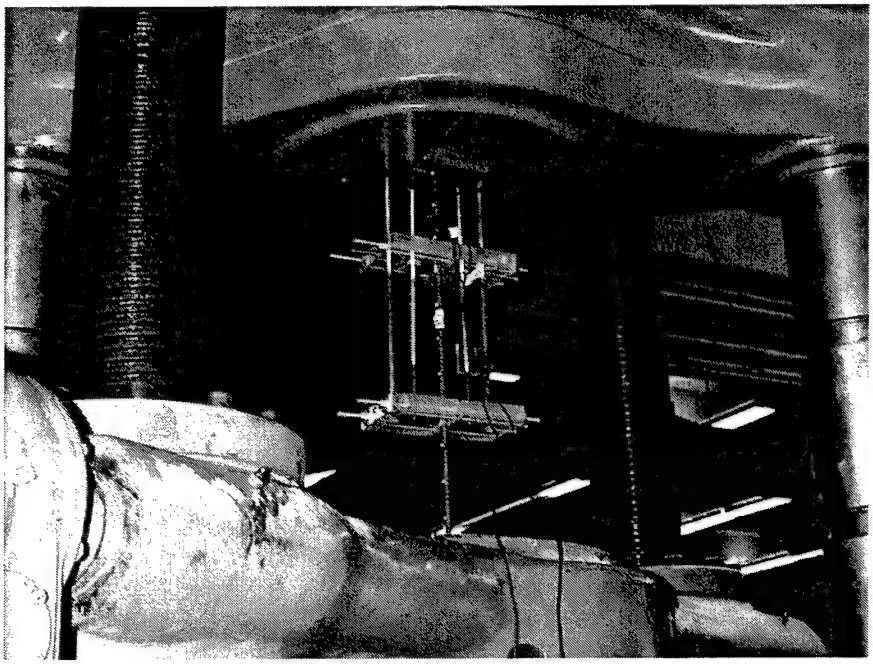

Figure 48. Typical rebar tensile test

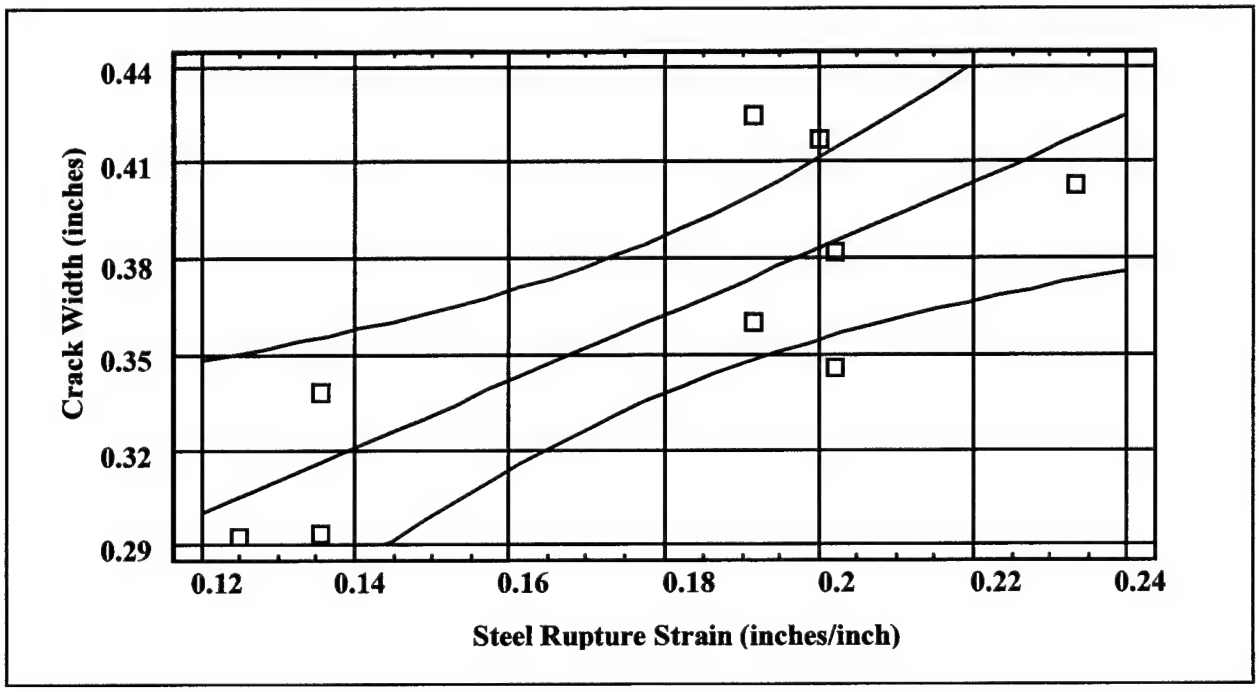

Figure 49. Plot of model predicting ultimate crack width from reinforcing steel rupture strain, including 95-percent confidence intervals

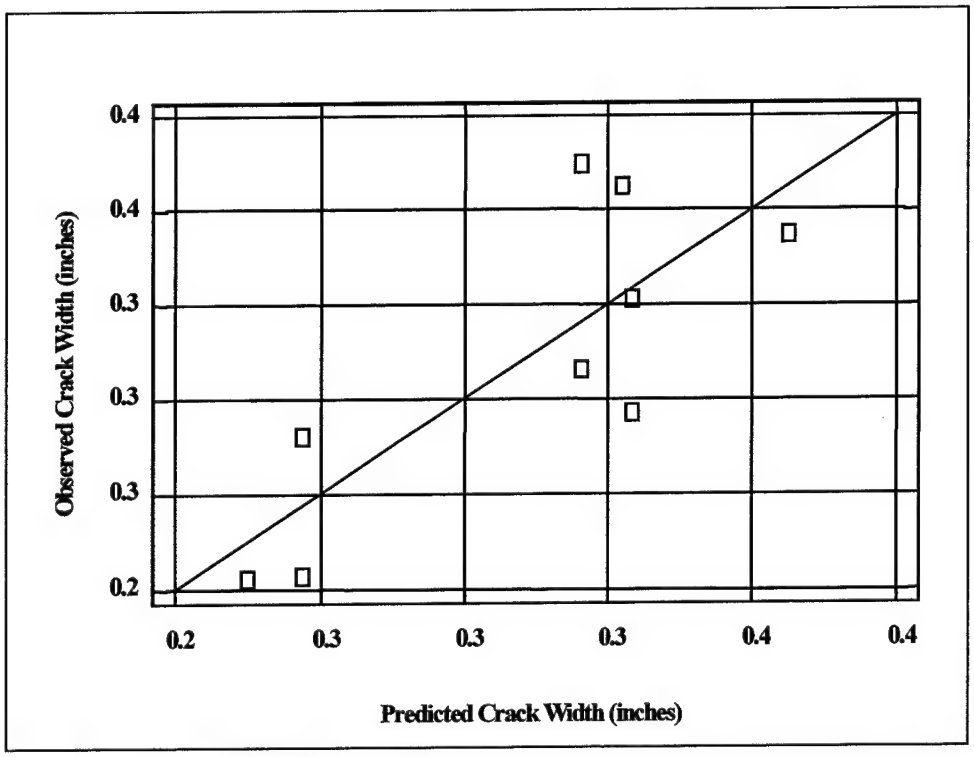

Figure 50. Ultimate crack width predicted from reinforcing steel rupture strain versus measured ultimate crack width for all nine experiments

With this model it is possible to directly calculate the expected ultimate crack width of a section given only the ultimate strain capacity of the reinforcing. Hence, the ultimate deflection capacity (δ_u) of the intake tower is dependent only on the ultimate strain capacity of the reinforcing and the elastic response of the tower above the crack. There is no need to calculate the strain penetration as an intermediate step. Recall that strain penetration is defined by the equation: Crack Width (C_u) = Strain Penetration (L_ε)*Ultimate Rupture Strain (ε_u). However, it was interesting to compare the strain penetration calculated by the equation and the measured strains in the experimental model. Figure 51 shows the strain penetration length back calculated from the final ultimate crack model, the measured crack width, as well as the upper and lower bounds of apparent yield as seen in the strain gage data for the experiment 5SLCH. For this and the other experiments, there was little correlation between the strain data and the calculated strain penetration length. In retrospect, the strain gages do not measure the strain penetration (L_ε) as defined by the equation. Strain penetration (L_ε) as defined by the equation is a parameter that relates crack width to rupture strain but does not necessarily relate to the actual state of strain in the model at failure. For this reason the strain gages shed little light on the response of the model. Fortunately, this was not needed to build the final equation of ultimate crack width and hence deflection capacity.

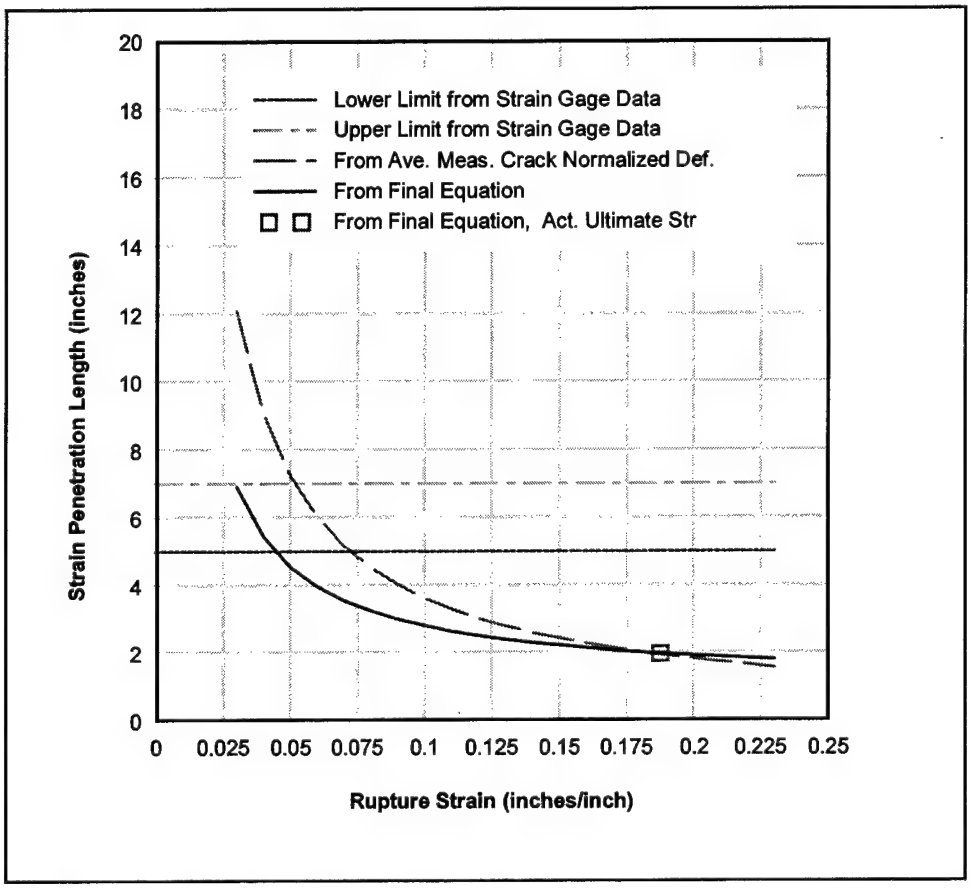

Figure 51. Example of calculated and experimental strain penetration lengths, experiment 5CLSH

5 Deflection-Based Analysis Technique

With the generation of the ultimate crack model, we now have all the tools needed to conduct a deflection analysis. The example presented here is a recent analysis of the Wappapello intake tower. The initial requirement is to determine the location of the critical section so that a simplified structural model can be constructed (Figure 52). This critical section is the expected location of the single crack assumed in the deflection analysis. In most towers, there is an obvious choice for the critical section as there is often a major change in stiffness where the tower section attaches to the much stiffer substructure. This is the case with the Wappapello tower (Figure 53) where there is a major reduction in stiffness at the 395-ft elevation. Also, the tower below this elevation is almost completely buried on three sides, further stiffening the sections below 395 ft. The critical section at 395 ft is shown in Figure 54. As you can see, the section geometry is relatively complicated. The section was simplified before calculating the moment-curvature relationship for the weak axis by combining all the open areas together and all the concrete areas together (Figure 55). The steel areas were summed in a similar manner.

The moment-curvature relationship was generated using the M-Phi program for the simplified section. A concrete strength of 3,000 psi, steel yield strength of 40,000 psi, and an ultimate strain of 5 percent was assumed. Multiplying the curvature (Phi) by an assumed strain penetration (plastic hinge) length of 9 in. yields the moment-rotation (M-Theta) relationship shown in Figure 56. The area under the cracked section M-Theta curve, up to failure, was calculated. This area was used to generate an equal-energy/equal-maximum rotation curve. This linear relationship is the rotational spring constant needed for the finite element model.

The next step was to conduct an ABAQUS response spectrum analysis. Only the modified response spectrum for a 1,000-year-return earthquake was modeled, as this is the most severe case (Figure 57). The element properties were consistent with those calculated by Dr. Truman for elements above the 395-ft elevation. Note that there is no added mass due to water as the maximum water level is below the critical section. The analysis shows that a maximum top deflection of 0.014 in. was calculated. This is the deflection demand placed on the system by the given earthquake.

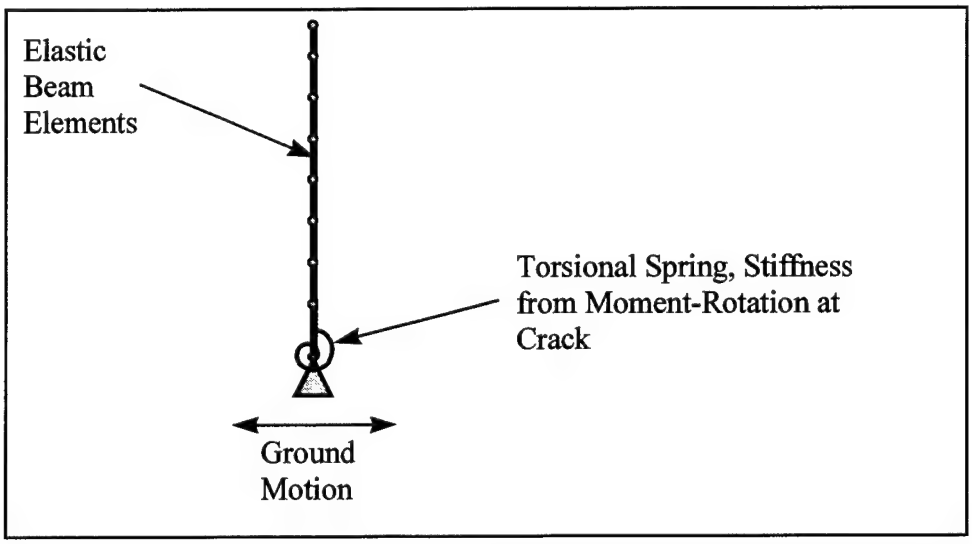

Figure 52. Simplified intake tower model

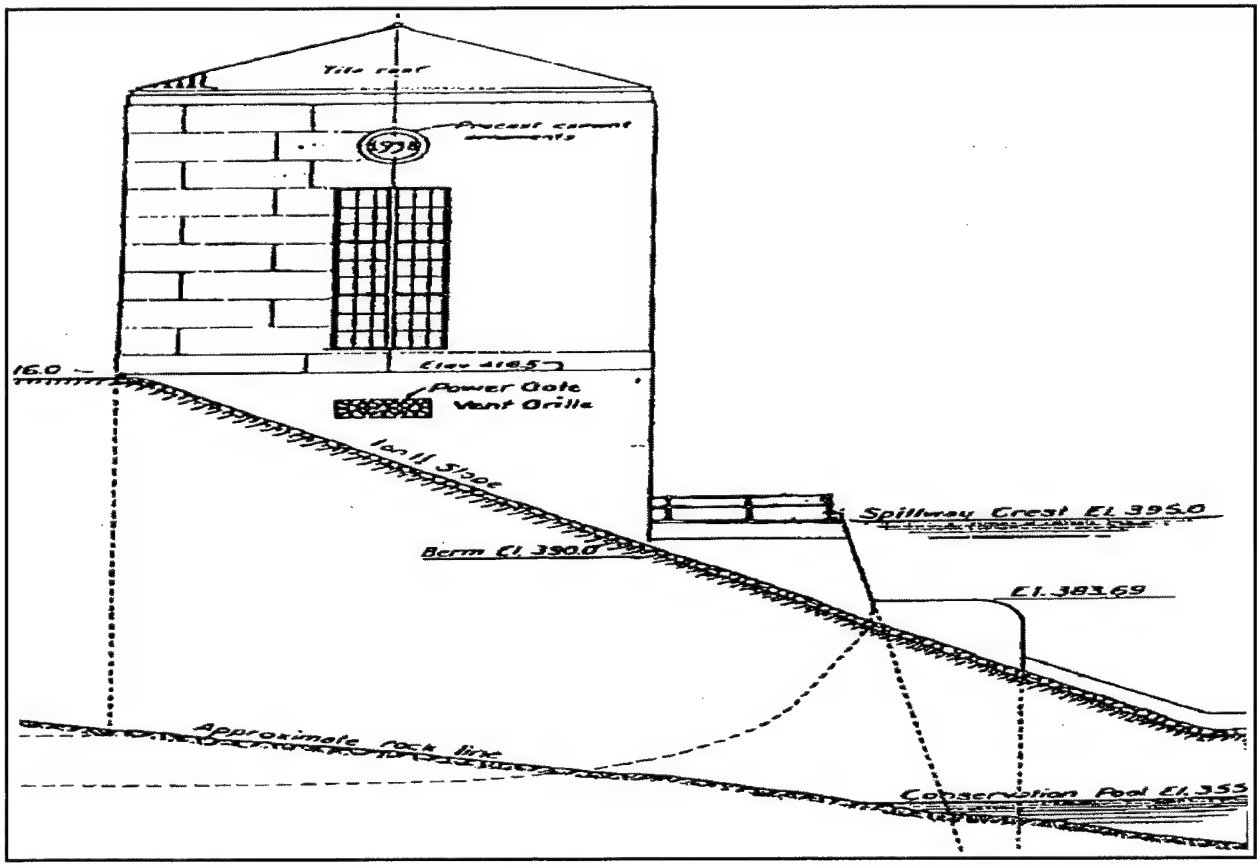

Figure 53. Side view of Wappapello Intake Tower

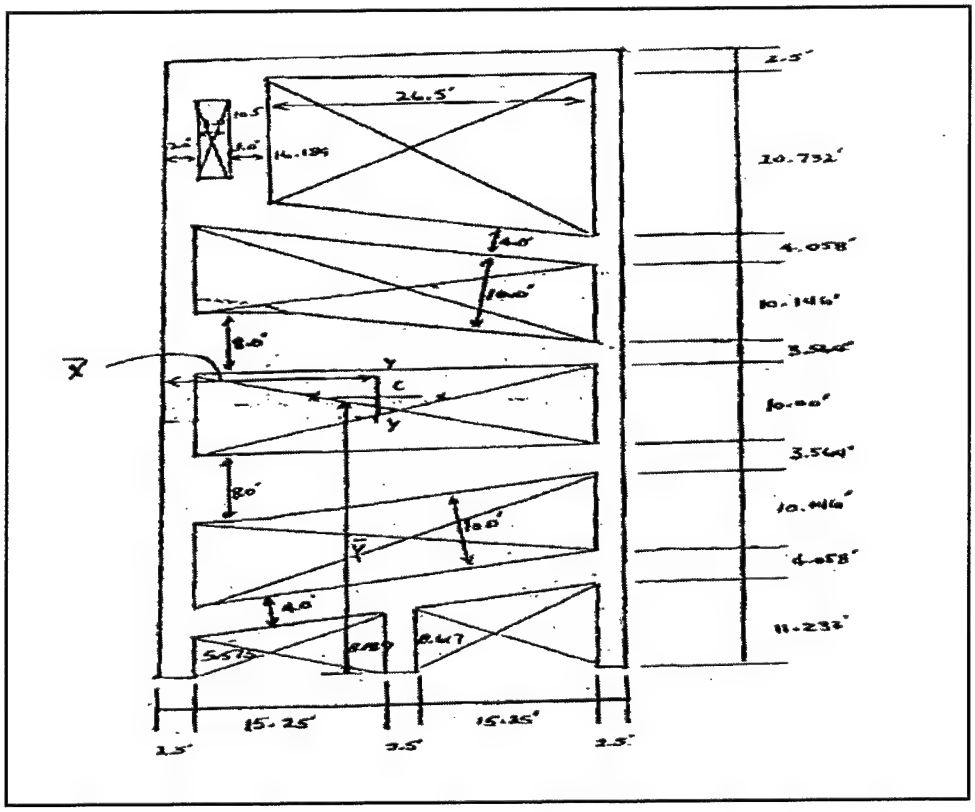

Figure 54. Schematic of critical section at 395-ft elevation

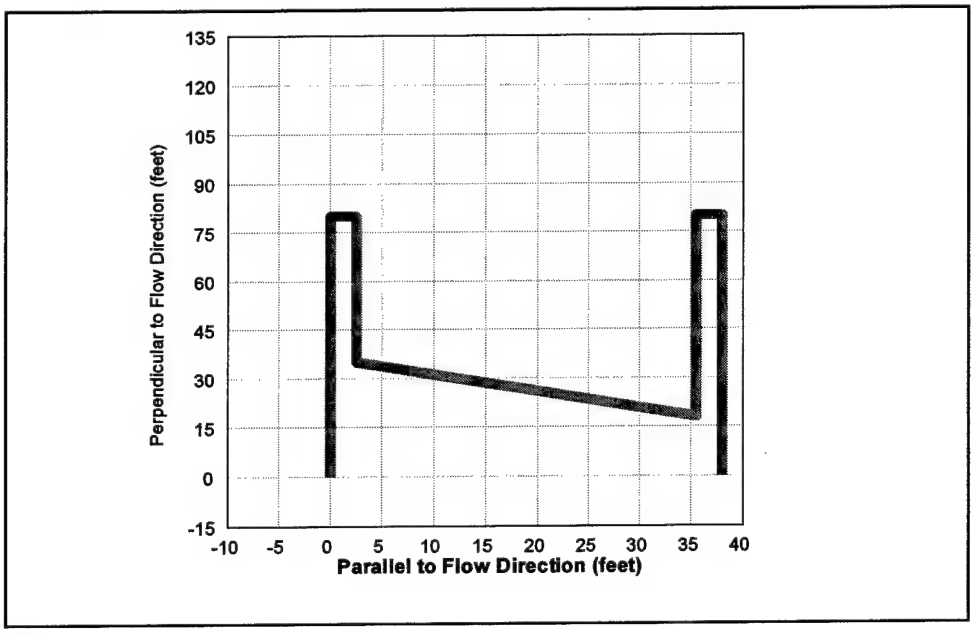

Figure 55. Outline of simplified critical section at 395-ft elevation

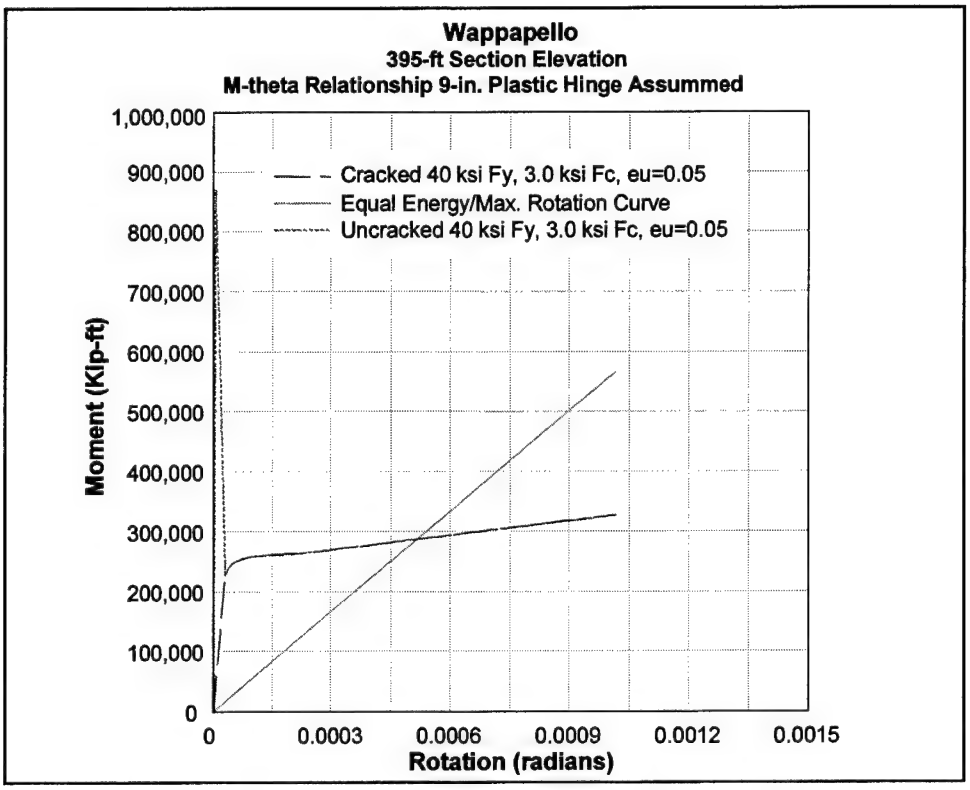

Figure 56. M-Theta relationship for critical section at 395-ft elevation

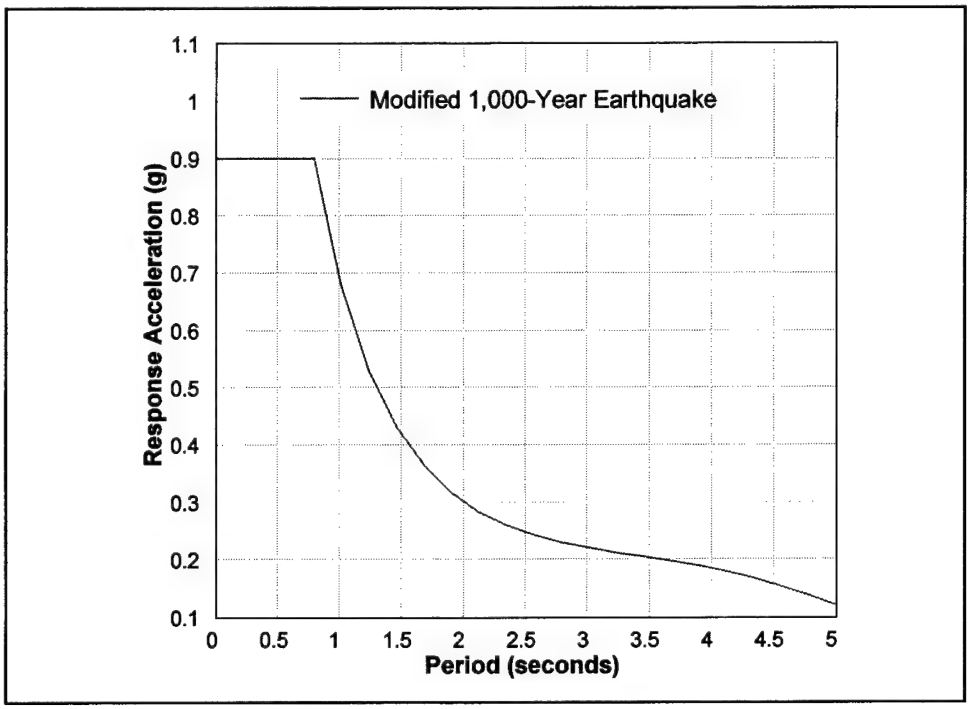

Figure 57. Modified response spectra, 1,000-year-return earthquake

In the final step of the analysis, the calculated demand deflection is compared to the deflection capacity. To calculate the deflection capacity, the crack width is first calculated:

$$C_u = 0.175913 + 1.03506 * \varepsilon_u$$

$$= 0.175913 + 1.03506 * (0.05)$$

$$= 0.23 \text{ in.}$$

Then the deflection capacity is calculated:

$$\delta_u = \frac{\phi_E l^2}{3} + \frac{C_u}{l_w} l \qquad \delta_u \sim \frac{0.23}{38} 61 = 0.37 \text{ in.}$$

This calculation assumes a conservative ultimate strain of 5 percent and ignores the contribution of the elastic response. The capacity far exceeds the demand, and the tower passes the analysis.

6 Conclusions and Recommendations

This experimental effort successfully generated a substantial amount of data on the strain penetration/failure deflection characteristics of the reinforcing steel in the failure zone of lightly reinforced intake towers. The subsequent analysis of the data provided information on the rotational capacity of the critical section at the base of the tower and, hence, to an estimation of the ultimate deflection capacity of existing intake towers. An empirical equation was generated for the estimation of the parameters required for this calculation, and the method was successfully applied to an example problem. This fulfills the objectives as initially stated in this report.

The most important finding was that the crack width in the failure zone is largely controlled by the steel rupture strain. Steel rupture strain is well understood and usually easy to obtain.

Given that there is a direct relationship between crack width and the ultimate structure deflection, the model provides a simple method of estimating deflection capacity, consistent with mechanics of the response of lightly reinforced structures. However, there remain some significant areas of concern. The first is, should crack width be scaled? Variation of bar size was not significant, implying scaling is not appropriate. If results are not scaled, can the model be extrapolated to larger bar diameters? Also, are model modifications needed for application to dynamic response? Some reduction of the rupture strain value may be needed to include strain rate effects.

In summary, we now have a deflection-based analysis procedure. However, the rotational spring model needs further development and the procedure must be verified for dynamic response and perhaps for larger bar sizes. It is recommended that further experimental and analytical work address these concerns.

References

Dove, R. C. (1996). "Structural parameter analysis of U.S. Army Corps of Engineers existing intake tower inventory," Technical Report SL-96-1, U.S. Army Engineer Waterways Experiment Station, Vicksburg, MS.

_____. (1998). "Performance of lightly reinforced concrete intake towers under selected loadings," Technical Report SL-98-1, U.S. Army Engineer Waterways Experiment Station, Vicksburg, MS.

Finn, and Ledbetter. (1999). "Earthquake induced tunnel loading," draft report prepared for the U.S. Army Corps of Engineers District, St. Louis, MO.

Headquarters, Department of the Army. (1995). "Structural analysis and design of intake structures for outlet works," Engineer Circular 1110-2-285, Washington, DC.

Truman, K. Z. (1996). "Seismic analysis of the Wappapello control structure," U.S. Army Engineer District, St. Louis, MO.

Appendix A
Model Construction Drawings

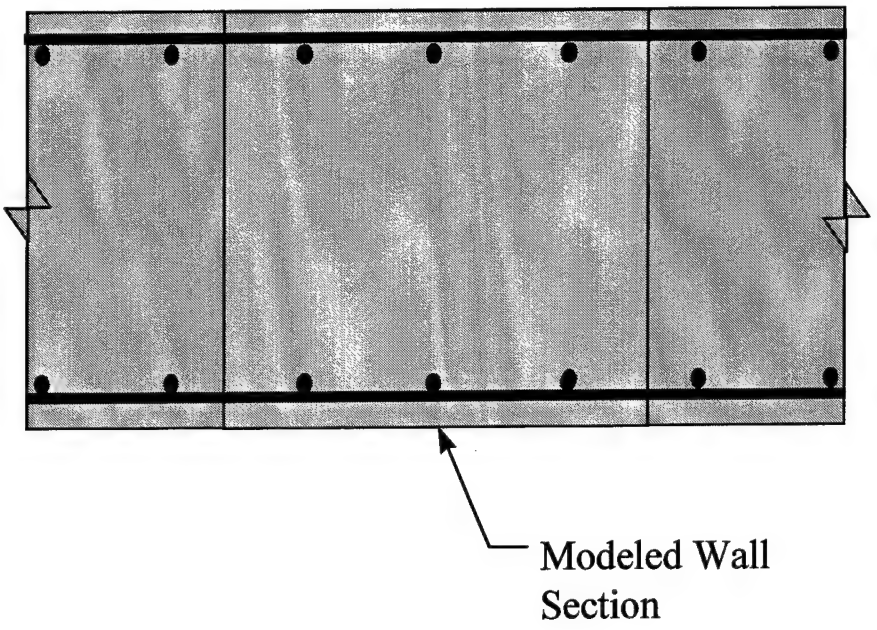

Figure A1. Schematic of modeled intake tower wall section

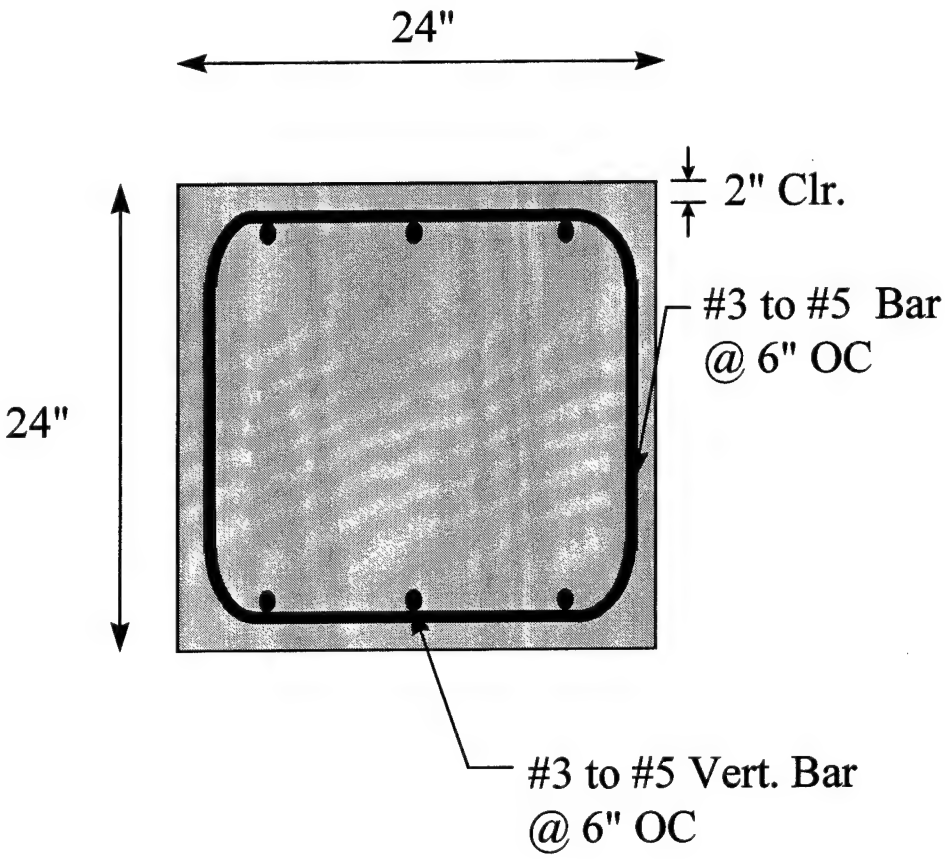

Figure A2. Plan view of model dimensions and reinforcing bar layout

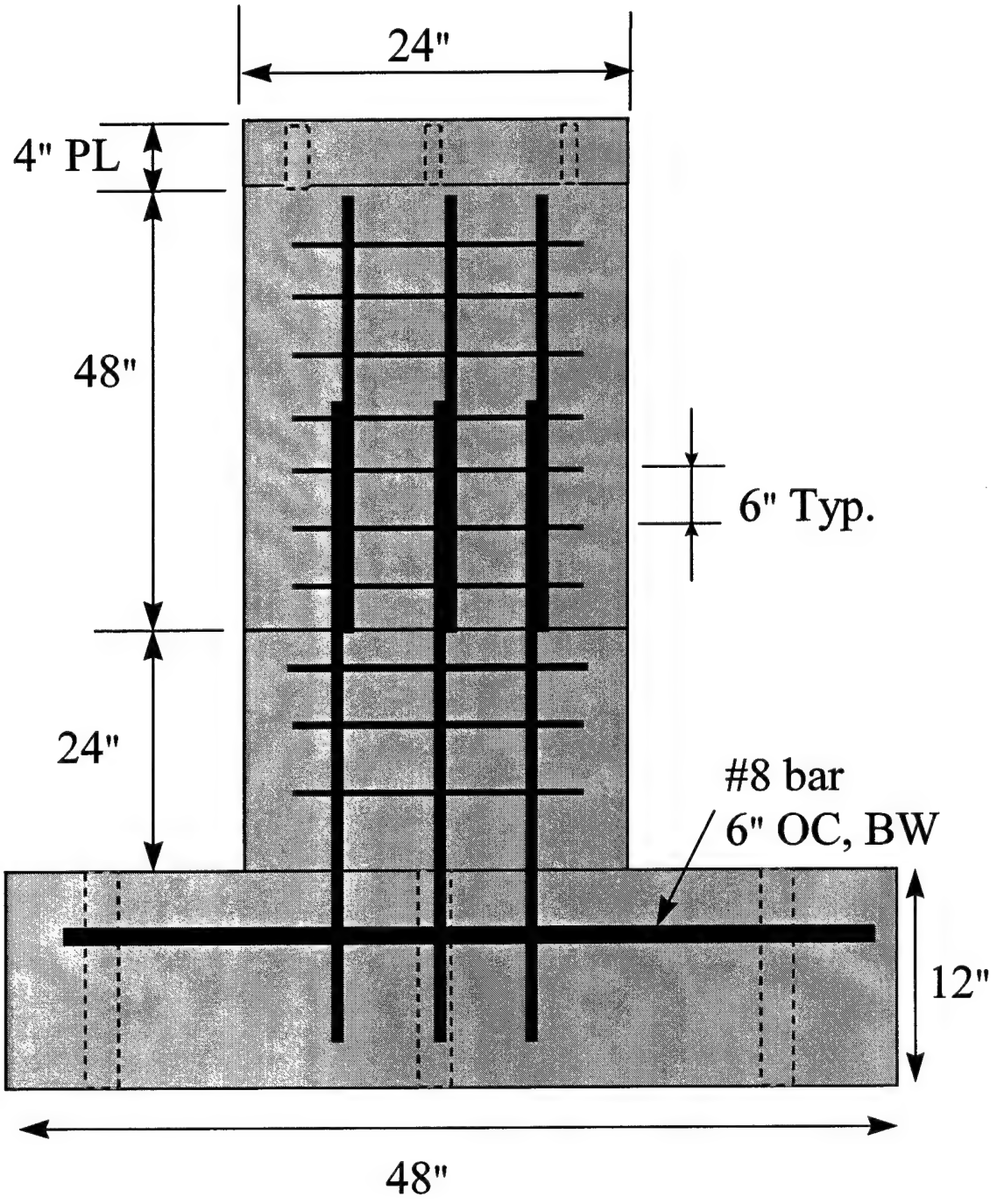

Figure A3. Side view of overall dimensions and rebar layout typical for all models

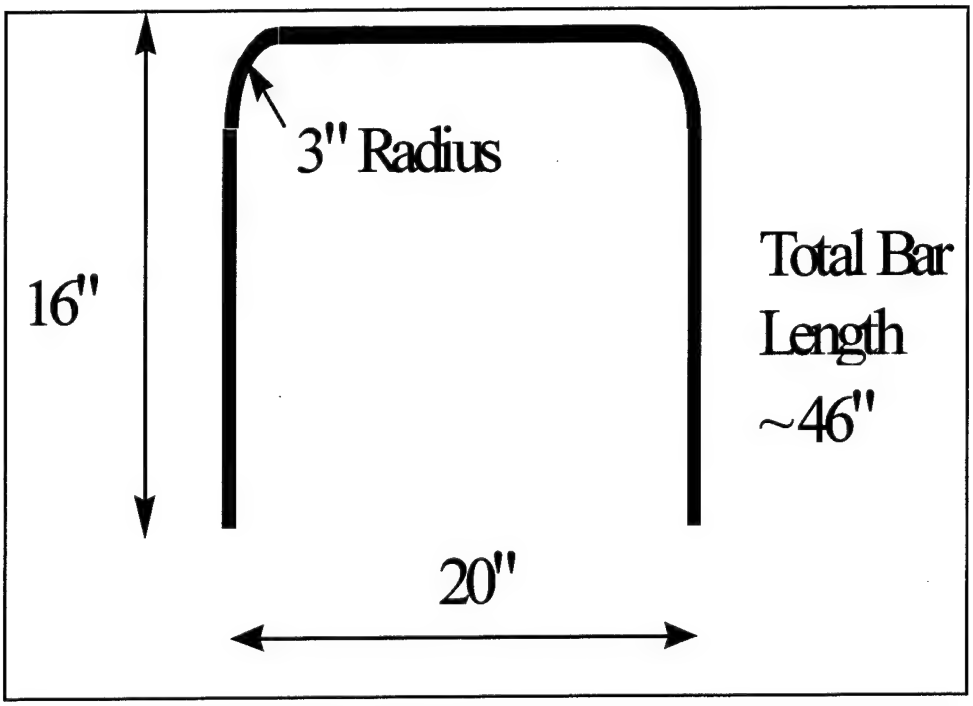

Figure A4. Dimensions of rebar hoops

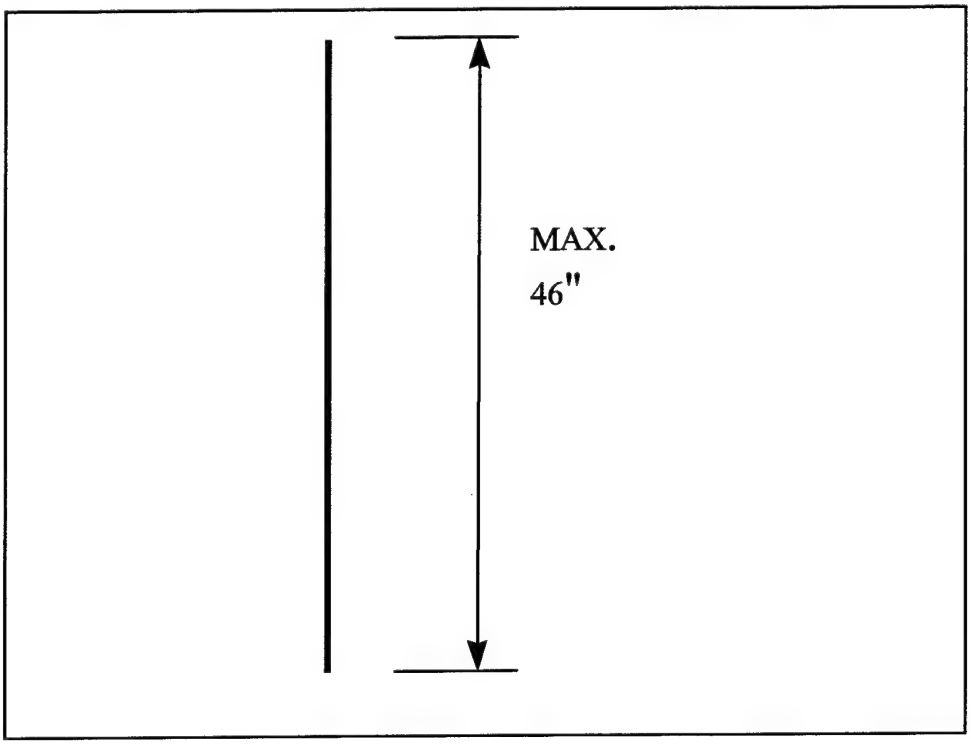

Figure A5. Dimensions of all upper rebar

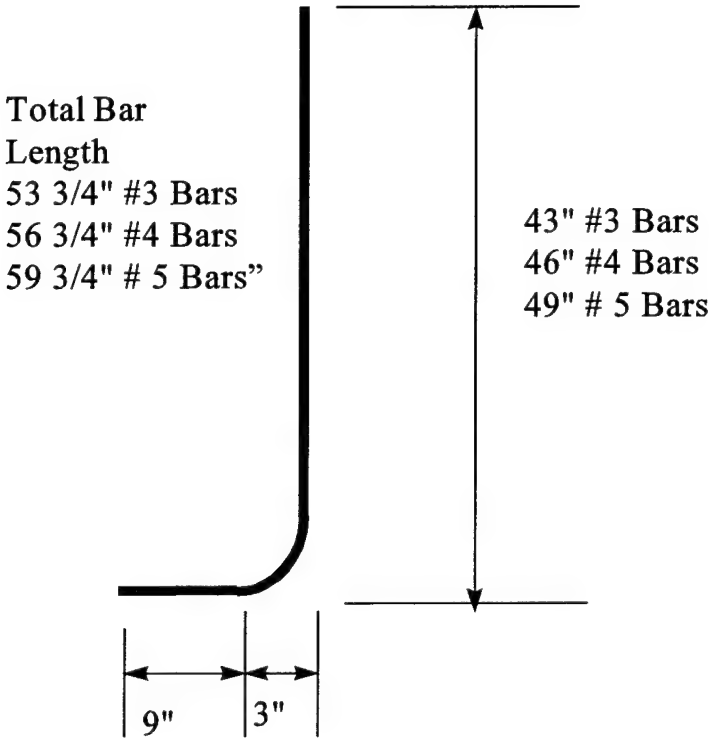

Figure A6. Dimensions of lower rebar

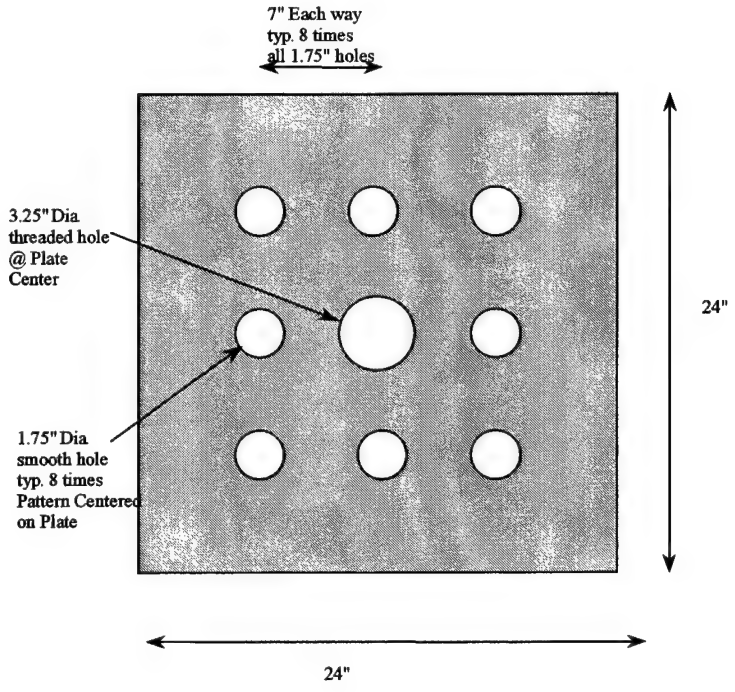

Figure A7. Dimensions of 4-in.-thick load plate

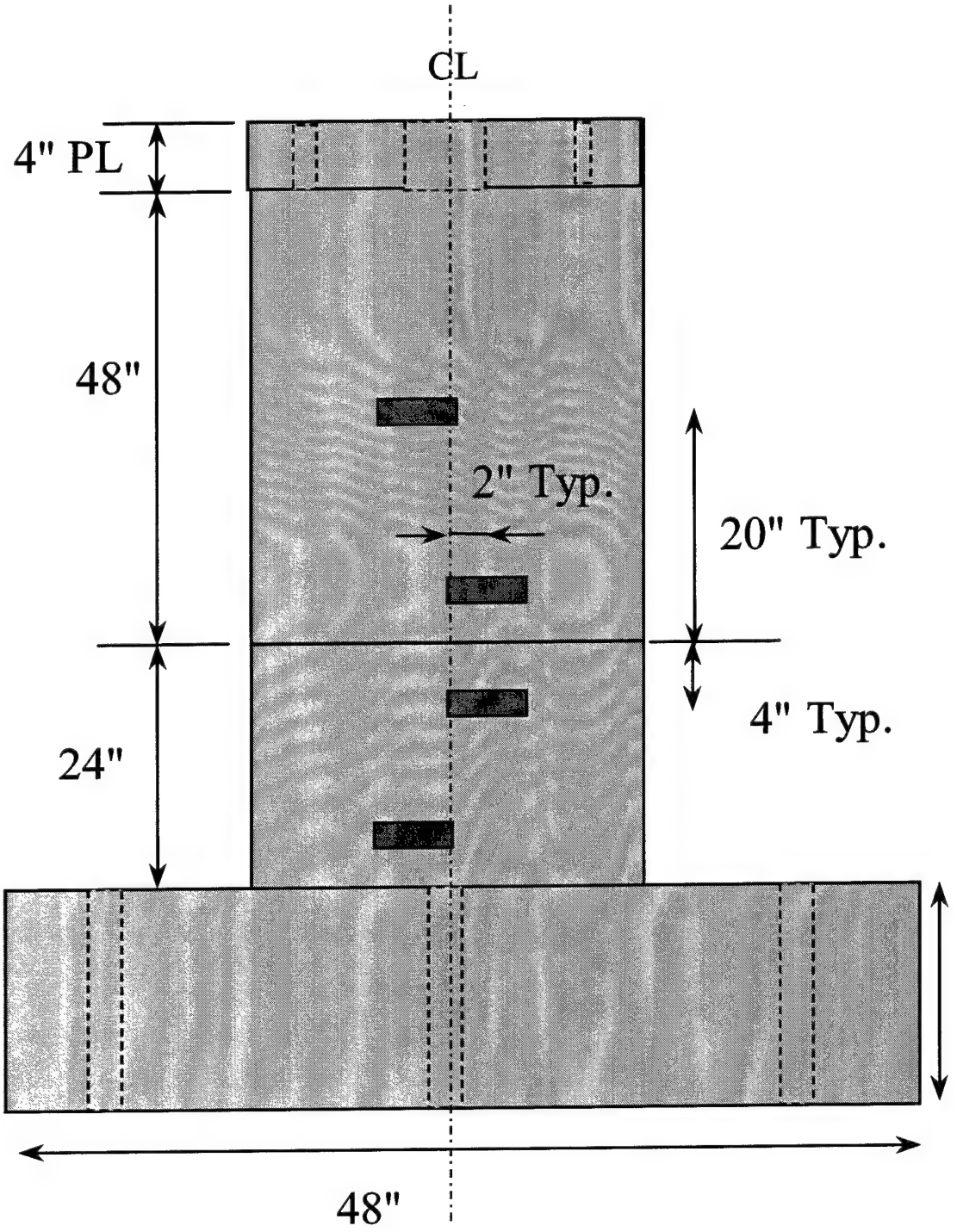

Figure A8. Initial deflection gage locations (modified during experimentation)

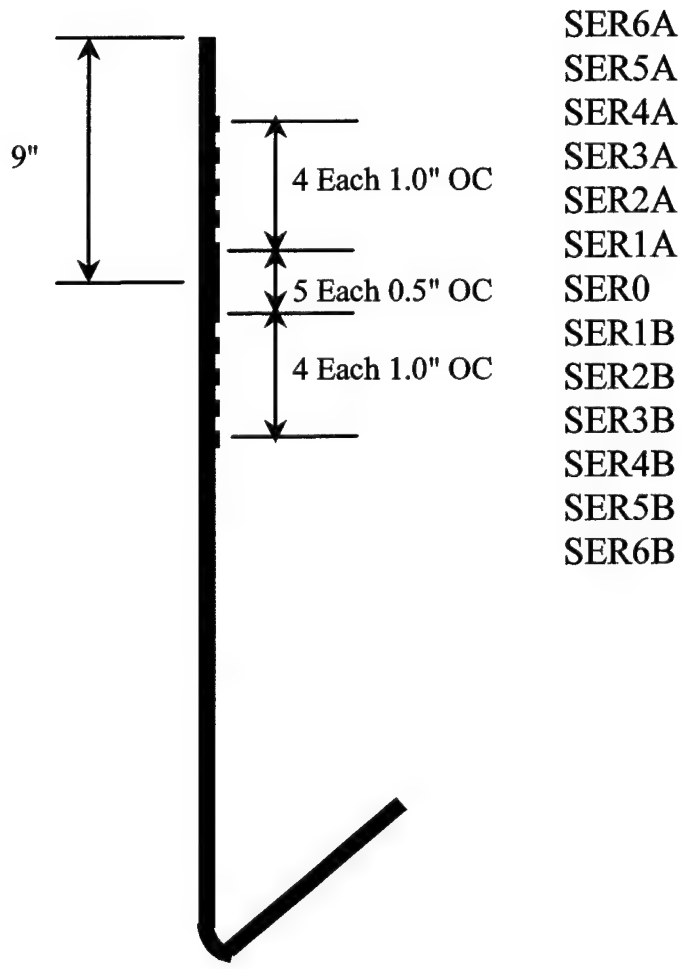

Figure A9. Strain gage locations and designations, east face of models 3SLCL, 3SLCH, 3SHCL, 3SHCH

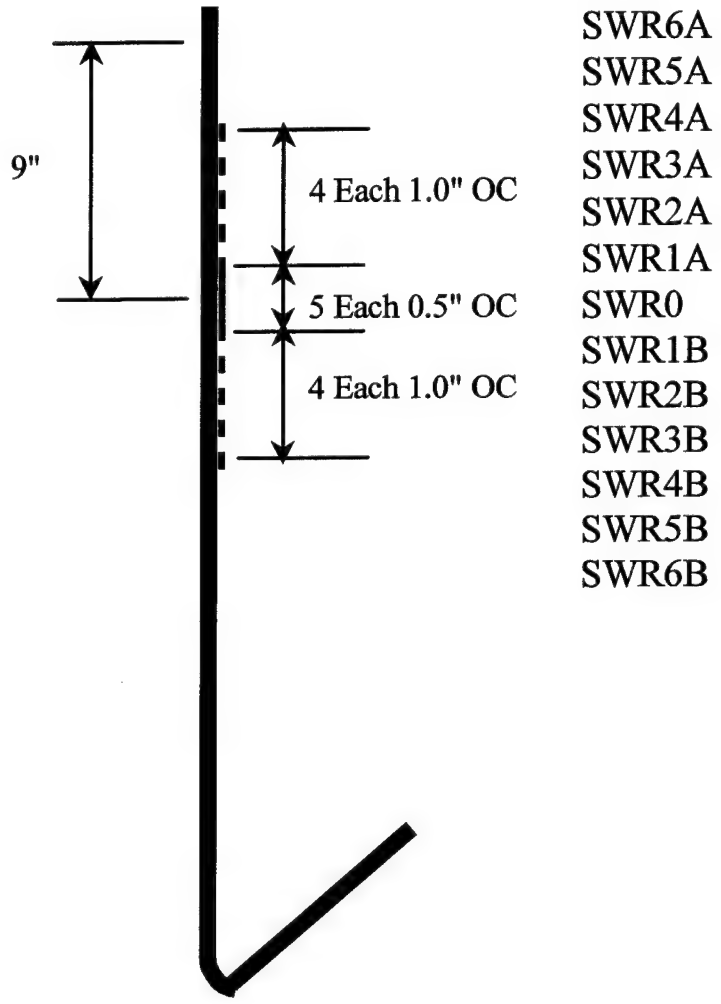

Figure A10. Strain gage locations and designations, west face of models 3SLCL, 3SLCH, 3SHCL, 3SHCH

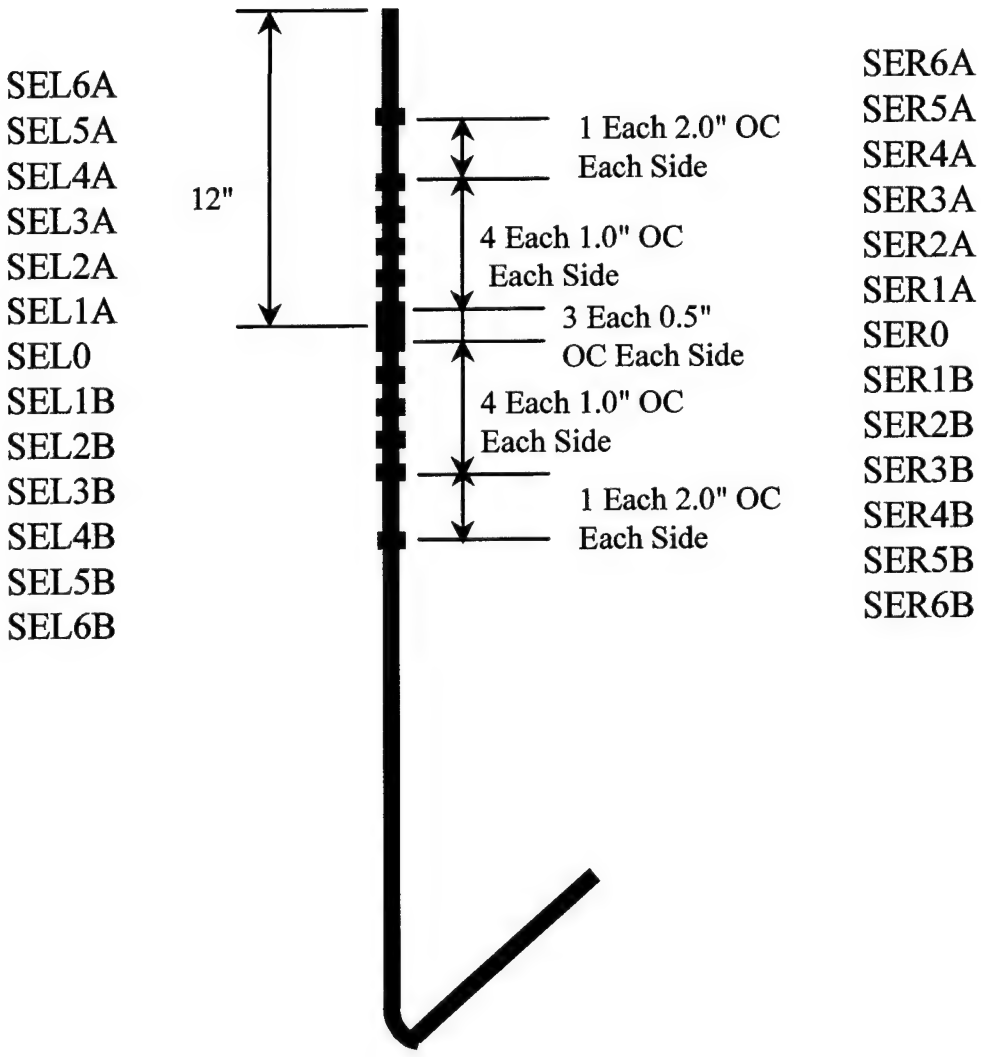

Figure A11. Strain gage locations and designations, east face of models 4SLCM, 4SHCM

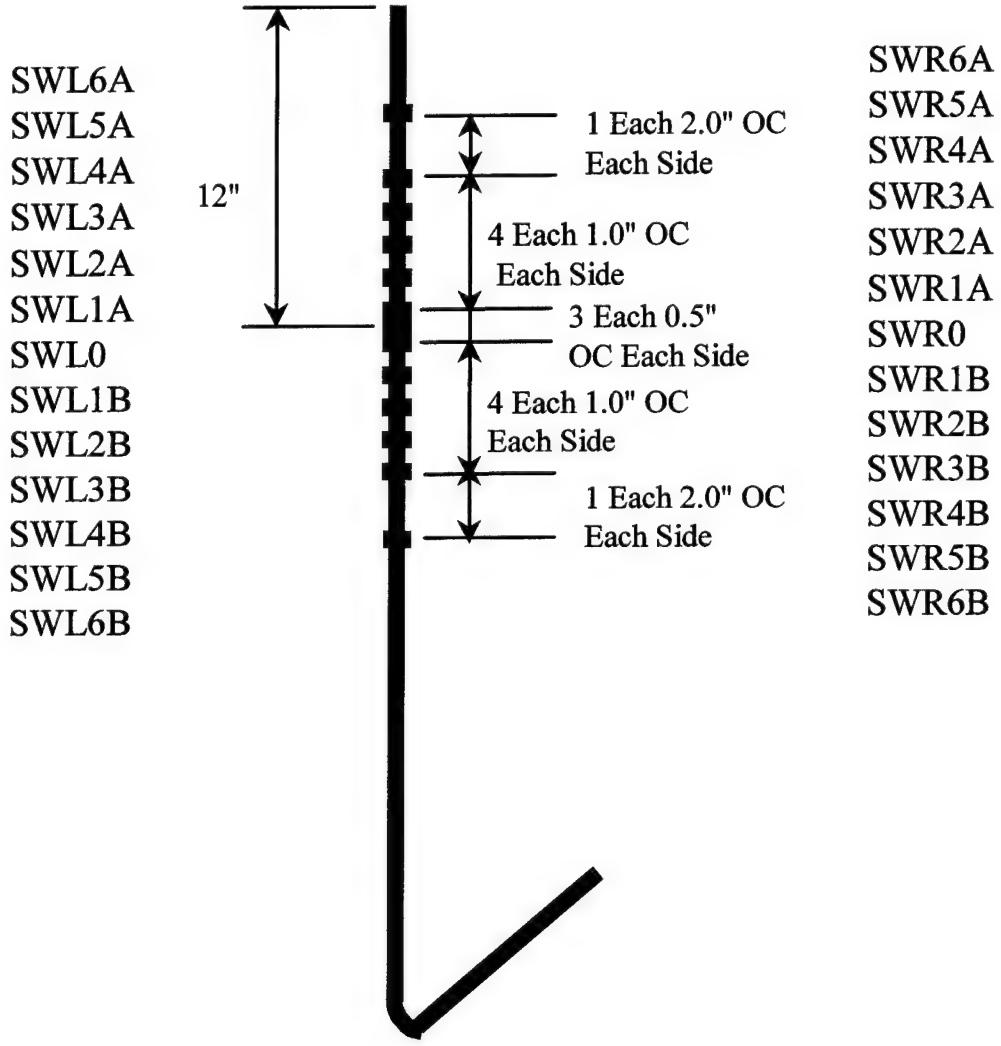

Figure A12. Strain gage locations and designations, west face of models 4SLCM, 4SHCM

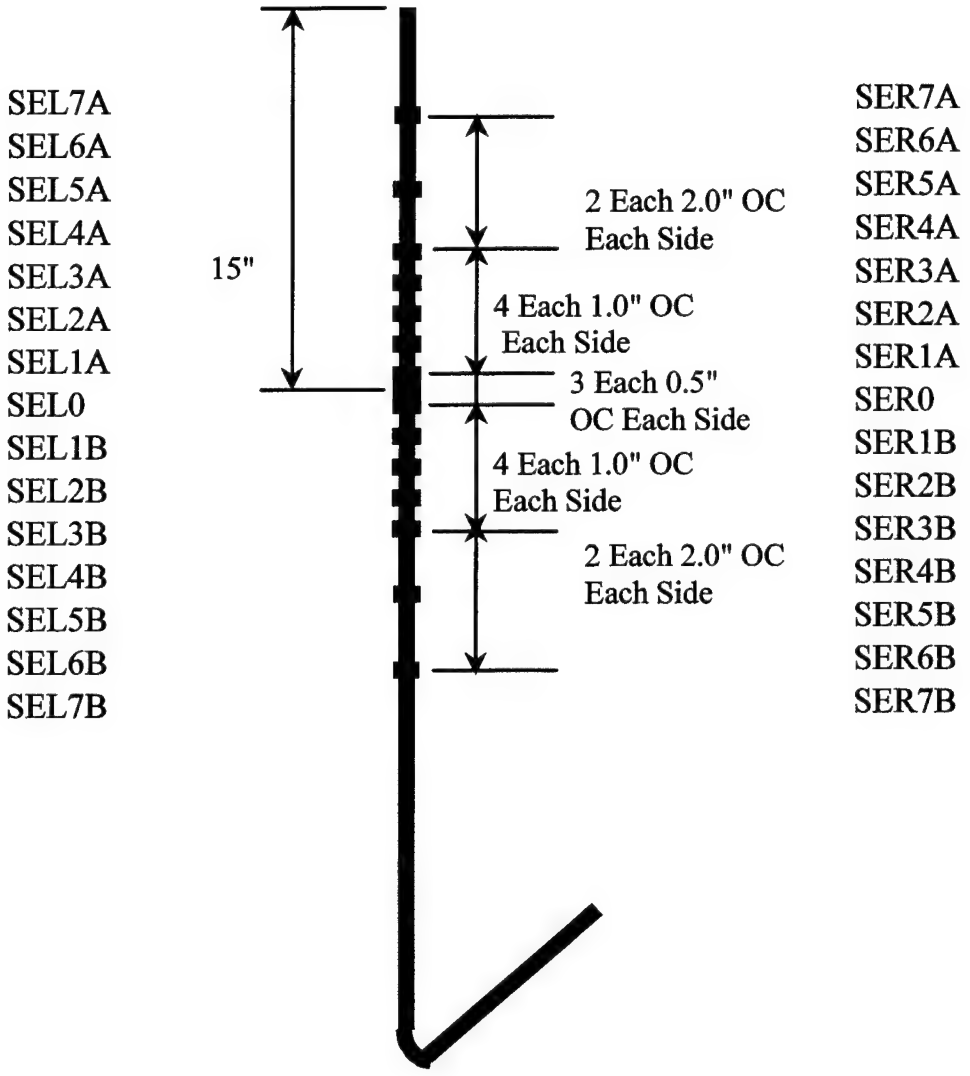

Figure A13. Strain gage locations and designations, east face of models 5SLCL, 5SLCH, 5SHCL, 5SHCH

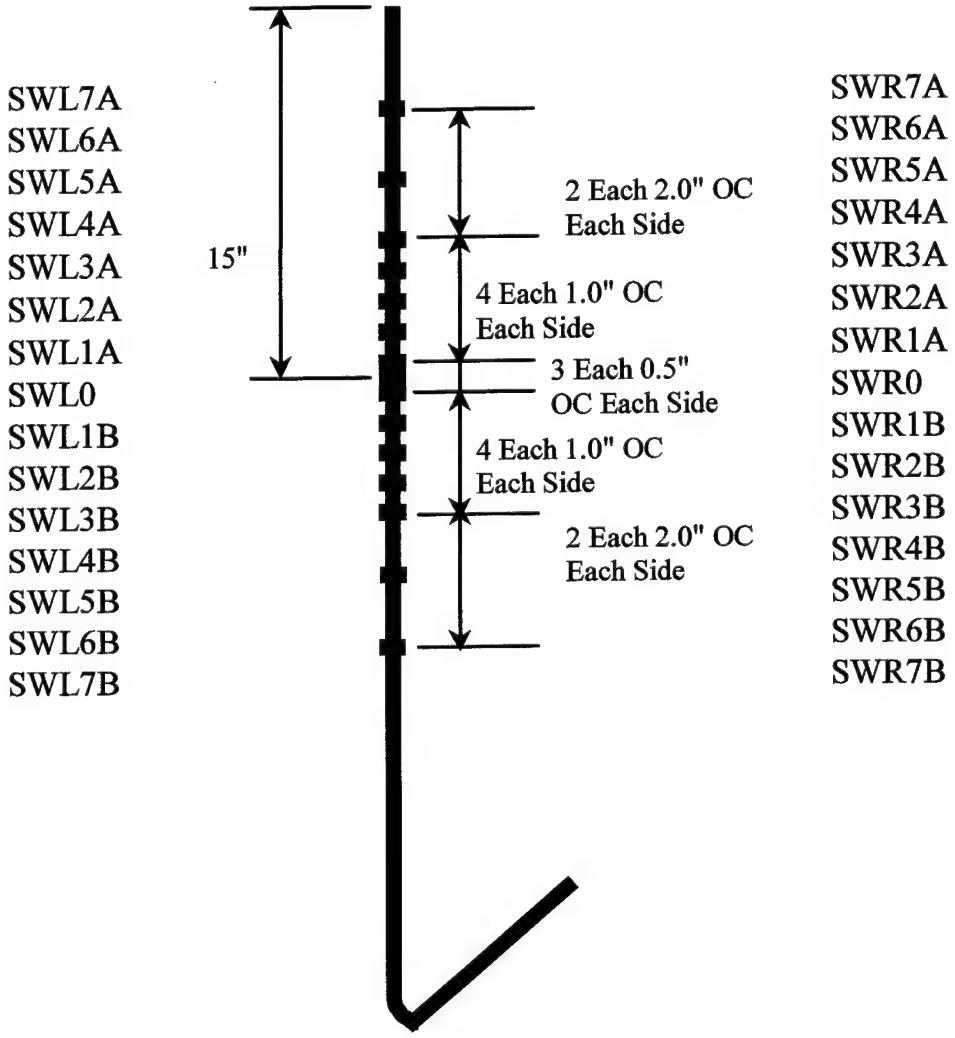

Figure A14. Strain gage locations and designations, west face of models 5SLCL, 5SLCH, 5SHCL, 5SHCH

Appendix B
Materials Properties

Table B1
Material Properties as Determined by Reinforcing Bar Tensile Tests

Experiment Name	Bar Diameter in.	Bar Area	Yield Strength (psi)	Yield Strain (in./in.)	Hardening Strain (in./in.)	Ultimate Strength (psi)	Rupture Strain (in./in.)
3 SLCL	3	0.11	58,309.66	0.00222857	0.02161	83,664.77	0.19375
3 SLCL	3	0.11	59,105.11	0.00223112	0.02067	86,349.43	0.2125
3 SLCL	3	0.11	58,551.14	0.00239104	0.02193	85,568.18	0.2
3 SHCL	3	0.11	77,755.68	0.00302442	0.014488	111,804	0.1375
3 SHCL	3	0.11	71,079.55	0.00304273	0.0107	105,497.20	0.15
3 SHCL	3	0.11	80,056.82	0.0028681	0.0151	113,394.90	0.11875
3 SLCH	3	0.11	58,309.66	0.00222857	0.02161	83,664.77	0.19375
3 SLCH	3	0.11	59,105.11	0.00223112	0.02067	86,349.43	0.2125
3 SLCH	3	0.11	58,551.14	0.00239104	0.02193	85,568.18	0.2
3 SHCH	3	0.11	77,755.68	0.00302442	0.014488	111,804	0.1375
3 SHCH	3	0.11	71,079.55	0.00304273	0.0107	105,497.20	0.15
3 SHCH	3	0.11	80,056.82	0.0028681	0.0151	113,394.90	0.11875
4 SLCM	4	0.2	50,453.12	0.00153769	0.01857	70,789.07	0.24375
4 SLCM	4	0.2	50,562.50	0.00206498	0.020528	71,351.55	0.24375
4 SLCM	4	0.2	50,531.25	0.00181127	0.0185537	71,117.20	0.2125
4 SHCM	4	0.2	57,570.31	0.00239409	0.018049	84,578.12	0.2125
4 SHCM	4	0.2	55,968.77	0.00219103	0.018258	82,335.94	0.175
4 SHCM	4	0.2	57,796.86	0.00232676	0.018407	85,148.41	0.2125
5 SLCL	5	0.31	55,912.30	0.00236614	0.016692	85,191.53	0.175
5 SLCL	5	0.31	54,959.68	0.00219919	0.0165002	84,183.47	0.1875
5 SLCL	5	0.31	55,660.29	0.00226015	0.0167563	84,974.80	0.2125
5 SHCL	5	0.31	66,091.58	0.00297583	0.00449521	108,254.30	0.13125
5 SHCL	5	0.31	64,947.97	0.00318848	0.0050236	105,468	0.13125
5 SHCL	5	0.31	66,278.06	0.00297778	0.00507613	108,561	0.1125
5 SLCH	5	0.31	55,912.30	0.00236614	0.016692	85,191.53	0.175
5 SLCH	5	0.31	54,959.68	0.00219919	0.0165002	84,183.47	0.1875
5 SLCH	5	0.31	55,660.29	0.00226015	0.0167563	84,974.80	0.2125

Table B2
Early Age Concrete Properties for Mixture Development

Mixture Development		Air Content %	Unit Weight lb/cu ft	Cylinder Name	Cylinder Number	Date Tested	Age In Days	Hardened Density lb/cu ft	Uncon. Comp. Strength psi
Mixture Name	Slump in.								
2,500 psi (1)	6.25	7.6	139.88	82 RD 2500	1	30-Mar-98	7	140.5	1,490
					2	30-Mar-98	7	140.6	1,530
					3	30-Mar-98	7	140.1	1,550
2,500 psi (2)	3.25	6.6	141.88	82 RD 2500	4	30-Mar-98	7	142.1	1,500
					5	30-Mar-98	7	142.6	1,470
					6	30-Mar-98	7	143.4	1,530
4,000 psi (1)	2.75	9.3	139.4	82 RD 4000	1	30-Mar-98	7	144.7	2,370
					2	30-Mar-98	7	144.8	2,440
					3	30-Mar-98	7	–	2,300
4,000 psi (2)	2.5	5.8	143.9	82 RD 4000	4	30-Mar-98	7	145	2,760
					5	30-Mar-98	7	144.3	2,650
					6	30-Mar-98	7	146.7	2,720
5,500 psi (1)	3	8.3	139.8	82 RD 5500	1	30-Mar-98	7	142	3,450
					2	30-Mar-98	7	140.6	971*
					3	30-Mar-98	7	141.7	3,550
5,500 psi (2)	3	6.2	143.1	82 RD 5500	4	30-Mar-98	7	146.3	3,640
					5	30-Mar-98	7	145.1	4,410
					6	30-Mar-98	7	144.7	4,380
					* Bad Data Point, disregard this test.				

Table B3
Material Properties of Low-Strength Concrete in Lower Section of Models, First Batch

Low-Strength Concrete		Test Specimen Number	Dove Tower Number	Date Tested	Age in Days	Type of Curing	Ultrasonic Pulse Velocity ft/sec	Hardened Density lb/cu ft	Uncon Comp. Strength psi
Batch Number	Test Specimen Name								
1	99 RD	1	1 & 2	7-May-98	28	Fog		145.4	2,660
Slump - 1 "	99 RD	2	1 & 2	7-May-98	28	Fog		145.3	2,560
UW - 144.7	99 RD	3	1 & 2	8-May-98	29	Fog		145.1	2,610
Lb/cu ft									
Air - 5 %	99 RD	4	1 & 2	4-Jun-98	56	Amb.		144.6	3,180
Temp - 72 °F	99 RD	5	1 & 2	4-Jun-98	56	Amb.		145.0	2,900
	99 RD	6	1 & 2	4-Jun-98	56	Amb.		145.1	3,080
	3 SLCL	1	1	18-Dec-98	253	Amb.		144.9	3,710
						Modulus of Elasticity, psi			5.05 × E6
	3 SLCL	2	1	18-Dec-98	253	Amb.		144.2	3,530
						Modulus of Elasticity, psi			4.74 × E6
	3 SLCL	3	1	18-Dec-98	253	Amb.		143.9	3,610
						Modulus of Elasticity, psi			4.75 × E6
	3 SHCL	1	2	11-Dec-98	246	Amb.	14,430	143.3	3,550
						Modulus of Elasticity, psi			4.65 × E6
	3 SHCL	2	2	11-Dec-98	246	Amb.	14,540	143.2	3,660
						Modulus of Elasticity, psi			4.85 × E6
	3 SHCL	3	2	11-Dec-98	246	Amb.	14,390	143.4	3,640
						Modulus of Elasticity, psi			4.90 × E6

Table B4
Material Properties of Low-Strength Concrete in Lower Section of Models, Second Batch

Low-Strength Concrete									
Batch Number	Test Specimen Name	Test Specimen Number	Dove Tower Number	Date Tested	Age in Days	Type of Curing	Ultrasonic Pulse Velocity ft/sec	Hardened Density lb/cu ft	Uncon Comp. Strength psi
2	99 RD	7	3 & 4	8-May-98	29	Fog		145.2	2,350
Slump - 0.5 "	99 RD	8	3 & 4	8-May-98	29	Fog		145.7	2,650
UW - 144.3	99 RD	9	3 & 4	8-May-98	29	Fog		145.1	2,540
Lb/cu ft									
Air - 5 %	99 RD	10	3 & 4	4-Jun-98	56	Amb.		144.5	2,840
Temp – 70 °F	99 RD	11	3 & 4	4-Jun-98	56	Amb.		144.1	2,840
	99 RD	12	3 & 4	4-Jun-98	56	Amb.		145.0	2,940
	5 SLCL	1	3	4-Mar-99	329	Amb.	13,760	144.1	3,600
						Modulus of Elasticity, psi			4.80 × E6
	5 SLCL	2	3	2-Feb-98	301	Amb.	-	-	3,630
	5 SLCL	3	3	2-Feb-98	301	Amb.	-	-	3,510
	5 SHCL	1	4	2-Feb-99	301	Amb.	-	-	3,600
	5 SHCL	2	4	4-Mar-99	329	Amb.	14,270	144.1	3,450
						Modulus of Elasticity, psi			4.40 × E6
	5 SHCL	3	4	4-Mar-99	329	Amb.	14,110	142.7	3,540
						Modulus of Elasticity, psi			4.70 × E6

Table B5
Material Properties of Medium-Strength Concrete in Lower Section of Models

Medium-Strength Concrete		Test Specimen Number	Dove Tower Number	Date Tested	Age in Days	Type of Curing	Ultrasonic Pulse Velocity ft/sec	Hardened Density lb/cu ft	Uncon Comp. Strength psi
Batch Number	Test Specimen Name								
3	99 RD	13	5 & 6	8-May-98	29	Fog		141.4	3,060
Slump - 1 "	99 RD	14	5 & 6	8-May-98	29	Fog		140.2	3,030
UW - 142.3	99 RD	15	5 & 6	8-May-98	29	Fog		140.4	3,120
Lb/cu ft									
Air - 6.8 %	99 RD	16	5 & 6	4-Jun-98	56	Amb.		140.4	3,150
Temp – 70 °F	99 RD	17	5 & 6	4-Jun-98	56	Amb.		140.2	3,190
	99 RD	18	5 & 6	4-Jun-98	56	Amb.		140.6	3,260
	4 SLCM	1	5	4-Feb-99	301	Amb.	-	144.1	3,600
	4 SLCM	2	5	4-Feb-99	301	Amb.	-	143.7	3,370
	4 SLCM	3	5	4-Feb-99	301	Amb.	-	143.1	3,780
	4 SHCM	1	6	2-Dec-98	237	Amb.	14,550	139.3	3,640
	4 SHCM	2	6	2-Dec-98	237	Amb.	14,500	139.4	3,720
	4 SHCM	3	6	2-Dec-98	237	Amb.	14,240	138.5	3,570

Table B6
Material Properties of High-Strength Concrete in Lower Section of Models, Fourth Batch

High-Strength Concrete								
Batch Number Test	Specimen Name	Test Specimen Number	Dove Tower Number	Date Tested	Age in Days	Type of Curing	Hardened Density lb/cu ft	Uncon Comp. Strength psi
4	99 RD	19	7 & 8	8-May-98	29	Fog	142.3	4,780
Slump - 2.5 "	99 RD	20	7 & 8	8-May-98	29	Fog	143.0	3,790
UW - 143.9	99 RD	21	7 & 8	8-May-98	29	Fog	142.3	5,210
Lb/cu ft								
Air - 5.8 %	99 RD	22	7 & 8	4-Jun-98	56	Ambient	141.5	5,030
Temp – 70 °F	99 RD	23	7 & 8	4-Jun-98	56	Ambient	142.2	5,330
	99 RD	24	7 & 8	4-Jun-98	56	Ambient	141.4	4,950
	3 SLCH	1	7	23-Oct-98	197	Ambient	140.7	5,940
						Modulus of Elasticity, psi		5.50 × E6
	3 SLCH	2	7	23-Oct-98	197	Ambient	141.3	5,760
						Modulus of Elasticity, psi		5.35 × E6
	3 SLCH	3	7	23-Oct-98	197	Ambient	140.5	5,700
						Modulus of Elasticity, psi		5.60 × E6
	3 SHCH	1	8	12-Jan-99	278	Ambient	-	5,630
	3 SHCH	2	8	12-Jan-99	278	Ambient	-	6,410
	3 SHCH	3	8	12-Jan-99	278	Ambient	-	5,850

Table B7
Material Properties of High-Strength Concrete in Lower Section of Models, Fifth Batch

High-Strength Concrete								
Batch Number	Test Specimen Name	Test Specimen Number	Dove Tower Number	Date Tested	Age in Days	Type of Curing	Hardened Density lb/cu ft	Uncon Comp. Strength psi
5	99 RD	25	9 & 10	8-May-98	29	Fog	143.2	5,170
Slump - 2.5 "	99 RD	26	9 & 10	8-May-98	29	Fog	142.7	5,140
UW - 143.3	99 RD	27	9 & 10	8-May-98	29	Fog	143.0	5,380
Lb/cu ft								
Air - 5.5 %	99 RD	28	9 & 10	4-Jun-98	56	Amb.	142.6	5,270
Temp – 70 °F	99 RD	29	9 & 10	4-Jun-98	56	Amb.	142.7	4,980
	99 RD	30	9 & 10	4-Jun-98	56	Amb.	142.8	5,110
	5 SLCH	1	9	1-Oct-98	175	Amb.	141.7	5,220
						Modulus of Elasticity, psi		5.40 × E6
	5 SLCH	2	9	1-Oct-98	175	Amb.	142.2	5,280
						Modulus of Elasticity, psi		5.55 × E6
	5 SLCH	3	9	1-Oct-98	175	Amb.	142.2	5,400
						Modulus of Elasticity, psi		5.70 × E6
	5 SHCH	1	10	22-Feb-99	319	Amb.	-	5,450
	5 SHCH	2	10	22-Feb-99	319	Amb.	-	6,660
	5 SHCH	3	10	22-Feb-99	319	Amb.	-	6,820

Table B8
Material Properties of Low-Strength Concrete in Upper Section of Models, First Batch

Low-Strength Concrete		Test Specimen Number	Dove Tower Number	Date Tested	Age in Days	Type of Curing	Hardened Density lb/cu ft	Uncon Comp. Strength psi
Batch Number	Test Specimen Name							
1	132 RD	1	1	9-Jun-98	28	Fog		2,310
Slump - 2.0 "	132 RD	2	1	9-Jun-98	28	Fog		2,430
UW - 142.3	132 RD	3	1	9-Jun-98	28	Fog		2,250
Lb/cu ft								
Air - 6.0 %	132 RD	4	1	7-Jul-98	56	Ambient	146.3	2,790
Temp – 70 °F	132 RD	5	1	7-Jul-98	56	Ambient	146.5	2,690
	132 RD	6	1	7-Jul-98	56	Ambient	146.2	3,020
	3 SLCL (Top)	1	1	18-Dec-98	220	Ambient	140.6	2,970
						Modulus of Elasticity, psi		4.30 × E6
	3 SLCL (Top)	2	1	18-Dec-98	220	Ambient	143.0	3,130
						Modulus of Elasticity, psi		4.45 × E6
	3 SLCL (Top)	3	1	18-Dec-98	220	Ambient	141.6	2,830
						Modulus of Elasticity, psi		4.15 × E6

Table B9
Material Properties of Low-Strength Concrete in Upper Section of Models, Second Batch

Low-Strength Concrete									
Batch Number	Test Specimen Name	Test Specimen Number	Dove Tower Number	Date Tested	Age in Days	Type of Curing	Ultrasonic Pulse Velocity ft/sec	Hardened Density lb/cu ft	Uncon Comp. Strength psi
2	132 RD	7	2	9-Jun-98	28	Fog			2,510
Slump - 1.5 "	132 RD	8	2	9-Jun-98	28	Fog			2,460
UW - 143.5	132 RD	9	2	9-Jun-98	28	Fog			2,360
Lb/cu ft									
Air - 5.5 %	132 RD	10	2	7-Jul-98	56	Ambient		146.8	3,200
Temp – 68 °F	132 RD	11	2	7-Jul-98	56	Ambient		146.4	2,730
	132 RD	12	2	7-Jul-98	56	Ambient		147.0	3,010
	3 SHCL (Top)	1	2	11-Dec-98	213	Ambient	14,170	142.7	3,320
						Modulus of Elasticity, psi			4.25 × E6
	3 SHCL (Top)	2	2	11-Dec-98	213	Ambient	14,210	143.1	3,490
						Modulus of Elasticity, psi			4.65 × E6
	3 SHCL (Top)	3	2	11-Dec-98	213	Ambient	14,140	143.1	3,190
						Modulus of Elasticity, psi			3.95 × E6

Table B10
Material Properties of Low-Strength Concrete in Upper Section of Models, Third and Fourth Batches

Low-Strength Concrete									
Batch Number	Test Specimen Name	Test Specimen Number	Dove Tower Number	Date Tested	Age in Days	Type of Curing	Ultrasonic Pulse Velocity ft/ sec	Hardened Density lb/cu ft	Uncon Comp. Strength psi
3	132 RD	13	3	9-Jun-98	28	Fog			2,160
Slump - 2.0 "	132 RD	14	3	9-Jun-98	28	Fog			2,310
UW - 142.7	132 RD	15	3	9-Jun-98	28	Fog			2,200
Lb/cu ft									
Air - 6.1 %	132 RD	16	3	7-Jul-98	56	Ambient		147.1	2,620
Temp – 70 °F	132 RD	17	3	7-Jul-98	56	Ambient		147.2	2,780
	132 RD	18	3	7-Jul-98	56	Ambient		145.1	2,670
	5 SLCL (Top)	1	3	2-Feb-99	268	Ambient	-	-	3,480
	5 SLCL (Top)	2	3	2-Feb-99	268	Ambient	-	-	3,550
	5 SLCL (Top)	3	3	2-Feb-99	268	Ambient	-	-	3,690
4	132 RD	19	4	9-Jun-98	28	Fog			
Slump - 2.25 "	132 RD	20	4	9-Jun-98	28	Fog			2,440
UW – 142.3	132 RD	21	4	9-Jun-98	28	Fog			2,510
Lb/cu ft									
Air - 5.9 %	132 RD	22	4	7-Jul-98	56	Ambient		148.0	2,990
Temp - 73 °F	132 RD	23	4	7-Jul-98	56	Ambient		147.5	2,840
	132 RD	24	4	7-Jul-98	56	Ambient		148.0	3,100
	5 SHCL (Top)	1	4	4-Mar-99	296	Ambient	13,570	142.8	3,200
						Modulus of Elasticity, psi			4.60 × E6
	5 SHCL (Top)	2	4	4-Mar-99	296	Ambient	13,660	144.7	3,110
						Modulus of Elasticity, psi			4.40 × E6
	5 SHCL (Top)	3	4	4-Mar-99	296	Ambient	14,040	142.3	3,260
						Modulus of Elasticity, psi			4.60 × E6

Table B11
Material Properties of Medium-Strength Concrete in Upper Section of Models

Medium -Strength Concrete		Test Specimen Number	Dove Tower Number	Date Tested	Age in Days	Type of Curing	Ultrasonic Pulse Velocity ft/sec	Hardened Density Lb/cu ft	Uncon Comp. Strength psi
Batch Number	Test Specimen Name								
5	132 RD	25	5	9-Jun-98	28	Fog			2,910
Slump - 2.5"	132 RD	26	5	9-Jun-98	28	Fog			2,530
UW - 142.7	132 RD	27	5	9-Jun-98	28	Fog			3,070
Lb/cu ft									
Air - 7.0 %	132 RD	28	5	7-Jul-98	56	Ambient		147.2	3,570
Temp – 73 °F	132 RD	29	5	7-Jul-98	56	Ambient		146.9	3,290
	132 RD	30	5	7-Jul-98	56	Ambient		147.9	3,470
	4 SLCM (Top)	1	5	4-Feb-99	268	Ambient		141.7	3,910
	4 SLCM (Top)	2	5	4-Feb-99	268	Ambient		141.9	3,880
	4 SLCM (Top)	3	5	4-Feb-99	268	Ambient		141.5	3,810
6	132 RD	31	6	9-Jun-98	28	Fog			3,260
Slump - 1.25 "	132 RD	32	6	9-Jun-98	28	Fog			3,390
UW – 144.3	132 RD	33	6	9-Jun-98	28	Fog			3,470
Lb/cu ft									
Air - 6.0 %	132 RD	34	6	7-Jul-98	56	Ambient		147.8	3,750
Temp – 73 °F	132 RD	35	6	7-Jul-98	56	Ambient		145.6	3,910
	132 RD	36	6	7-Jul-98	56	Ambient		148.0	3,760
	4 SHCM (Top)	1	6	2-Dec-98	204	Ambient	14,290	141.6	4,290
	4 SHCM (Top)	2	6	2-Dec-98	204	Ambient	14,750	142.3	4,190
	4 SHCM (Top)	3	6	2-Dec-98	204	Ambient	14,520	143.1	4,390
						Modulus of Elasticity, psi			4.67 × E6

Table B12
Material Properties of High-Strength Concrete in Upper Section of Models, First and Second Batches

High-Strength Concrete								
Batch Number	Test Specimen Name	Test Specimen Number	Dove Tower Number	Date Tested	Age in Days	Type of Curing	Hardened Density lb/cu ft	Uncon Comp. Strength psi
1	133 RD	1	7	10-Jun-98	28	Fog	139.6	3,910
Slump-4.25 "	133 RD	2	7	10-Jun-98	28	Fog	140.2	4,580
UW-142.7	133 RD	3	7	10-Jun-98	28	Fog	138.9	4,550
Lb/cu ft								
Air - 6.8 %	133 RD	4	7	8-Jul-98	56	Ambient		4,830
Temp.-75 °F	133 RD	5	7	8-Jul-98	56	Ambient		5,080
	133 RD	6	7	8-Jul-98	56	Ambient		4,900
	3 SLCH (Top)	1	7	23-Oct-98	163	Ambient	141.9	4,360
						Modulus of Elasticity, psi		5.50 × E6
	3 SLCH (Top)	2	7	23-Oct-98	163	Ambient	142.2	5,690
						Modulus of Elasticity, psi		5.20 × E6
	3 SLCH (Top)	3	7	23-Oct-98	163	Ambient	142.8	4,850
						Modulus of Elasticity, psi		5.20 × E6
2	133 RD	7	8	10-Jun-98	28	Fog	142.7	5,000
Slump-2.5 "	133 RD	8	8	10-Jun-98	28	Fog	142.7	4,900
UW-144.4	133 RD	9	8	10-Jun-98	28	Fog	143.3	4,980
Lb/cu ft								
Air - 6.1 %	133 RD	10	8	8-Jul-98	56	Ambient		5,410
Temp.-73 °F	133 RD	11	8	8-Jul-98	56	Ambient		5,020
	133 RD	12	8	8-Jul-98	56	Ambient		5,060
	3 SHCH (Top)	1	8	12-Jan-99	244	Ambient	-	5,800
	3 SHCH (Top)	2	8	12-Jan-99	244	Ambient	-	5,950
	3 SHCH (Top)	3	8	12-Jan-99	244	Ambient	-	6,220

Table B13
Material Properties of High-Strength Concrete in Upper Section of Models, Third and Fourth Batches

High-Strength Batch Number	High-Strength Test Specimen Name	Test Specimen Number	Dove Tower Number	Date Tested	Age in Days	Type of Curing	Ultrasonic Pulse Velocity ft/sec	Hardened Density lb/cu ft	Uncon Comp. Strength psi
3	133 RD	13	9	10-Jun-98	28	Fog		142.7	5,170
Slump-2.25 "	133 RD	14	9	10-Jun-98	28	Fog		142.0	4,170
UW-143.1	133 RD	15	9	10-Jun-98	28	Fog		142.0	5,010
Lb/cu ft									
Air - 6.3%	133 RD	16	9	8-Jul-98	56	Ambient			5,630
Temp.-72 °F	133 RD	17	9	8-Jul-98	56	Ambient			5,340
	133 RD	18	9	8-Jul-98	56	Ambient			5,350
	5 SLCH (Top)	1	9	1-Oct-98	141	Ambient		142.2	5,030
						Modulus of elasticity, psi			5.30 × E6
	5 SLCH (Top)	2	9	1-Oct-98	141	Ambient		142.2	5,360
						Modulus of Elasticity, psi			5.20 × E6
	5 SLCH (Top)	3	9	1-Oct-98	141	Ambient		141.2	5,620
						Modulus of Elasticity, psi			5.25 × E6
4	133 RD	19	10	10-Jun-98	28	Fog		143.3	5,010
Slump-2.75 "	133 RD	20	10	10-Jun-98	28	Fog		141.4	4,900
UW-143.9	133 RD	21	10	10-Jun-98	28	Fog		141.4	4,800
Lb/cu ft									
Air - 6.3 %	133 RD	22	10	8-Jul-98	56	Ambient			5,320
Temp.-74 °F	133 RD	23	10	8-Jul-98	56	Ambient			5,210
	133 RD	24	10	8-Jul-98	56	Ambient			5,540
	5 SHCH (Top)	1	10	5-Mar-99	296	Ambient	14,650	140.7	6,010
						Modulus of Elasticity, psi			5.10 × E6
	5 SHCH (Top)	2	10	5-Mar-99	296	Ambient	14,430	141.2	6,300
						Modulus of Elasticity, psi			5.10 × E6
	5 SHCH (Top)	3	10	5-Mar-99	296	Ambient	14,800	141.1	6,280
						Modulus of Elasticity, psi			5.40 × E6

Appendix C
Strain Data

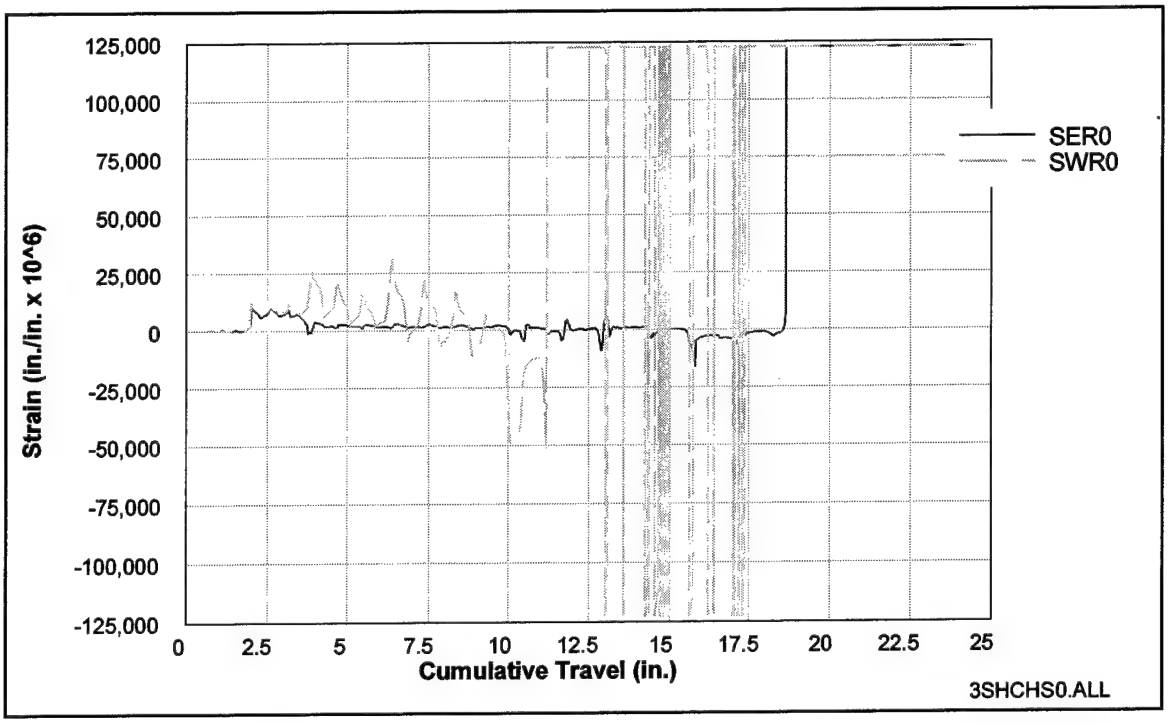

Figure C1. Strains measured at cold joint, 3SHCH

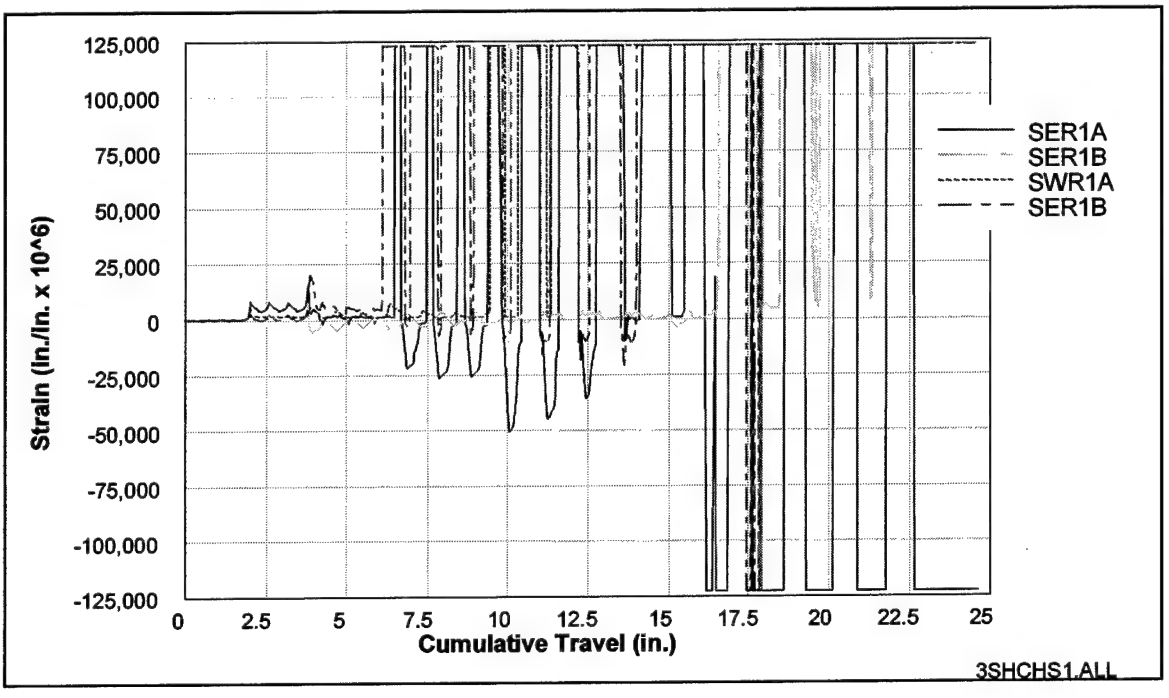

Figure C2. Strains measured 0.5 in. above and below cold joint, 3SHCH

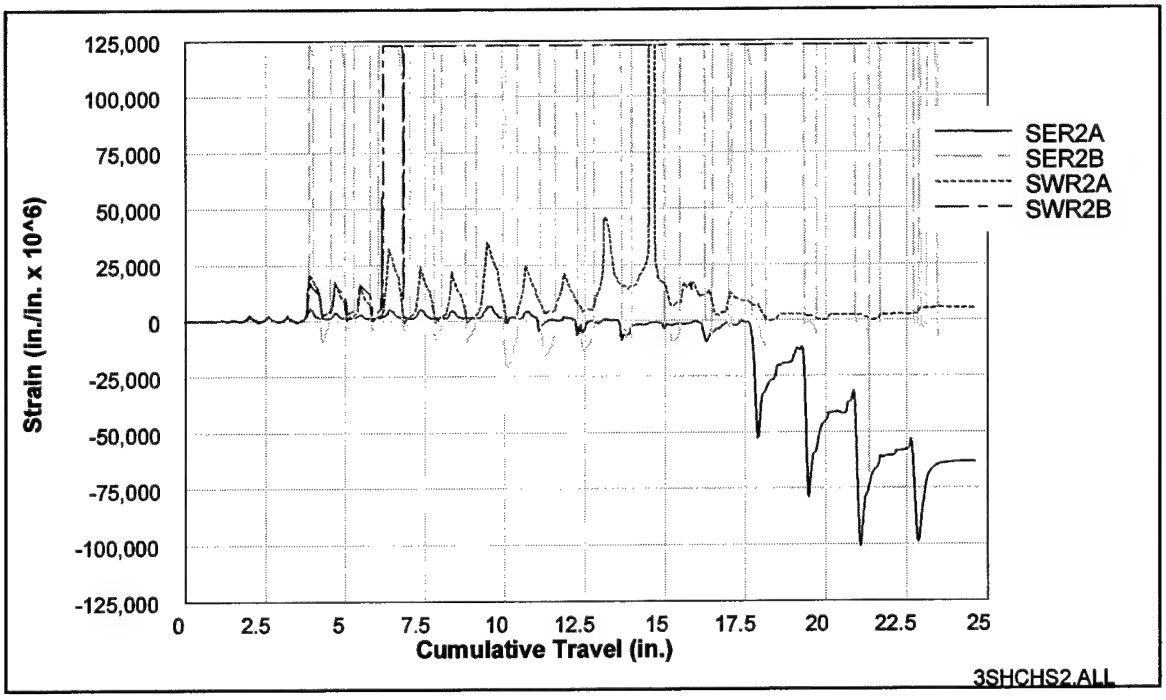

Figure C3. Strains measured 1.0 in. above and below cold joint, 3SHCH

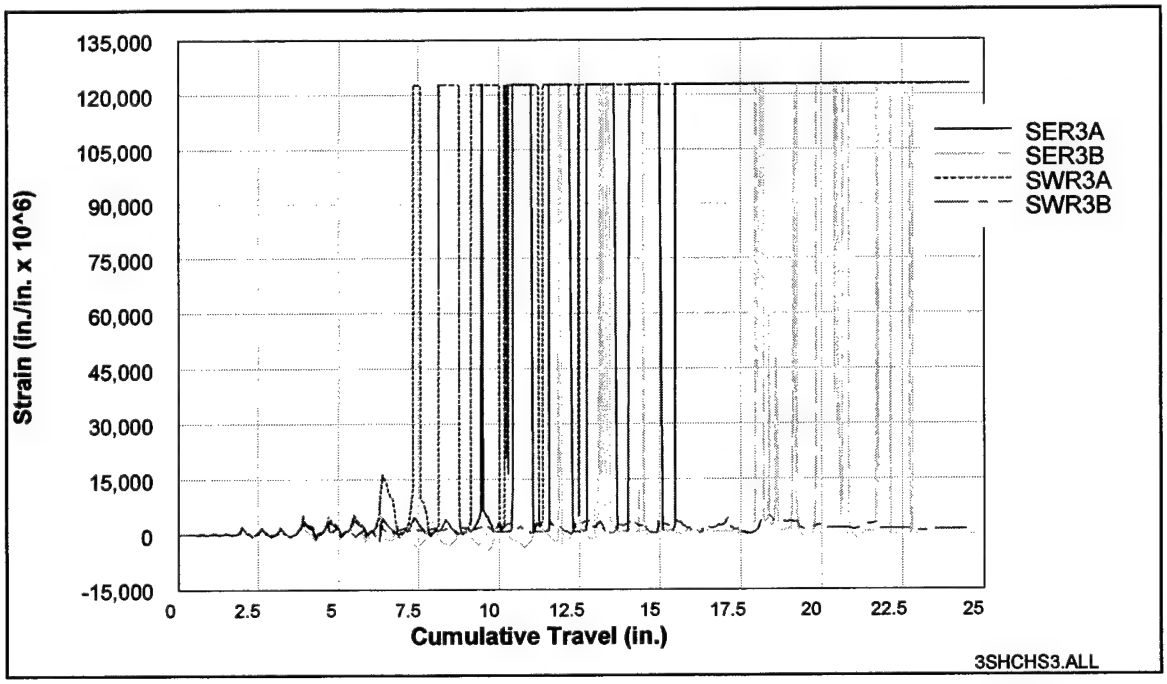

Figure C4. Strains measured 2.0 in. above and below cold joint, 3SHCH

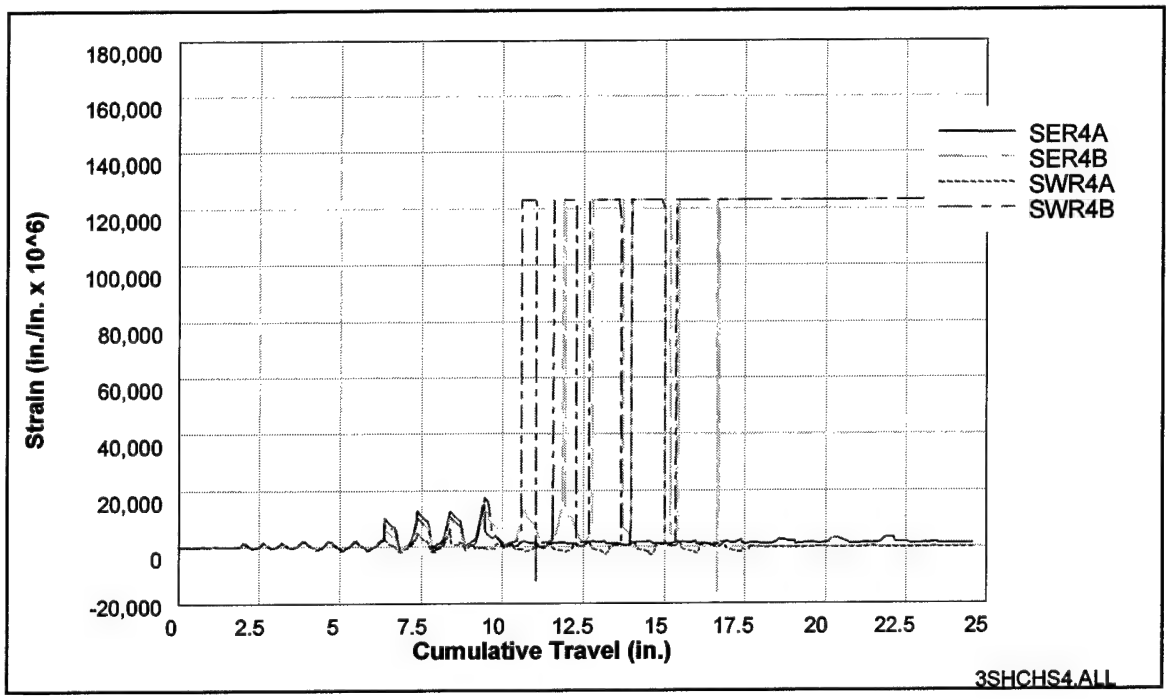

Figure C5. Strains measured 3.0 in. above and below cold joint, 3SHCH

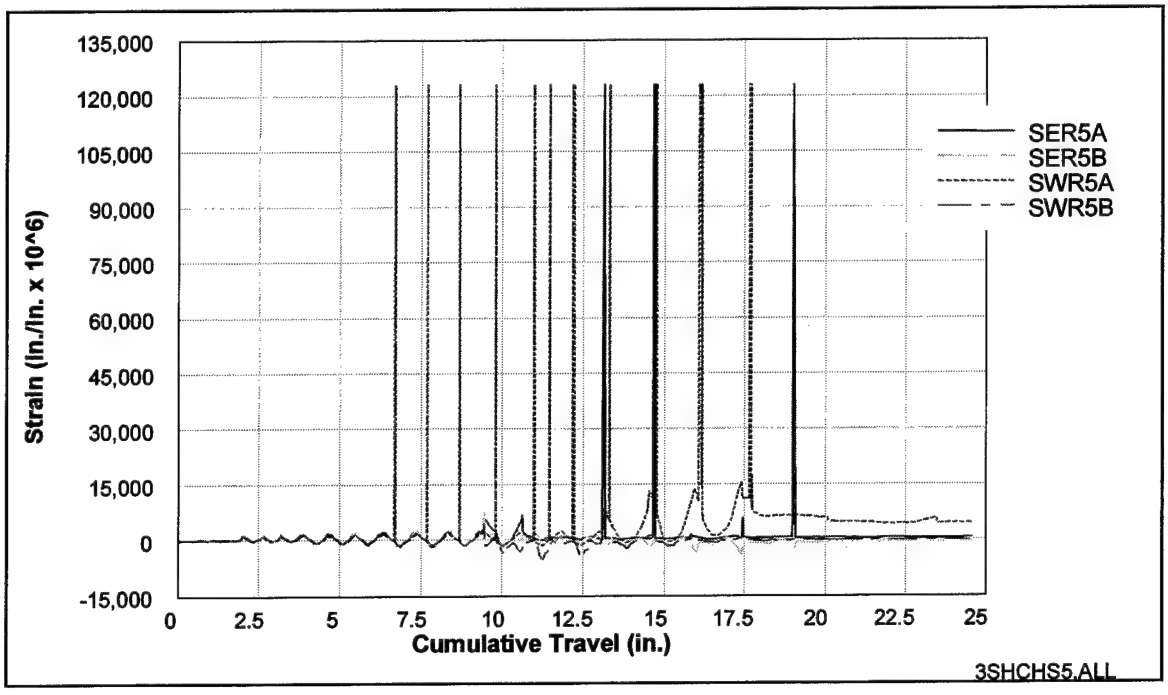

Figure C6. Strains measured 4.0 in. above and below cold joint, 3SHCH

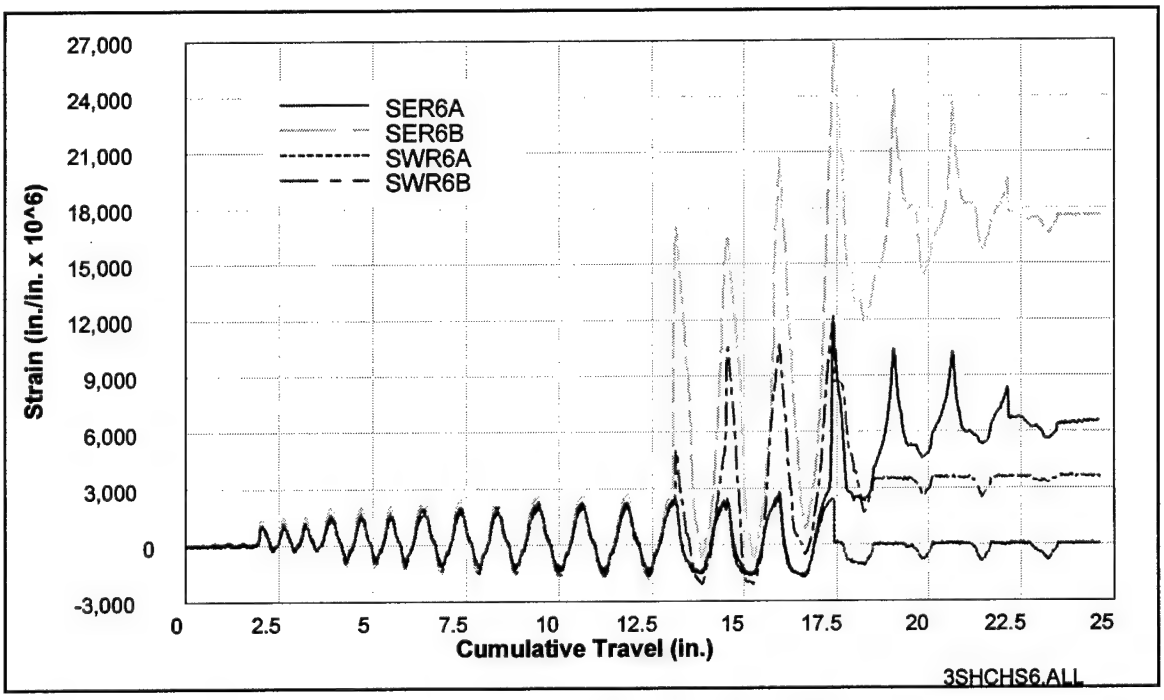

Figure C7. Strains measured 5.0 in. above and below cold joint, 3SHCH

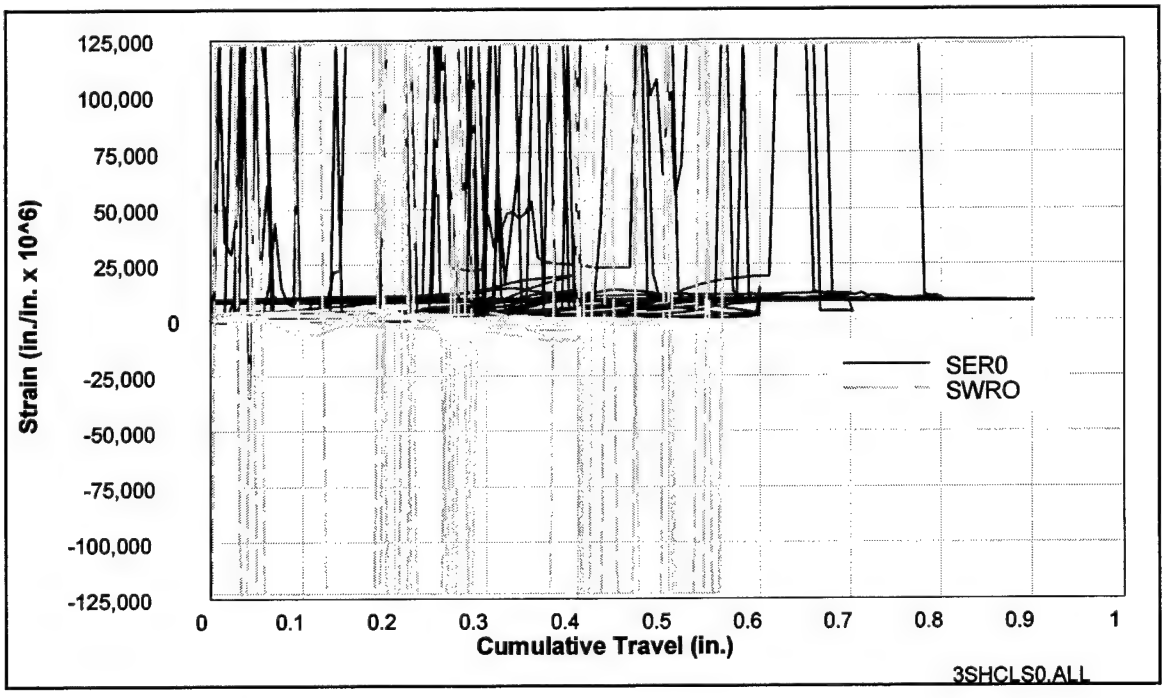

Figure C8. Strains measured at cold joint, 3SHCL

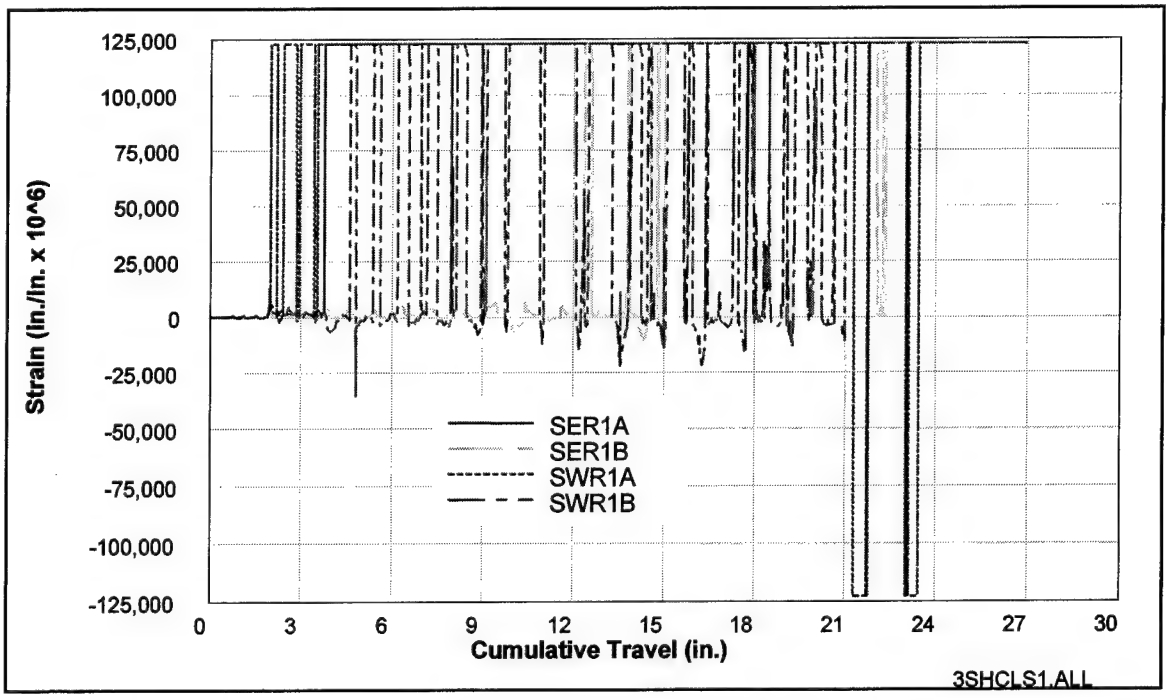

Figure C9. Strains measured 0.5 in. above and below cold joint, 3SHCL

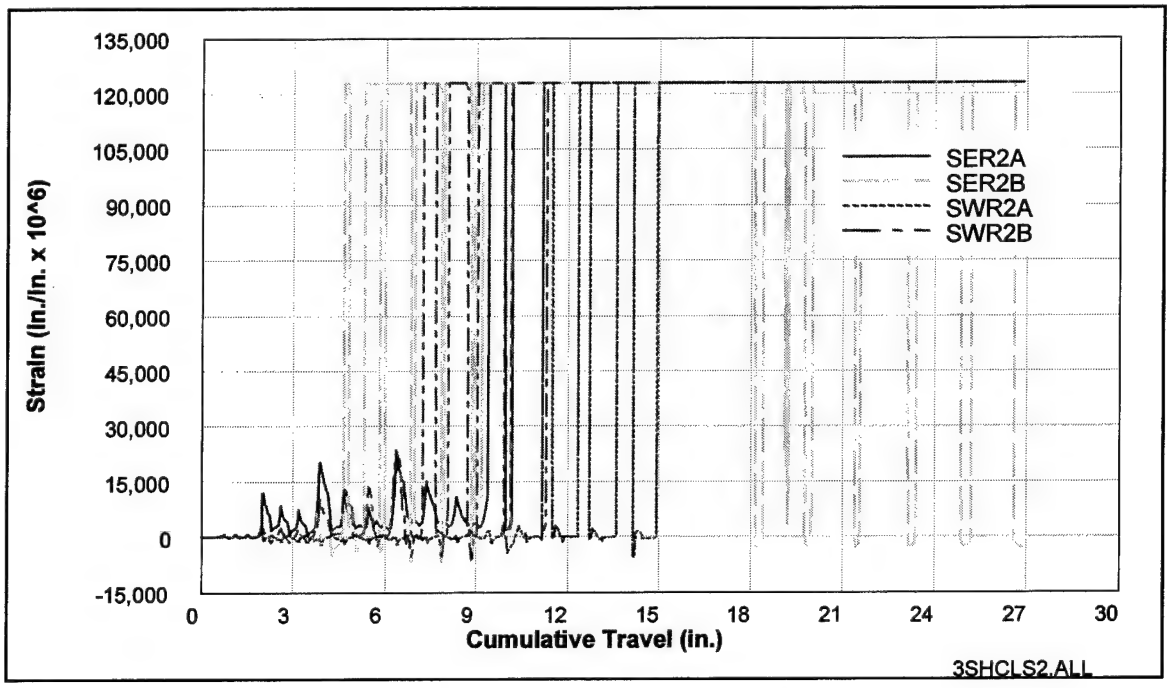

Figure C10. Strains measured 1.0 in. above and below cold joint, 3SHCL

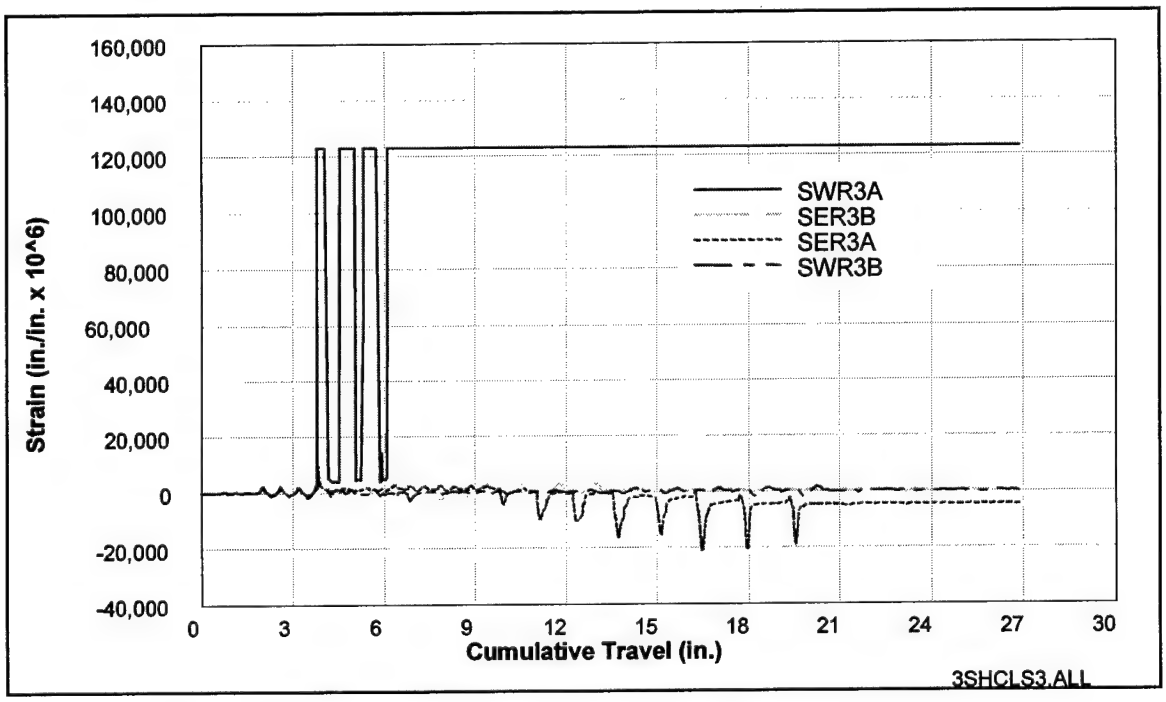

Figure C11. Strains measured 2.0 in. above and below cold joint, 3SHCL

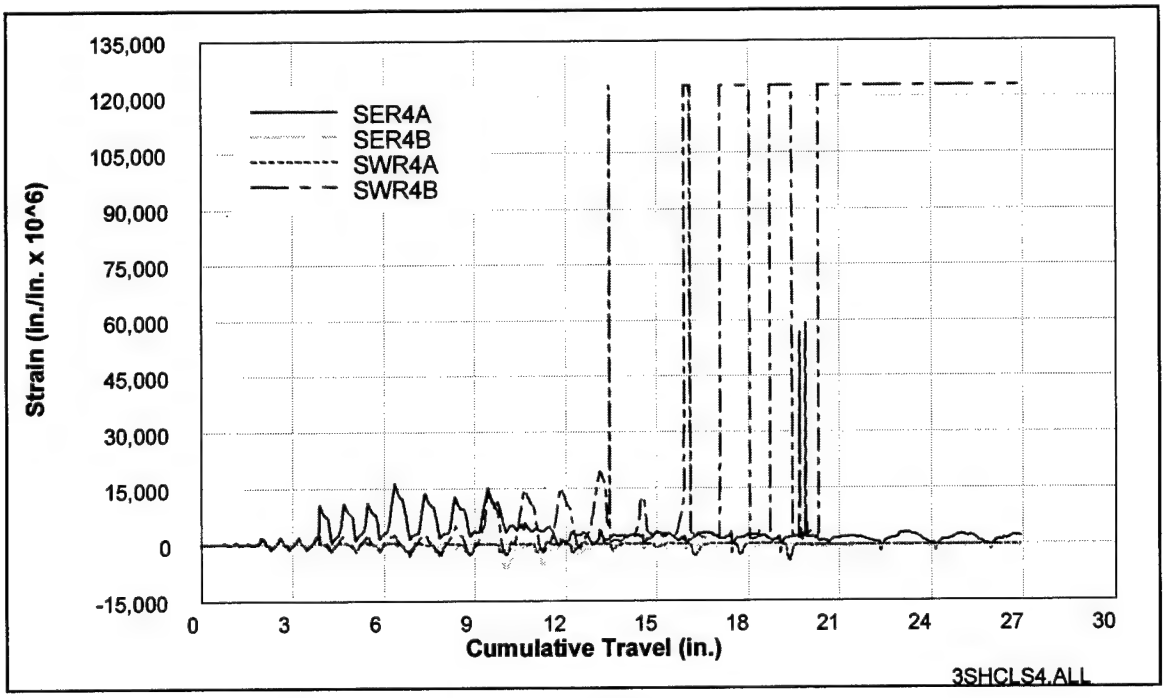

Figure C12. Strains measured 3.0 in. above and below cold joint, 3SHCL

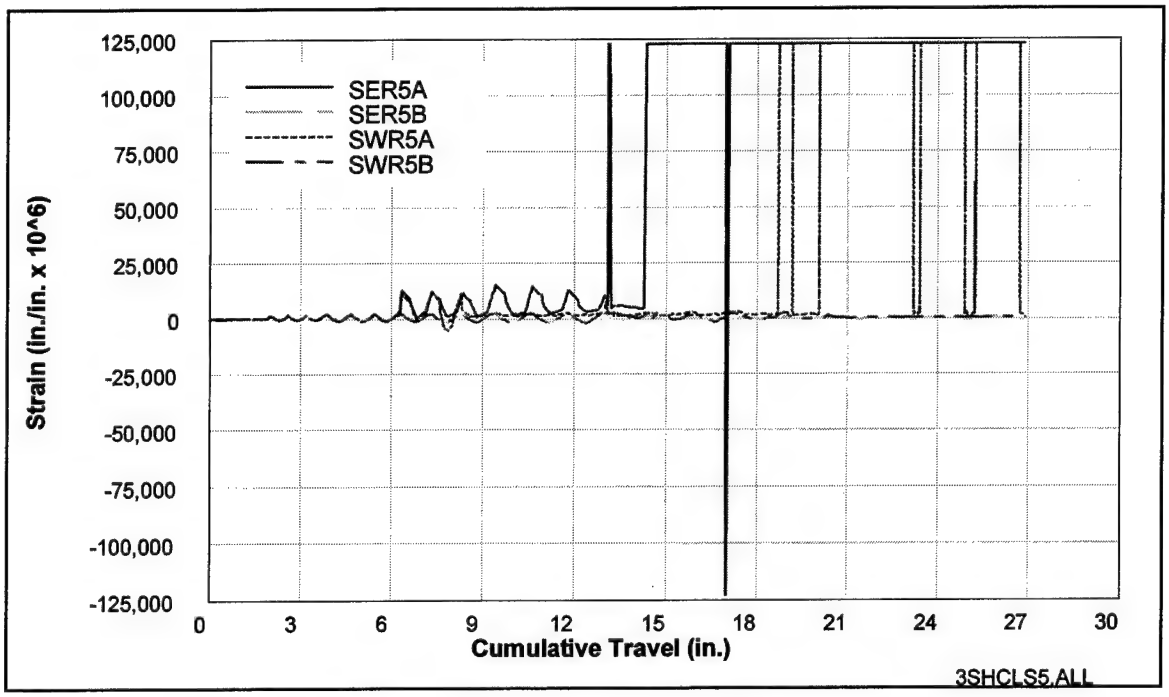

Figure C13. Strains measured 4.0 in. above and below cold joint, 3SHCL

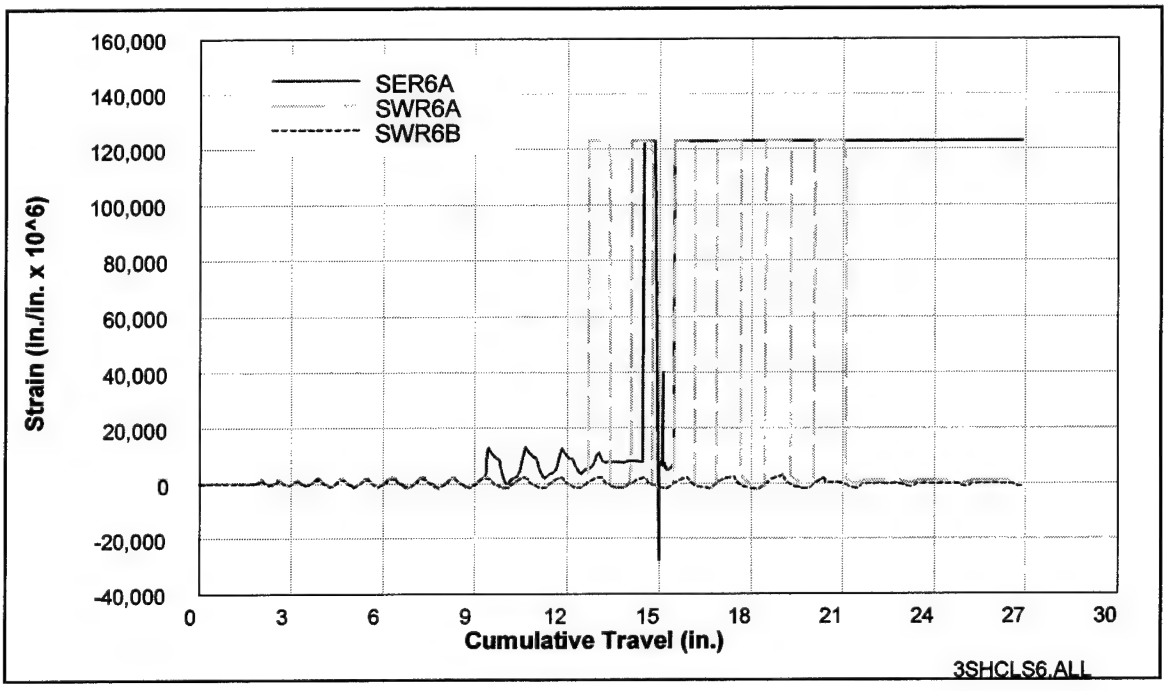

Figure C14. Strains measured 5.0 in. above and below cold joint, 3SHCL

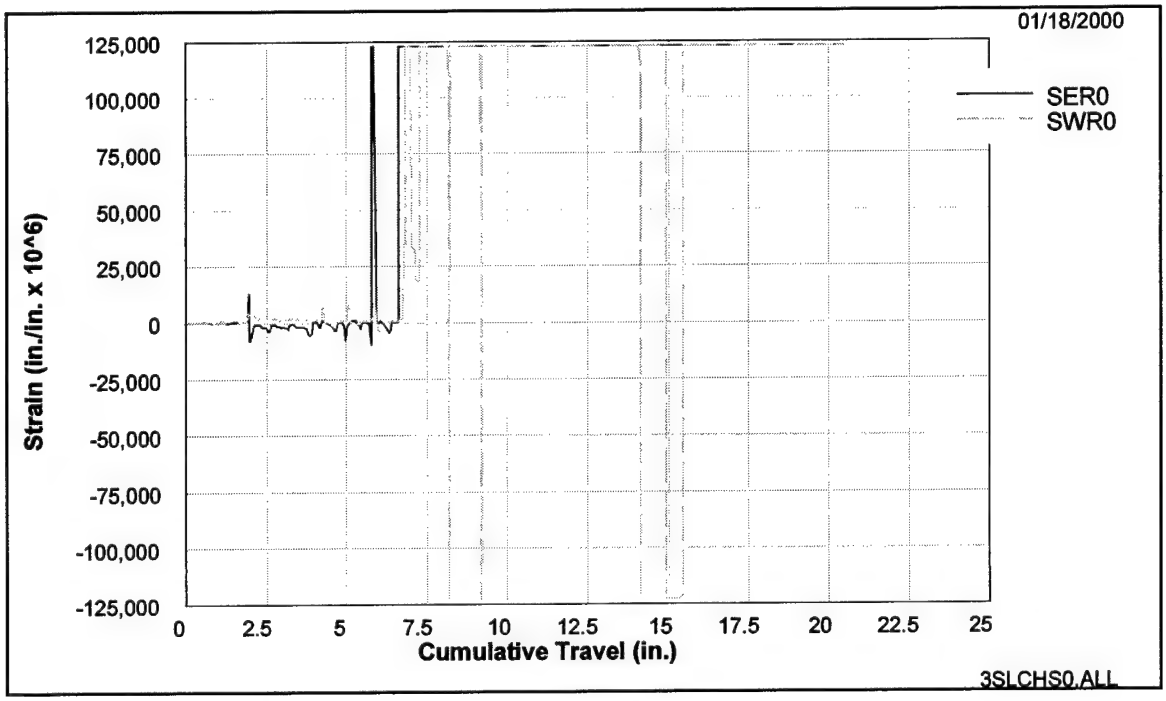

Figure C15. Strains measured at cold joint, 3SLCH

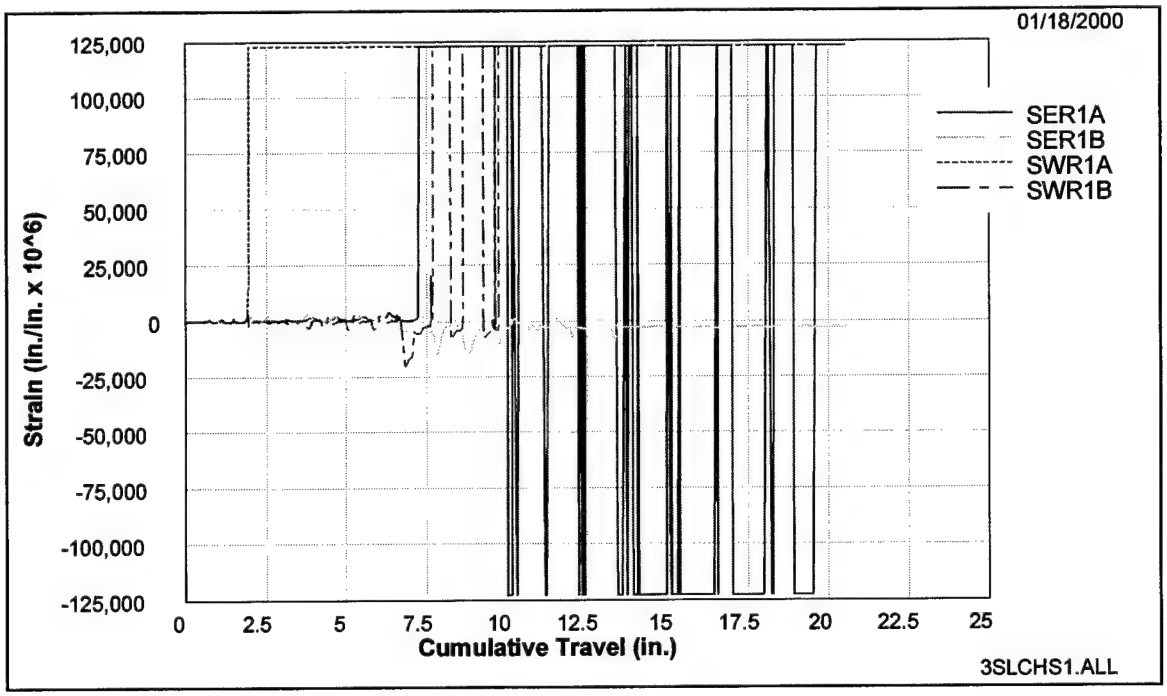

Figure C16. Strains measured 0.5 in. above and below cold joint, 3SLCH

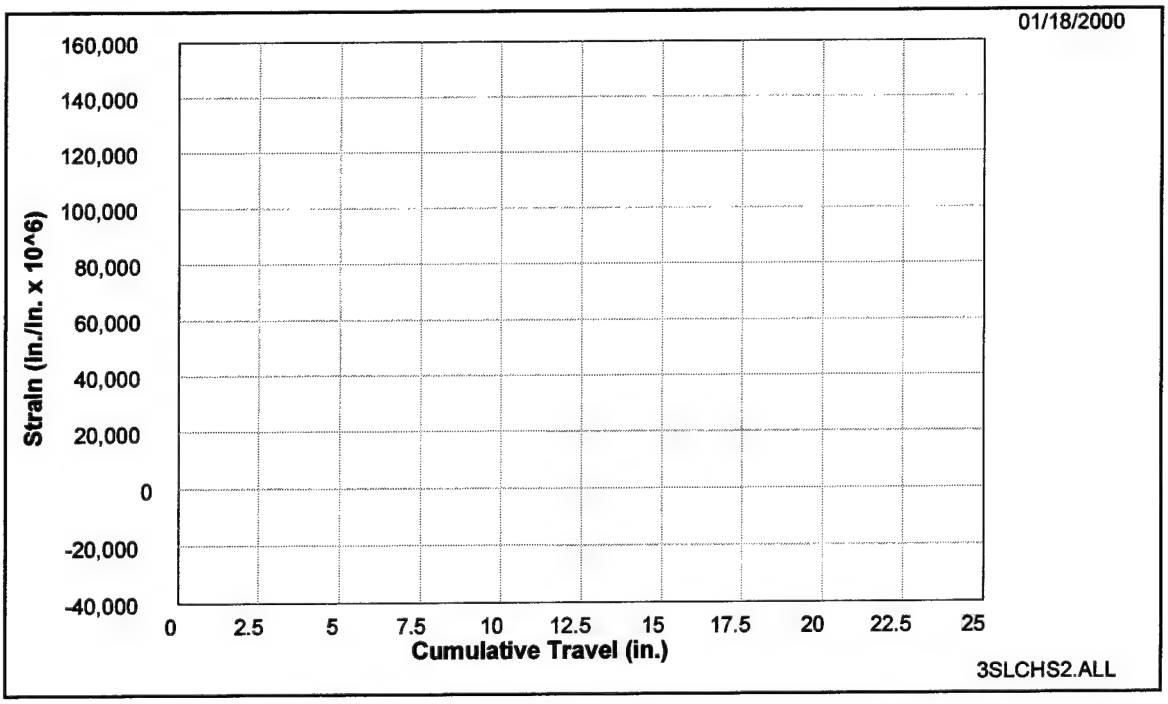

Figure C17. Strains measured 1.0 in. above and below cold joint, 3SLCH

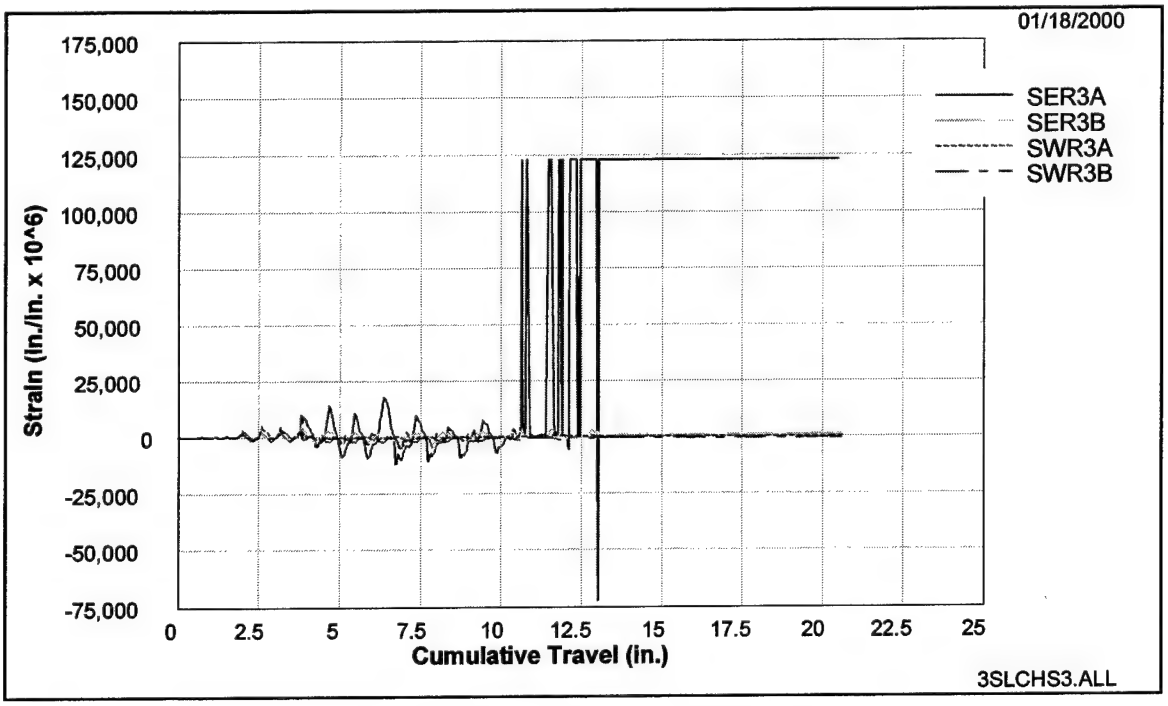

Figure C18. Strains measured 2.0 in. above and below cold joint, 3SLCH

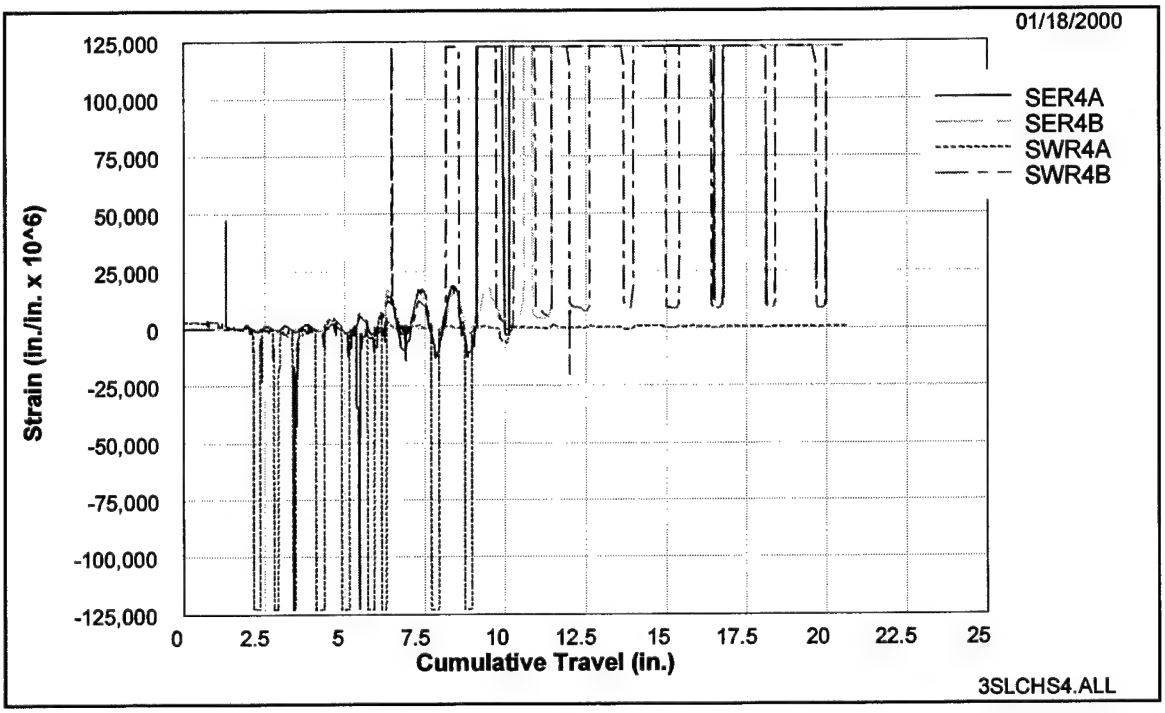

Figure C19. Strains measured 3.0 in. above and below cold joint, 3SLCH

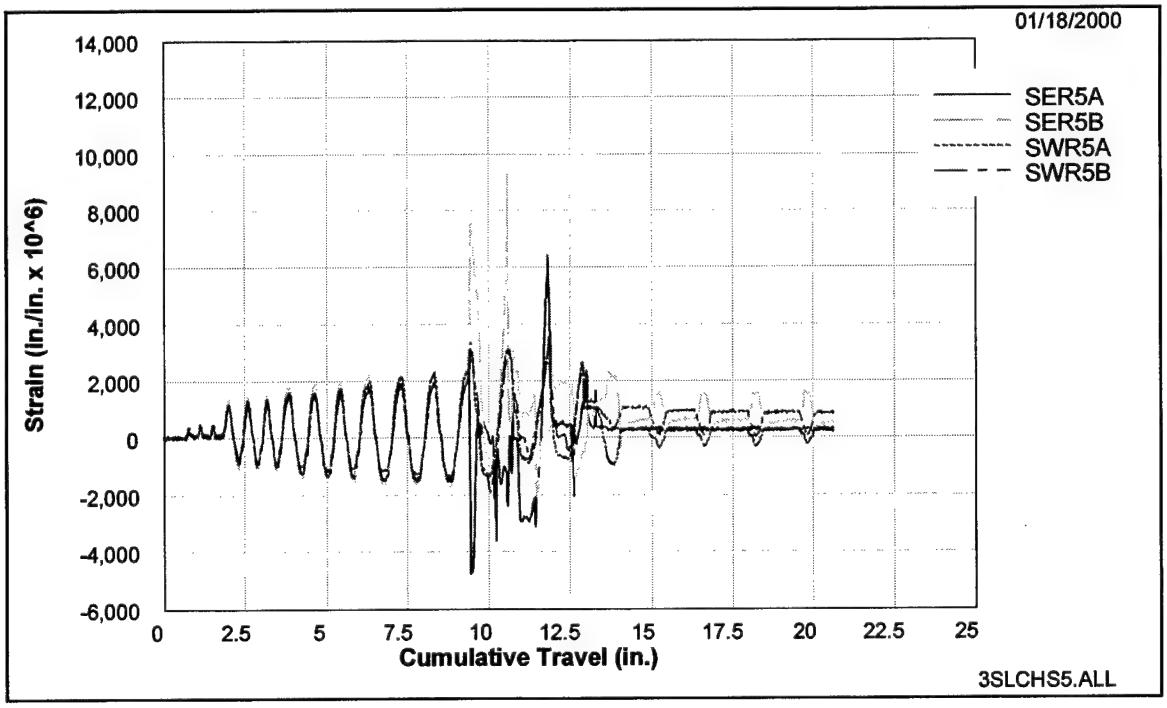

Figure C20. Strains measured 4.0 in. above and below cold joint, 3SLCH

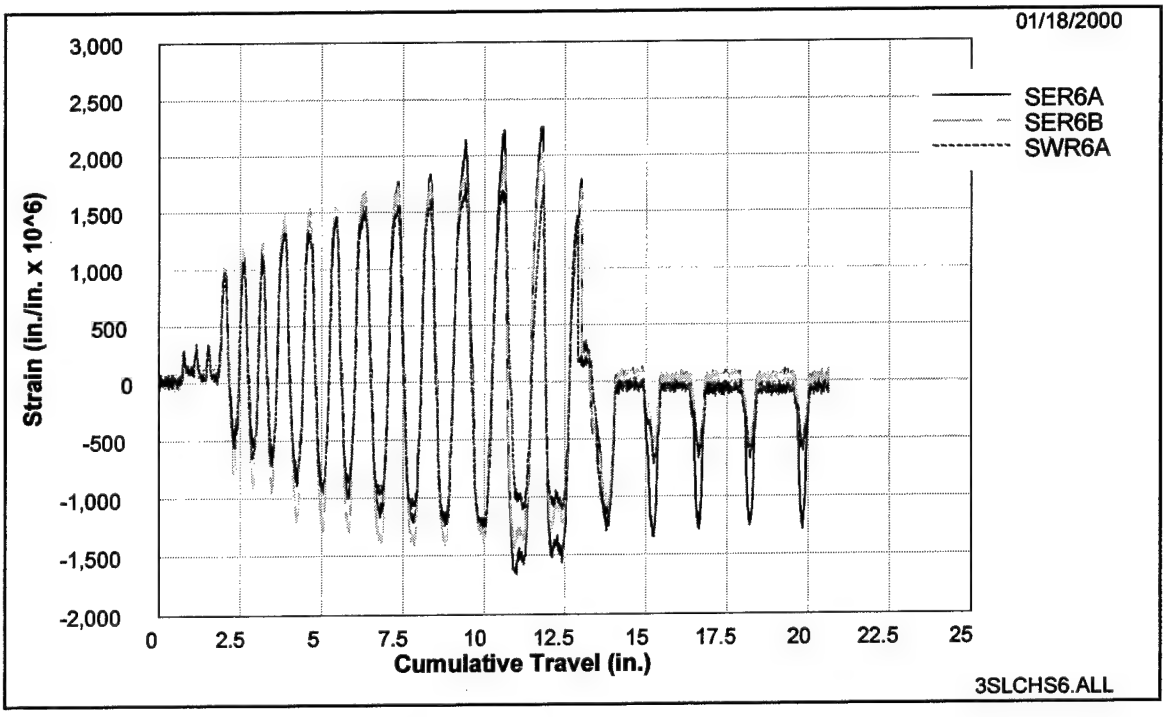

Figure C21. Strains measured 5 in. above and below cold joint, 3SLCH

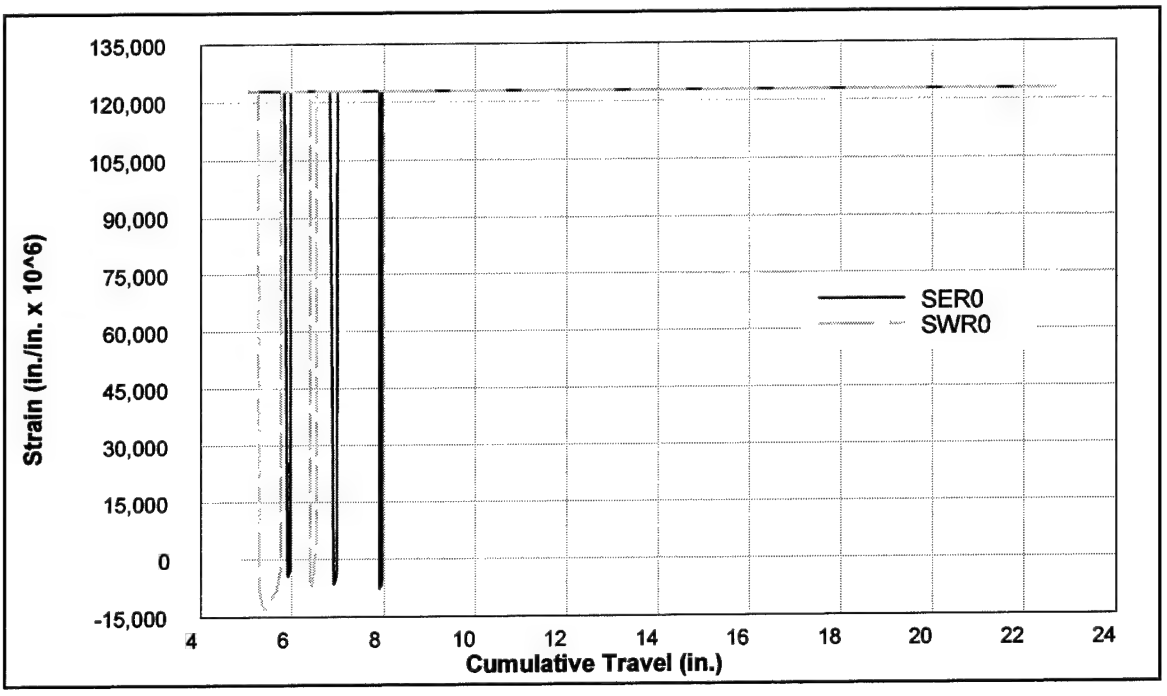

Figure C22. Strains measured at cold joint, 3SLCL

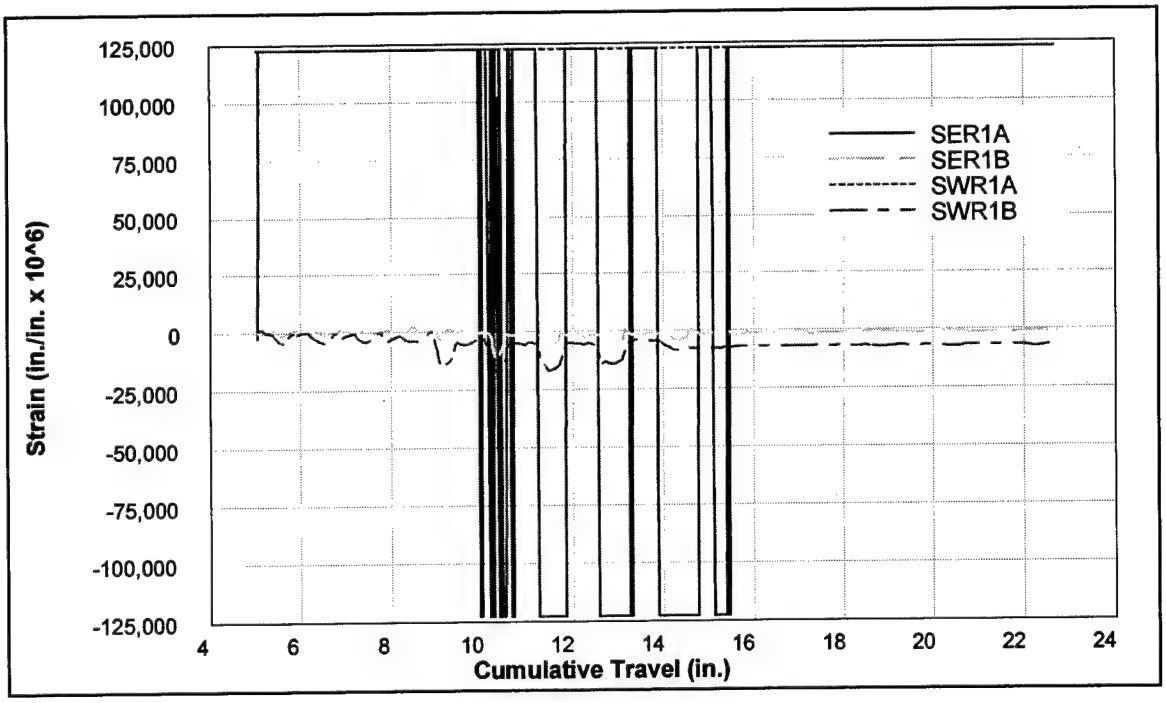

Figure C23. Strains measured 0.5 in. above and below cold joint, 3SLCL

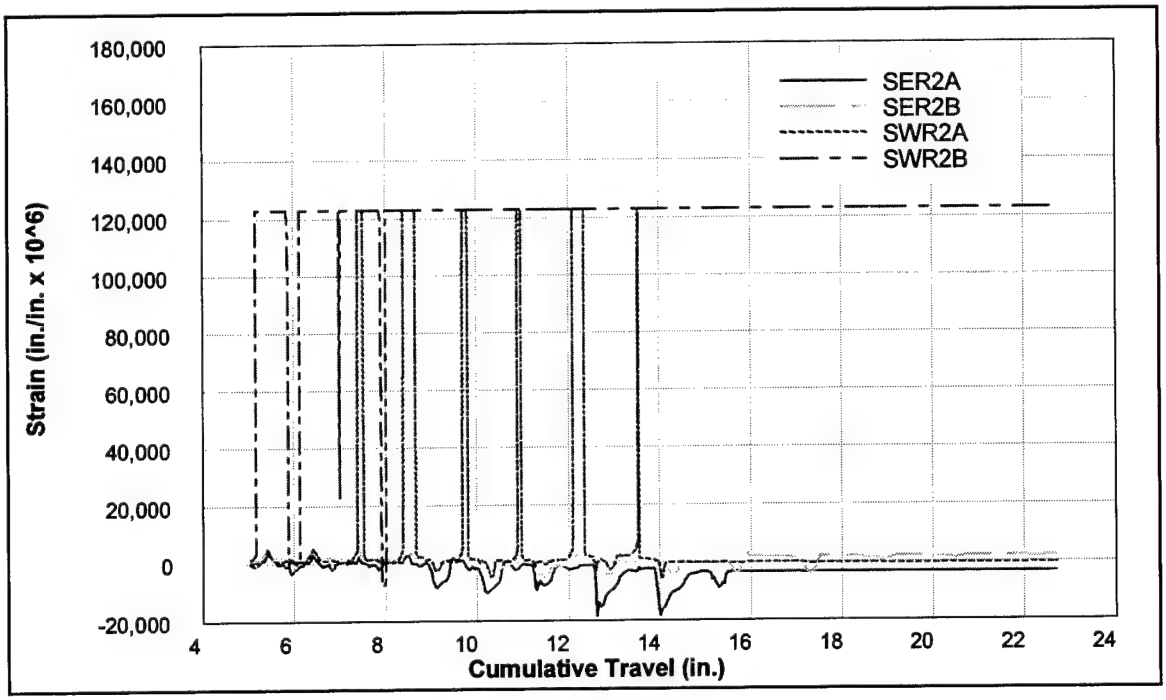

Figure C24. Strains measured 1.0 in. above and below cold joint, 3SLCL

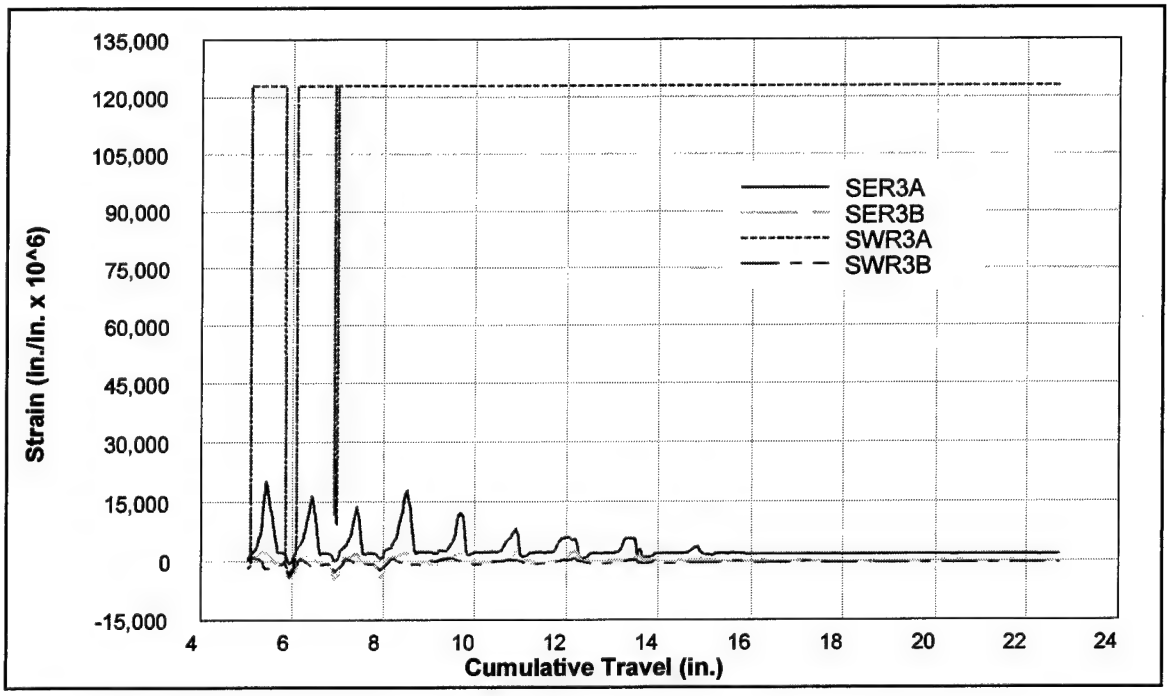

Figure C25. Strains measured 2.0 in. above and below cold joint, 3SLCL

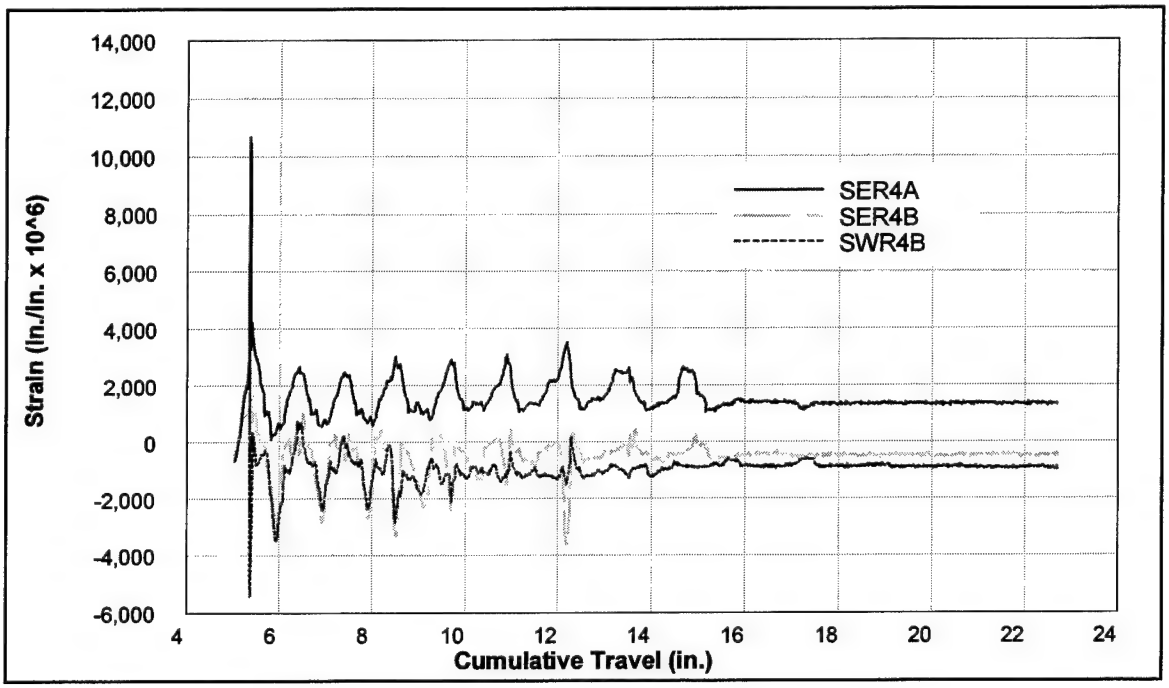

Figure C26. Strains measured 3.0 in. above and below cold joint, 3SLCL

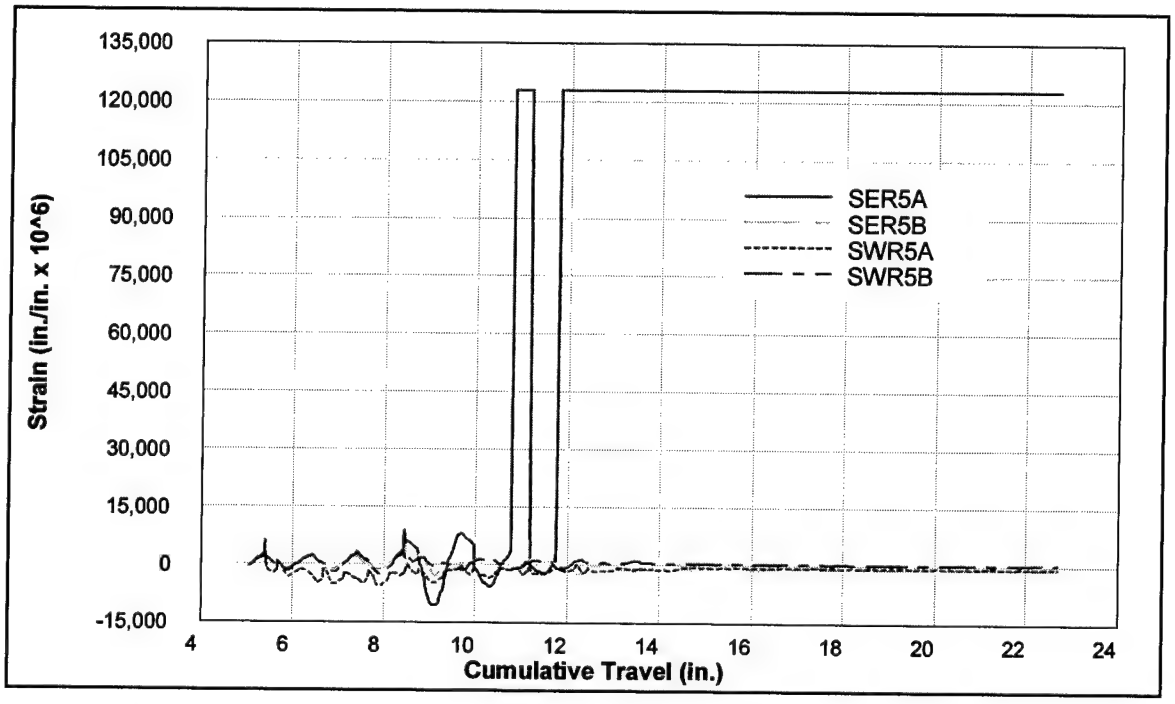

Figure C27. Strains measured 4.0 in. above and below cold joint, 3SLCL

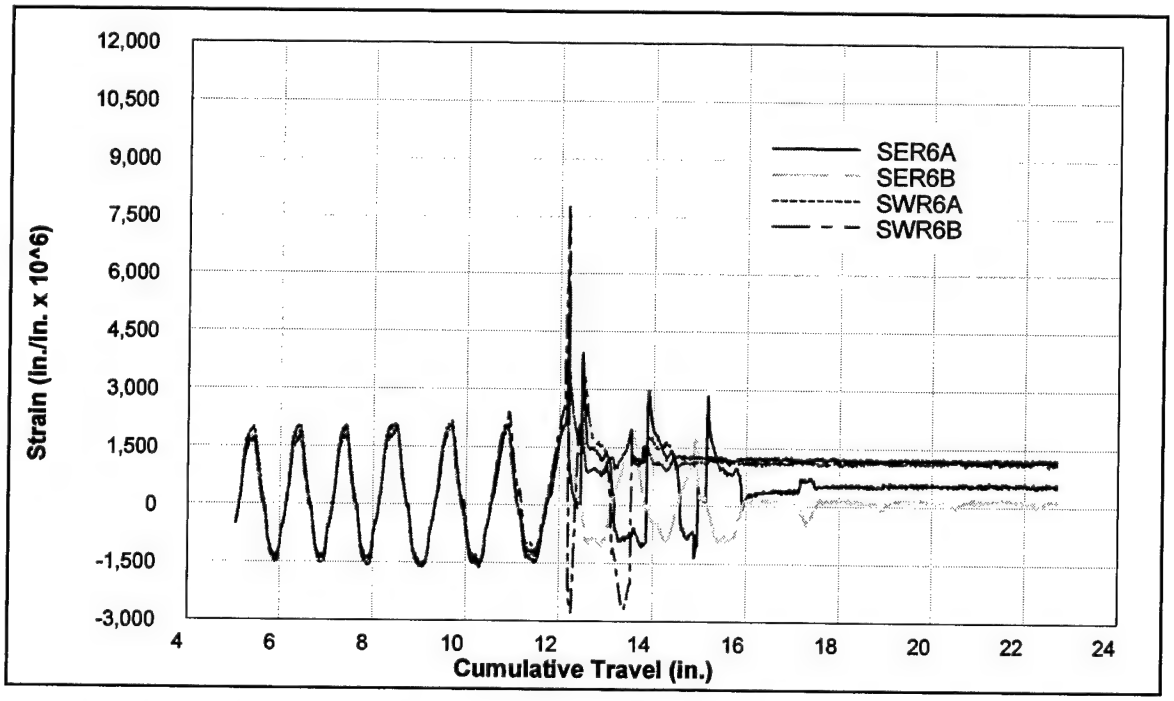

Figure C28. Strains measured 5 in. above and below cold joint, 3SLCL

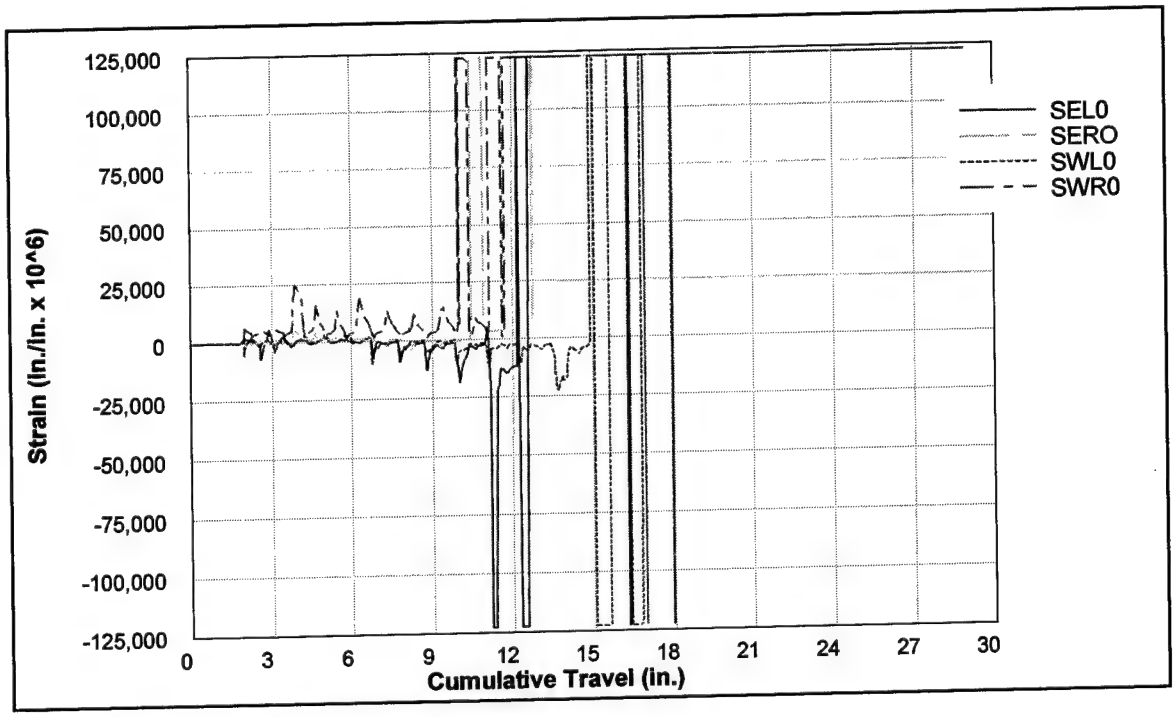

Figure C29. Strains measured at cold joint, 4SHCM

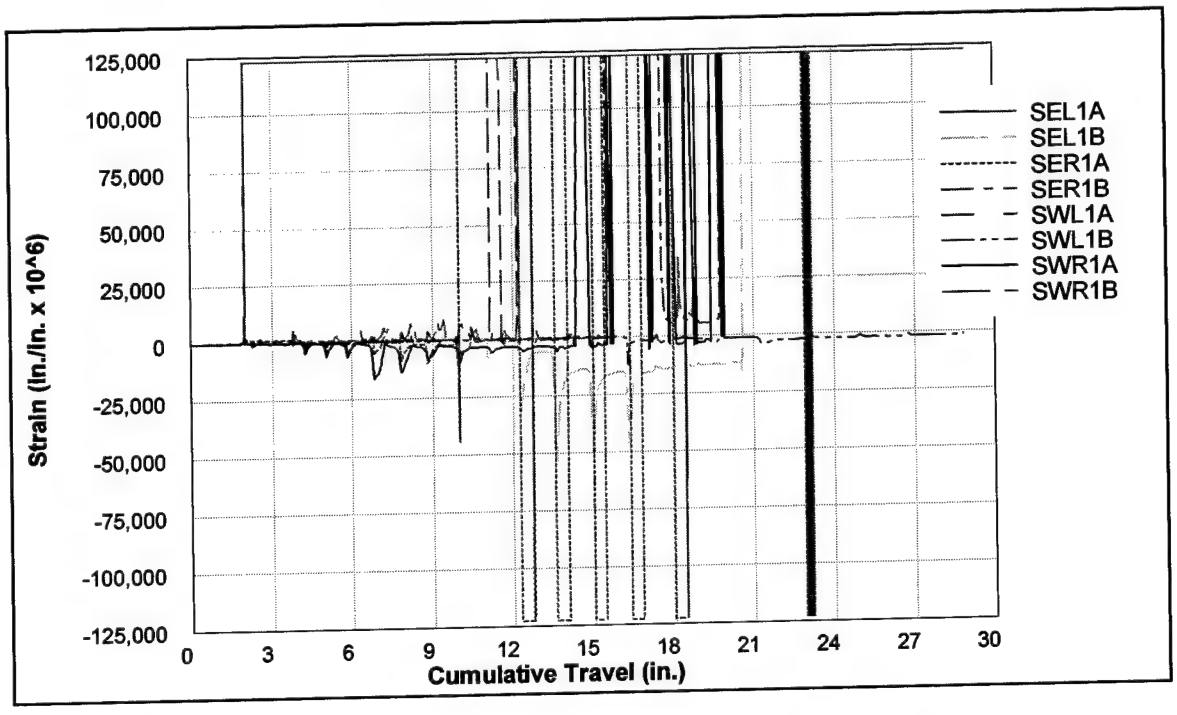

Figure C30. Strains measured 0.5 in. above and below cold joint, 4SHCM

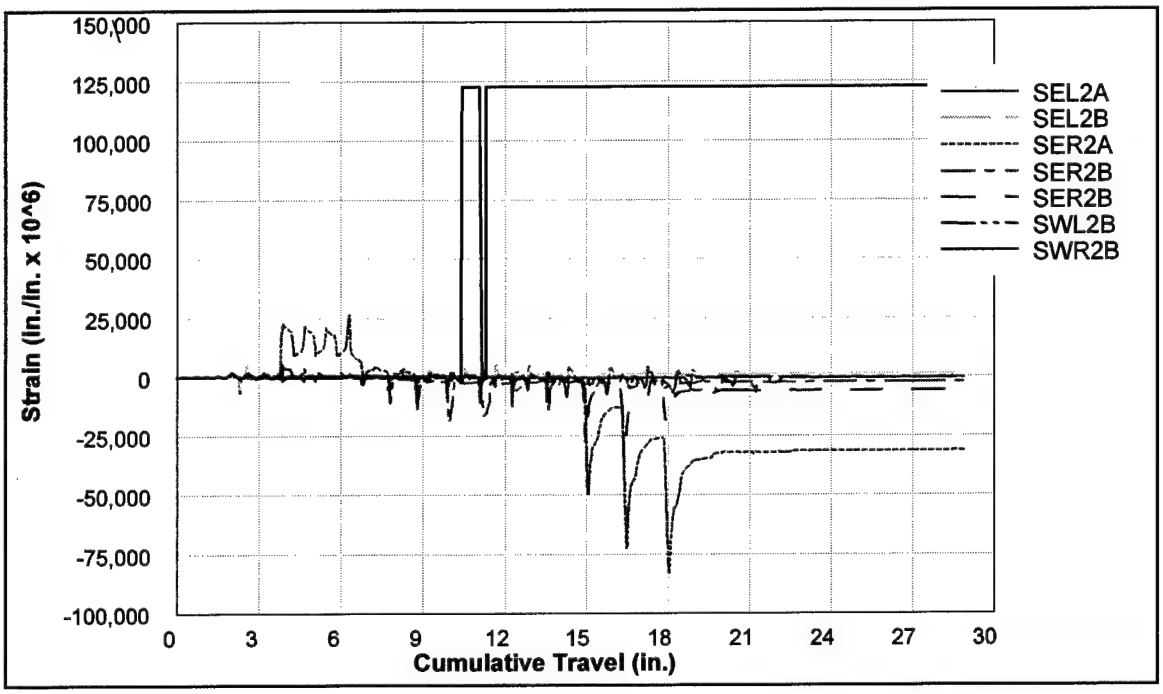

Figure C31. Strains measured 1.5 in. above and below cold joint, 4SHCM

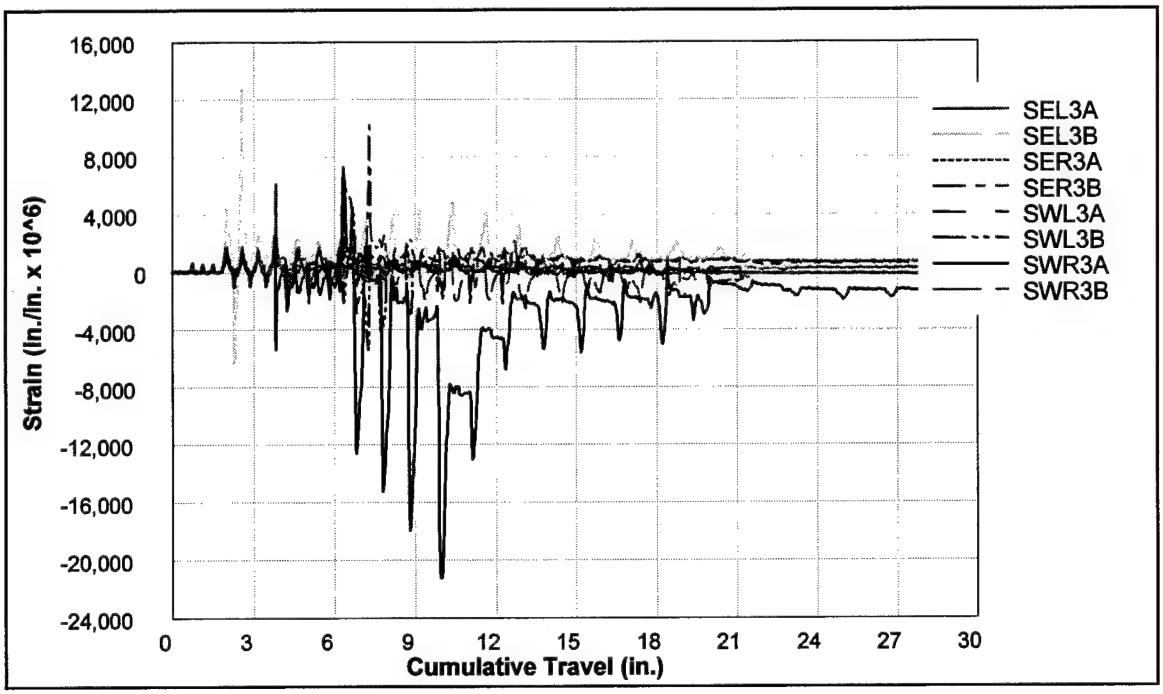

Figure C32. Strains measured 2.5 in. above and below cold joint, 4SHCM

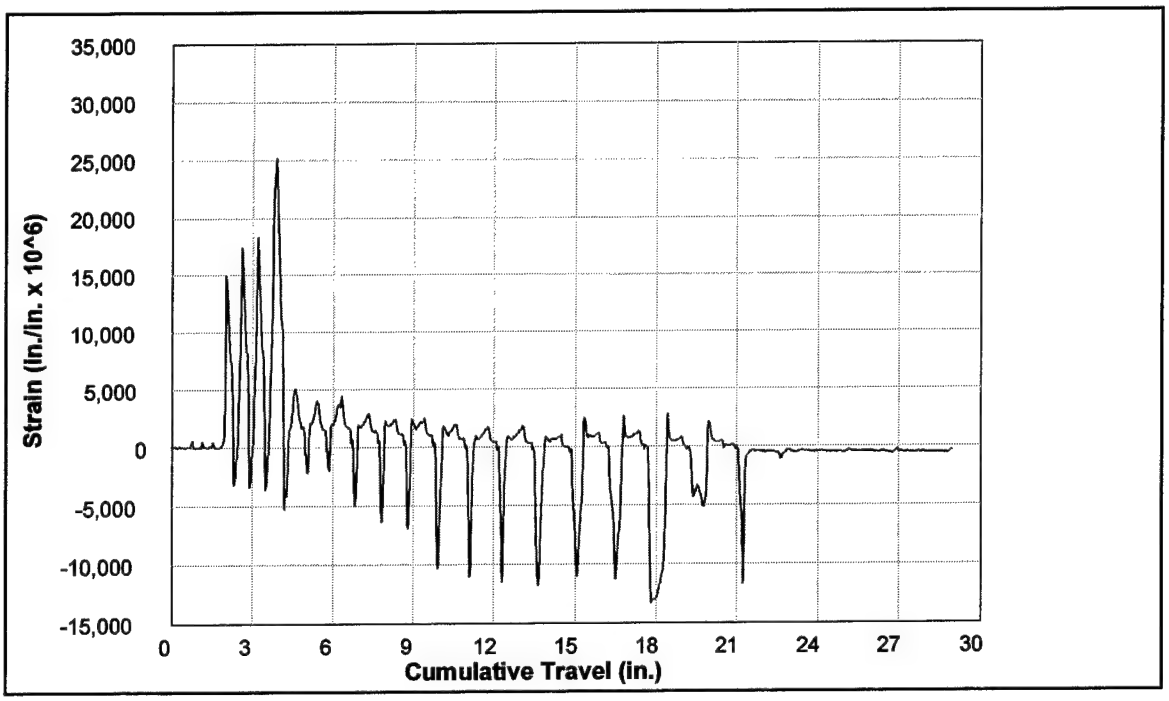

Figure C33. Strains measured 3.5 in. above and below cold joint, 4SHCM

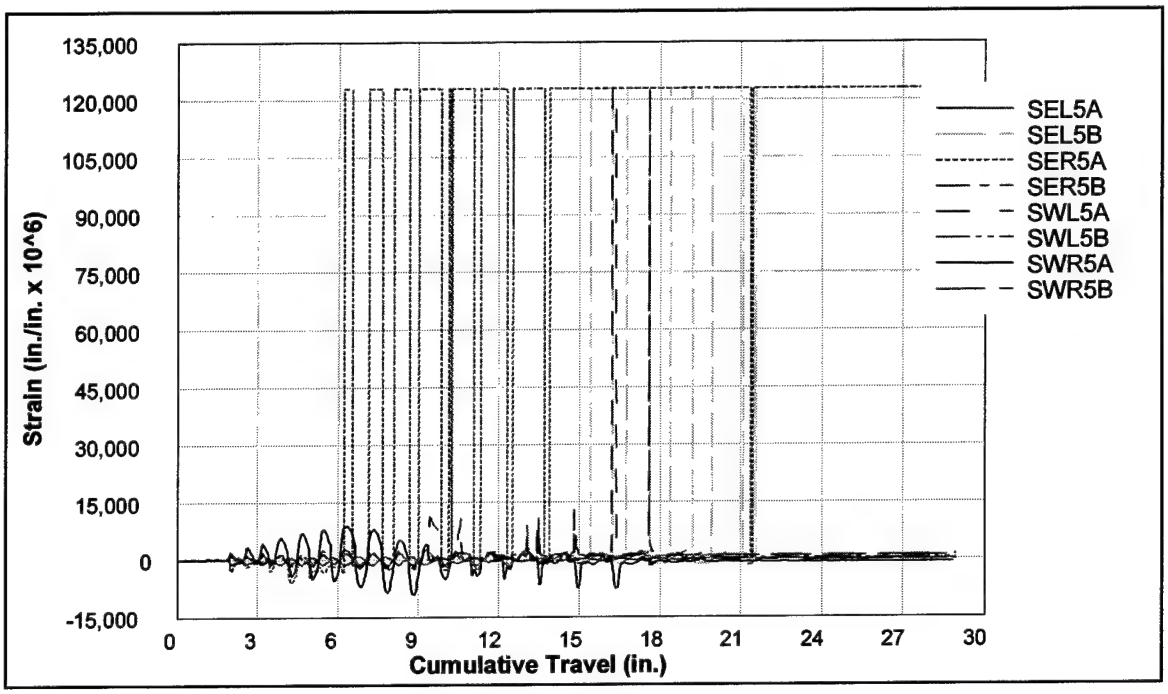

Figure C34. Strains measured 4.5 in. above and below cold joint, 4SHCM

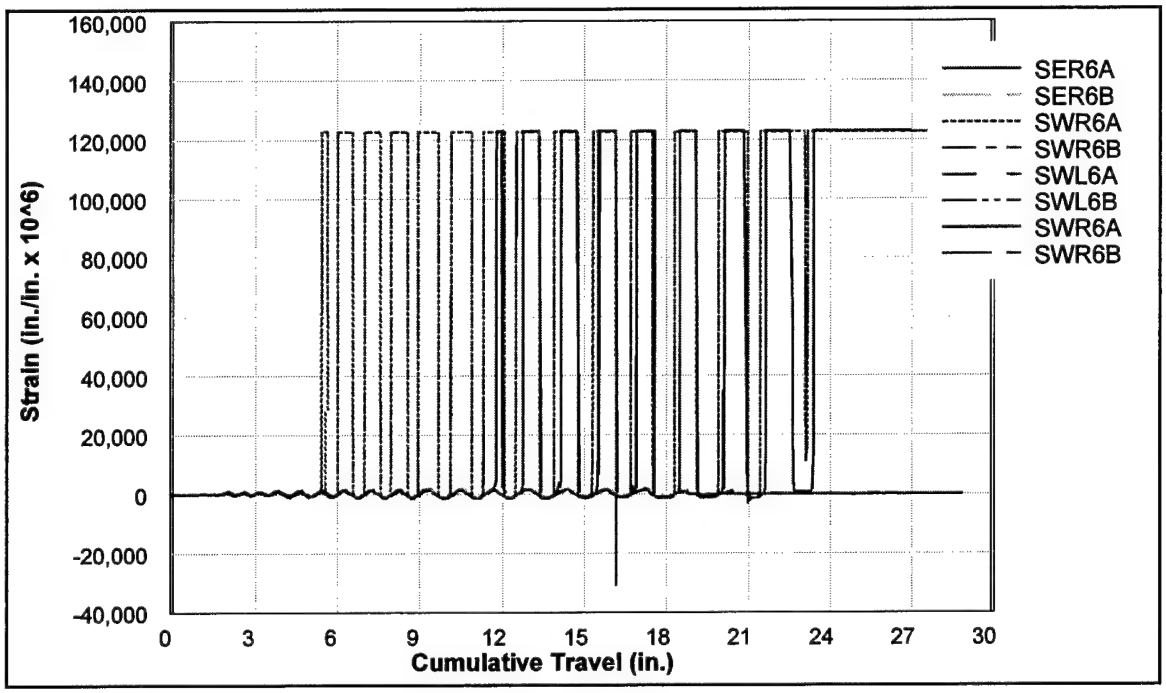

Figure C35. Strains measured 6.5 in. above and below cold joint, 4SHCM

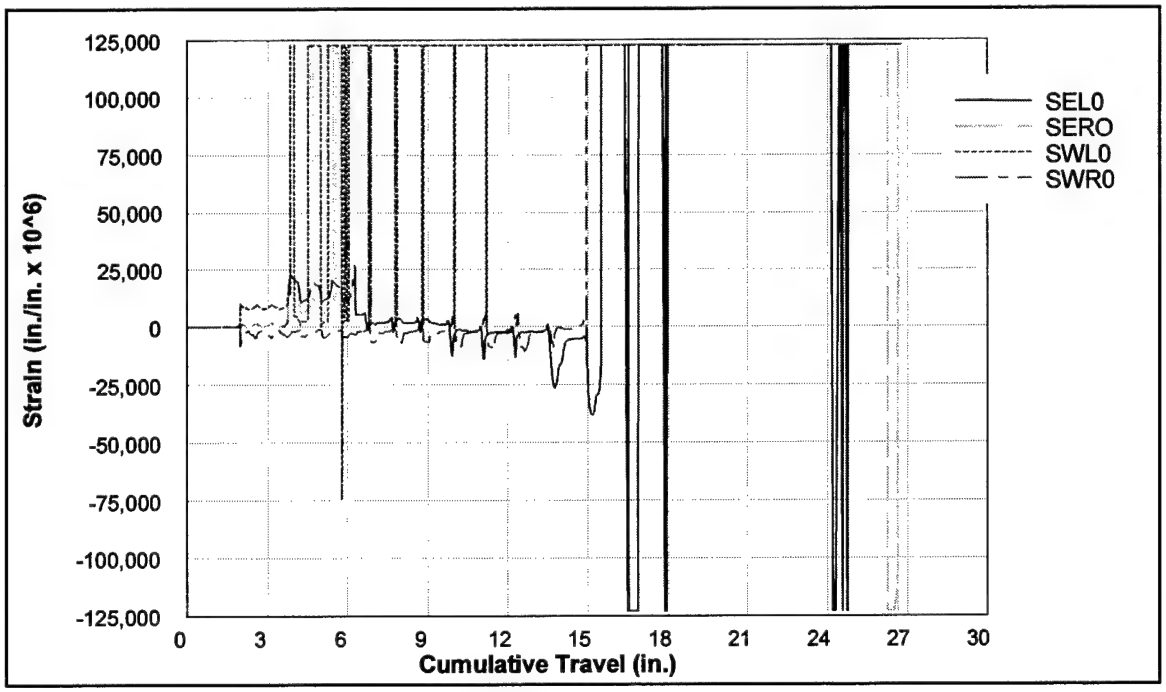

Figure C36. Strains measured at cold joint, 4SLCM

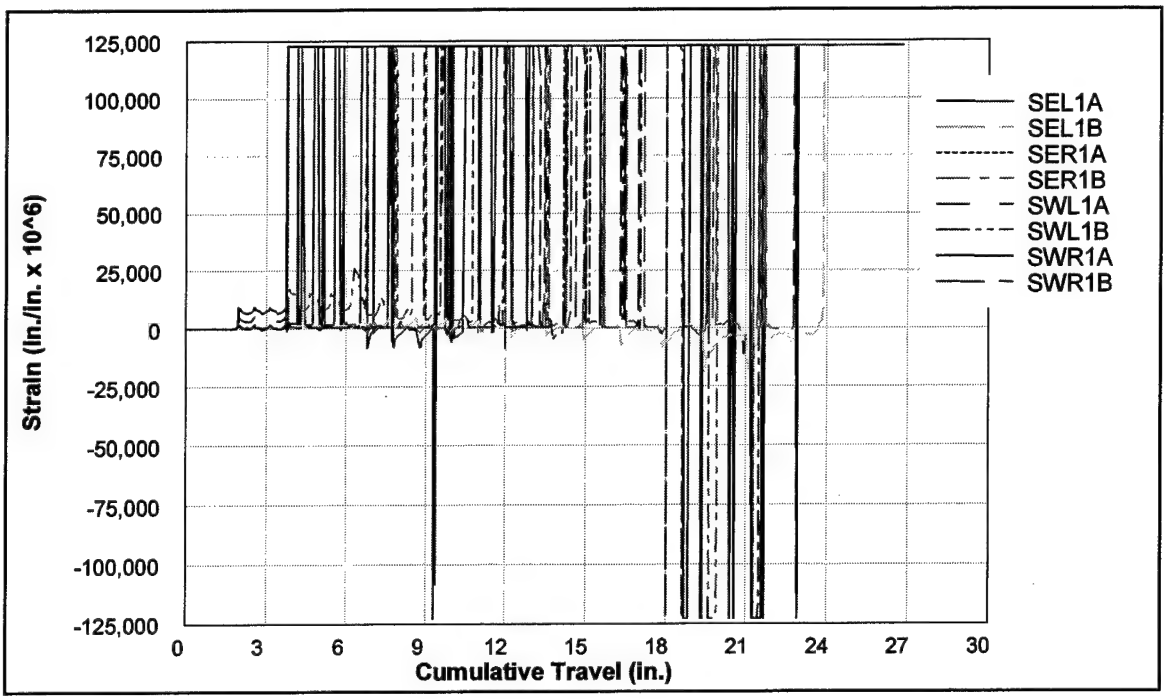

Figure C37. Strains measured 0.5 in. above and below cold joint, 4SLCM

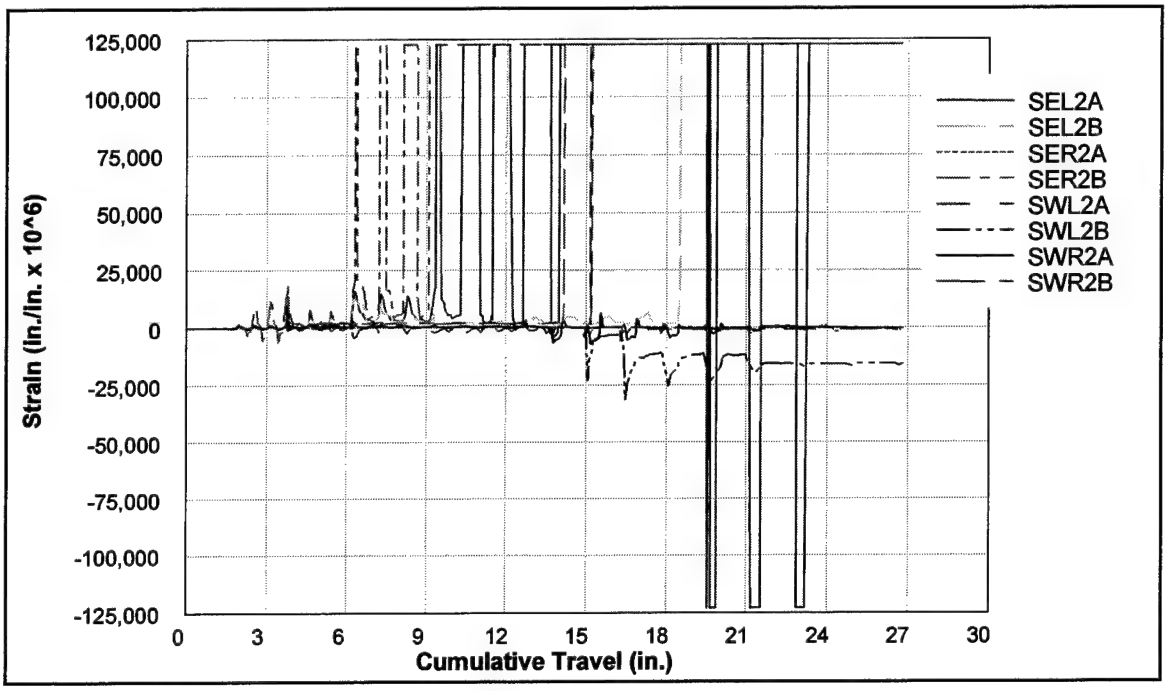

Figure C38. Strains measured 1.5 in. above and below cold joint, 4SLCM

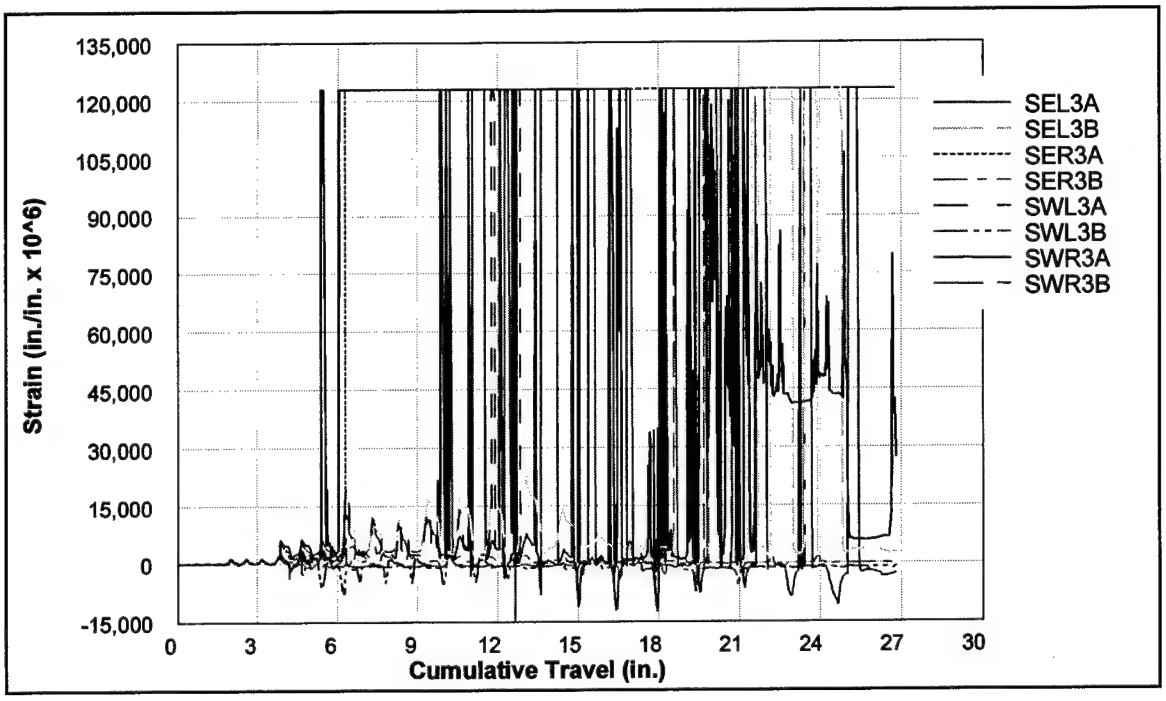

Figure C39. Strains measured 2.5 in. above and below cold joint, 4SLCM

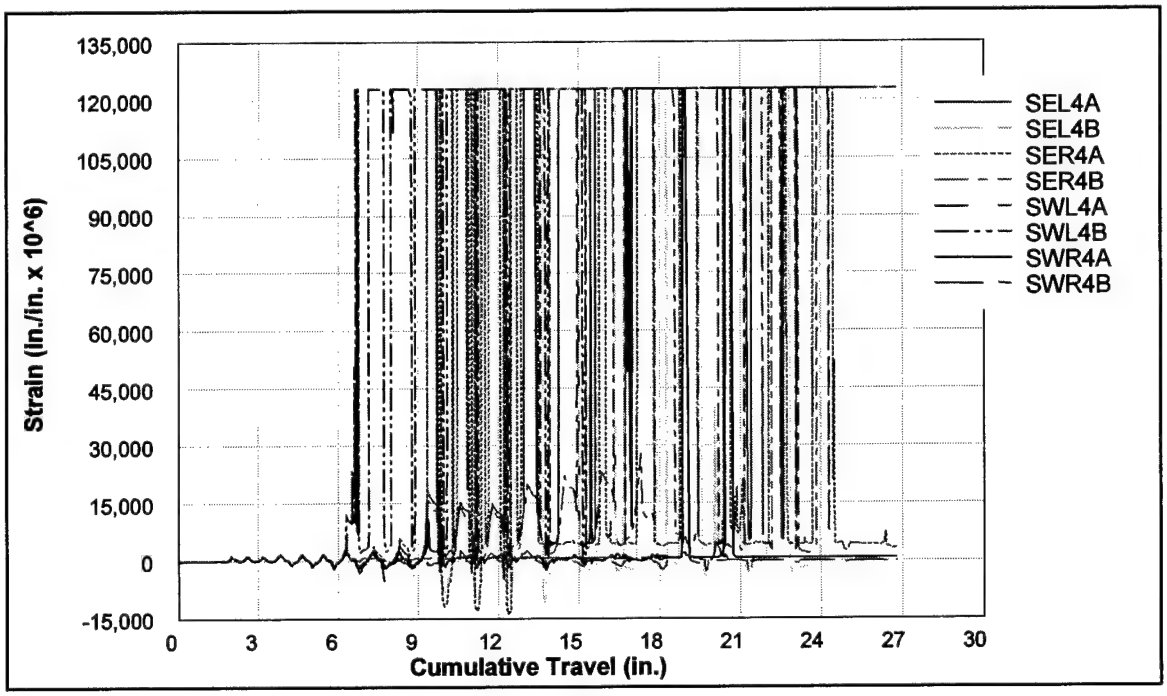

Figure C40. Strains measured 3.5 in. above and below cold joint, 4SLCM

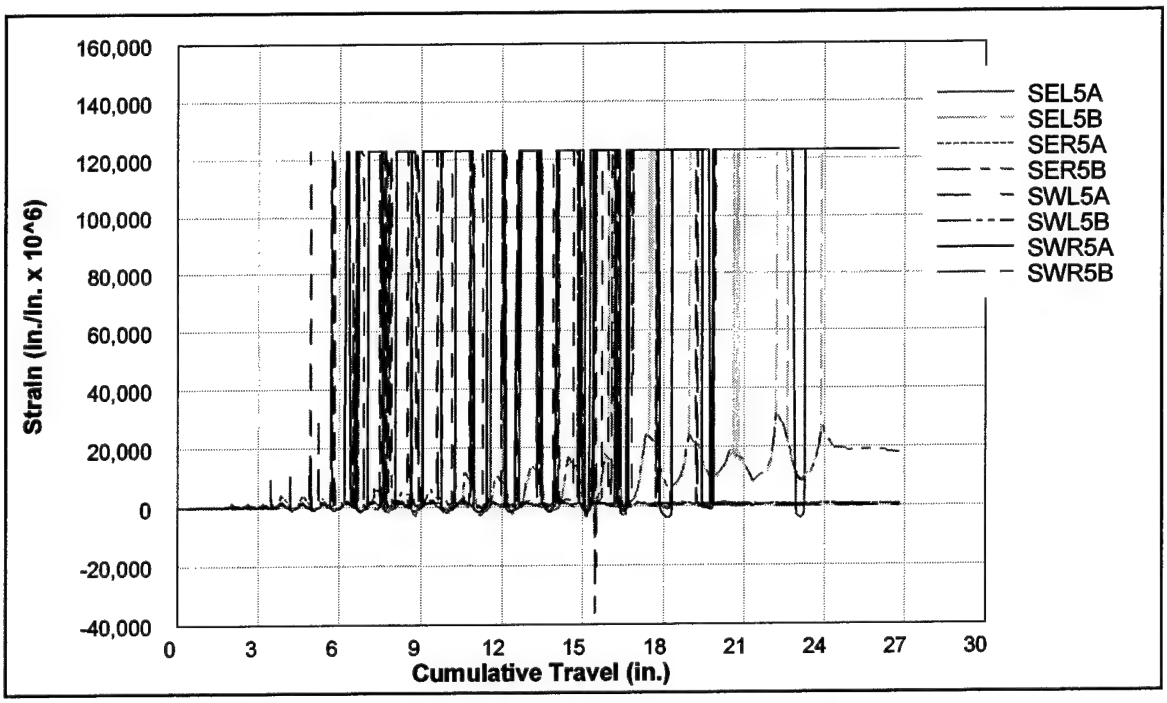

Figure C41. Strains measured 4.5 in. above and below cold joint, 4SLCM

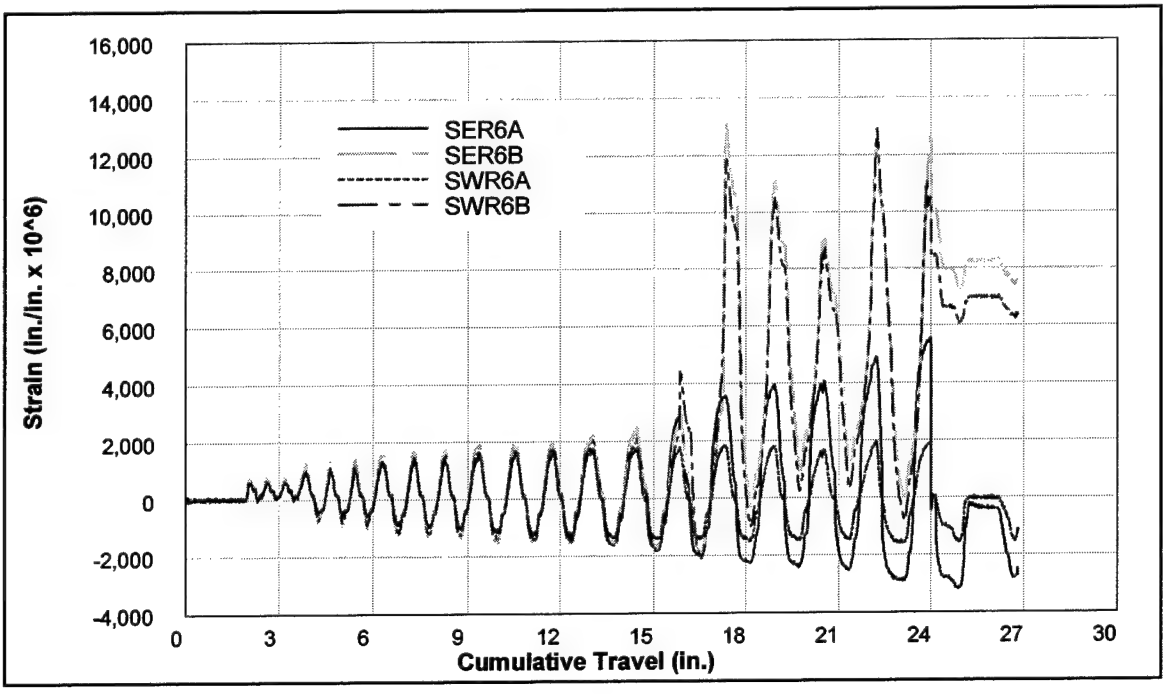

Figure C42. Strains measured 6.5 in. above and below cold joint, 4SLCM

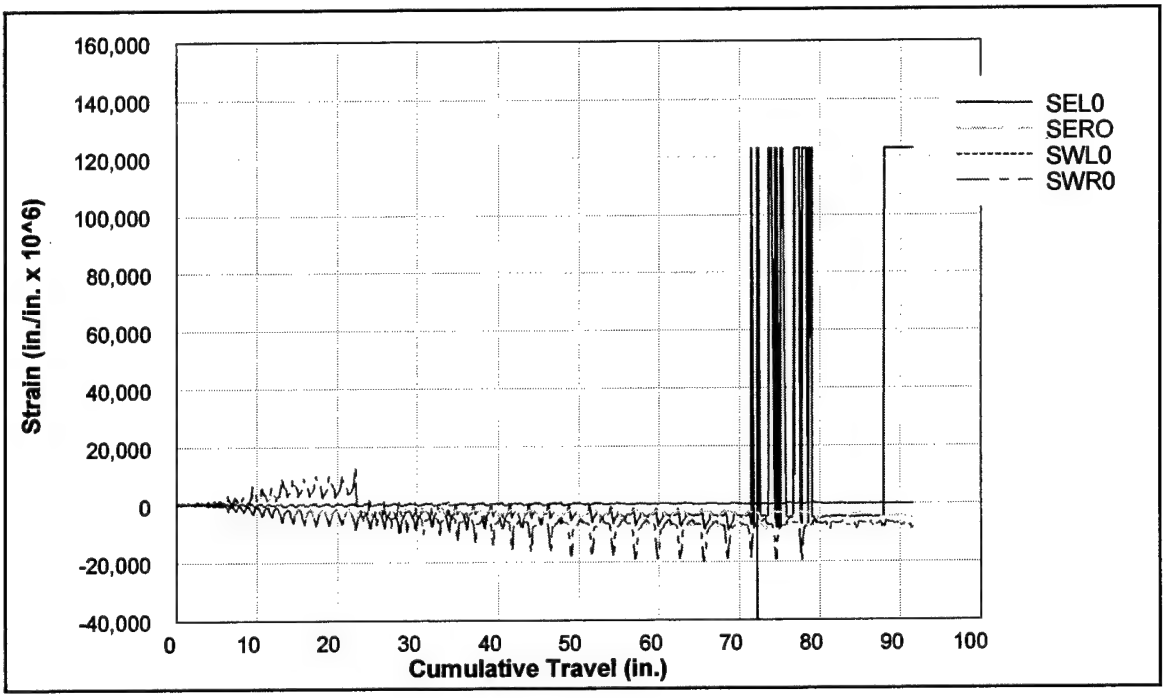

Figure C43. Strains measured at cold joint, 5SHCL

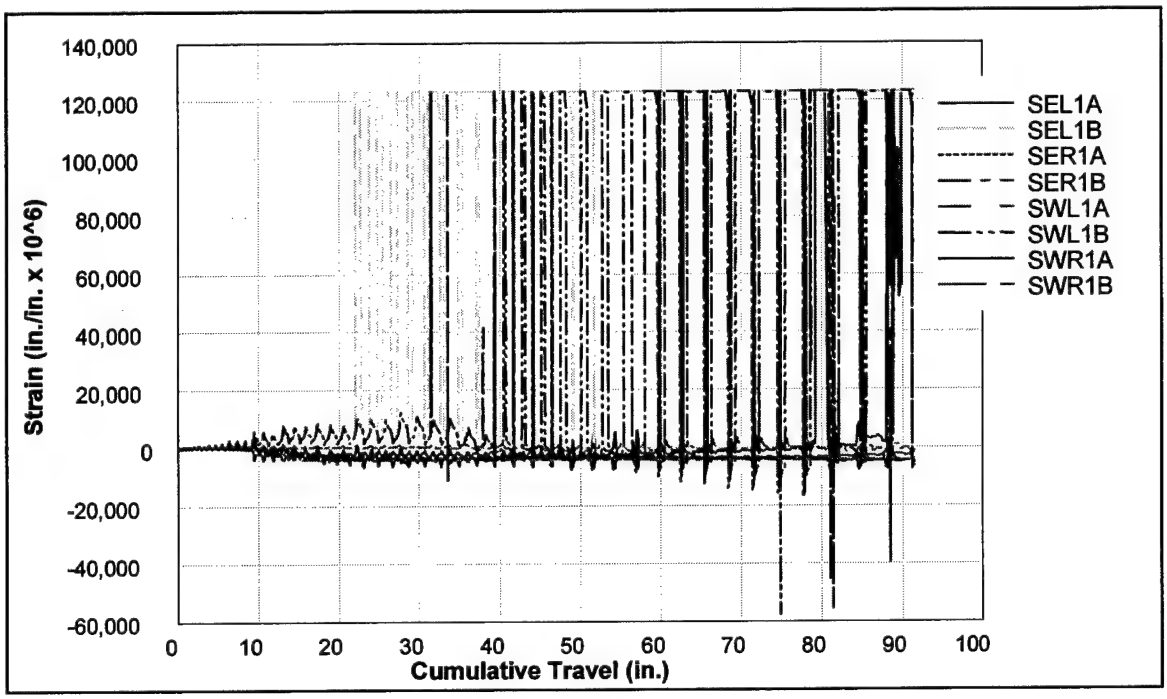

Figure C44. Strains measured 0.5 in. above and below cold joint, 5SHCL

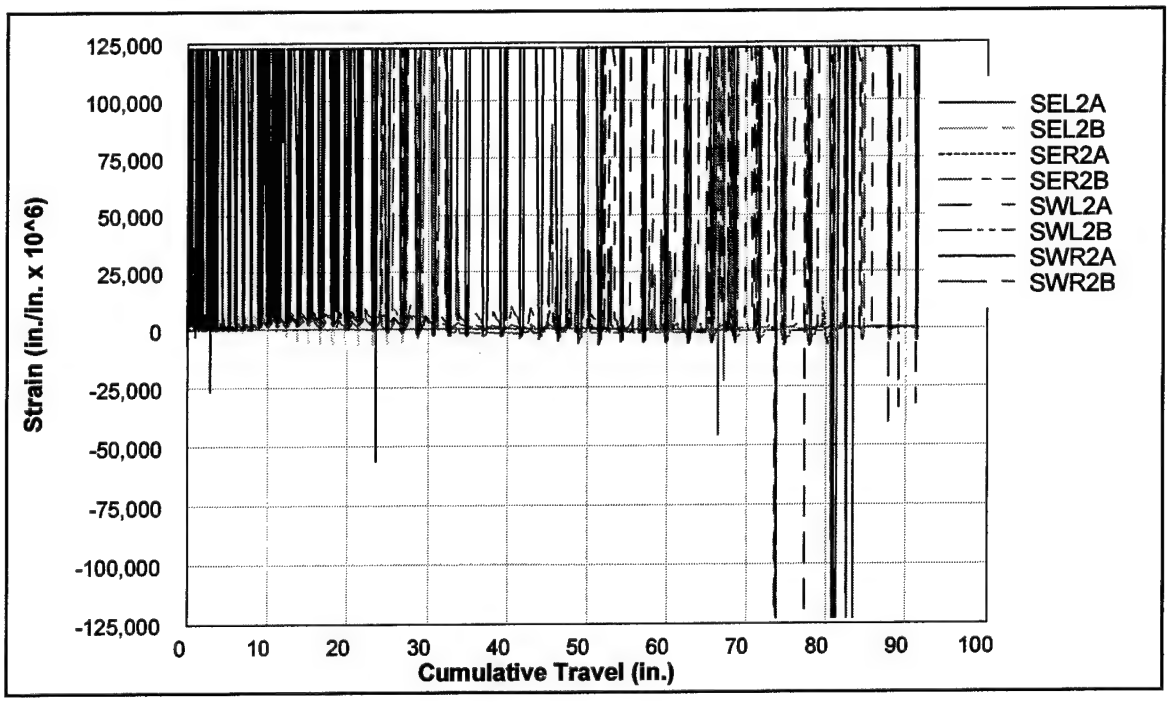

Figure C45. Strains measured 1.5 in. above and below cold joint, 5SHCL

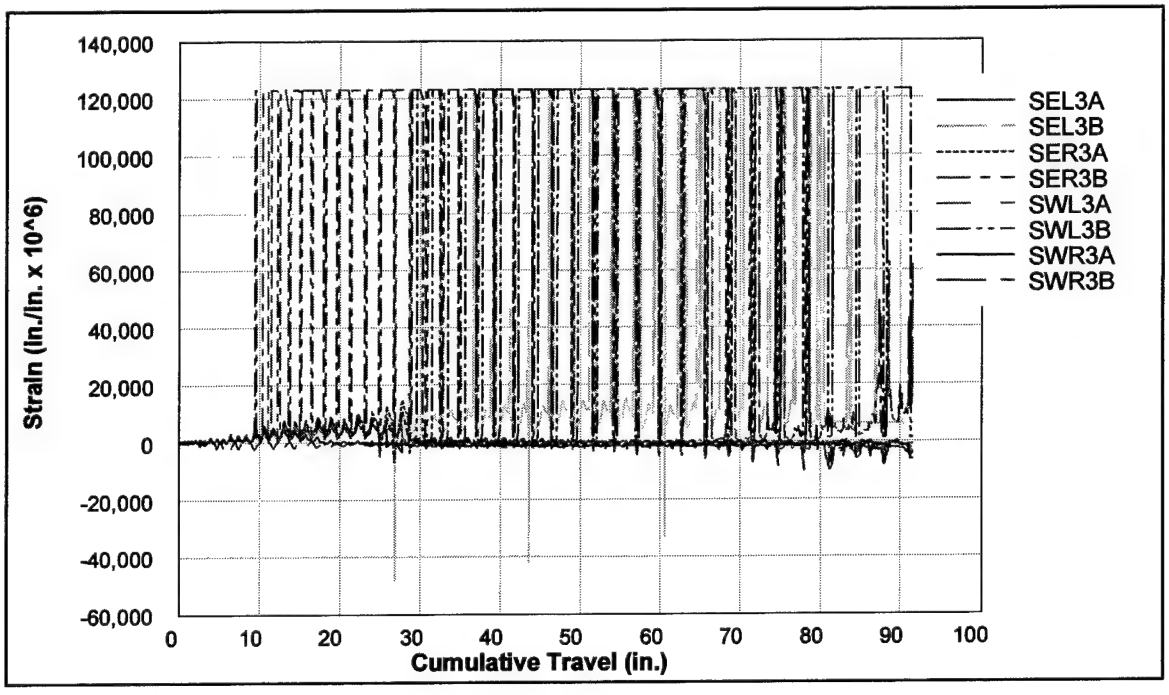

Figure C46. Strains measured 2.5 in. above and below cold joint, 5SHCL

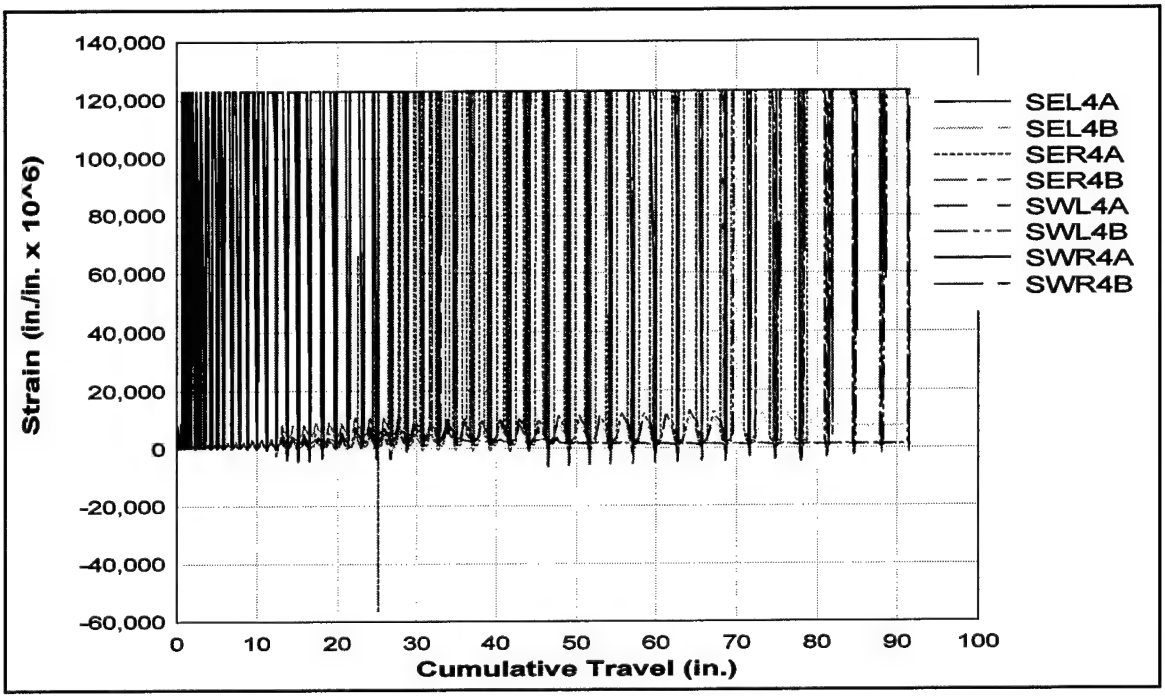

Figure C47. Strains measured 3.5 in. above and below cold joint, 5SHCL

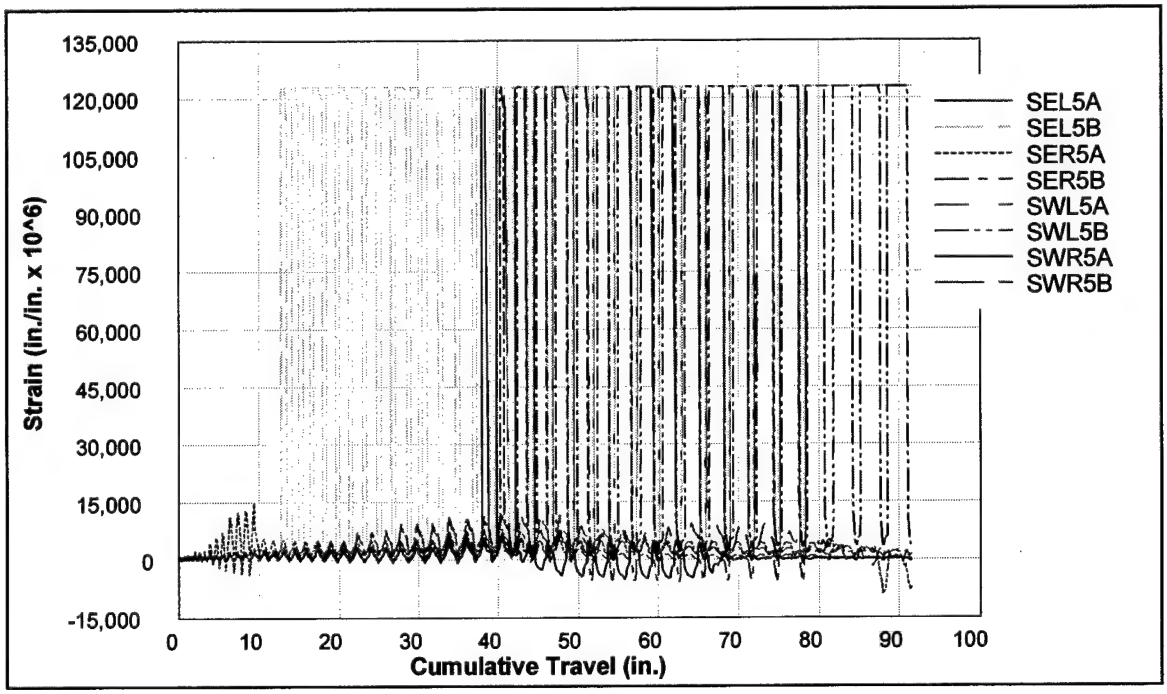

Figure C48. Strains measured 4.5 in. above and below cold joint, 5SHCL

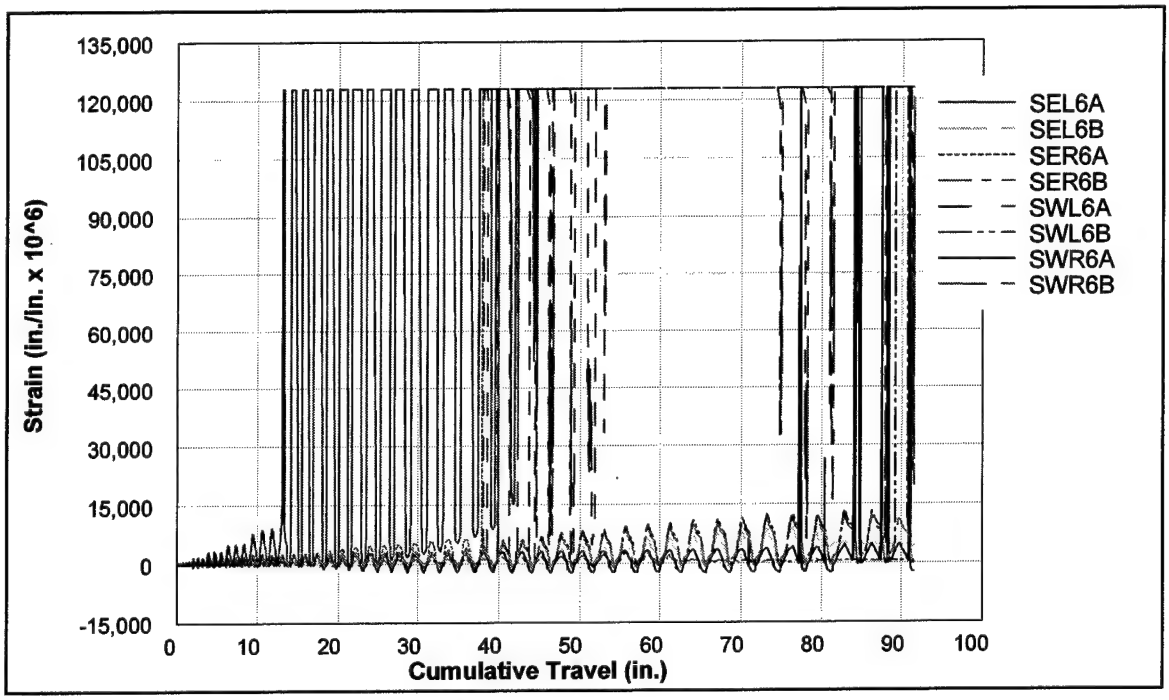

Figure C49. Strains measured 6.5 in. above and below cold joint, 5SHCL

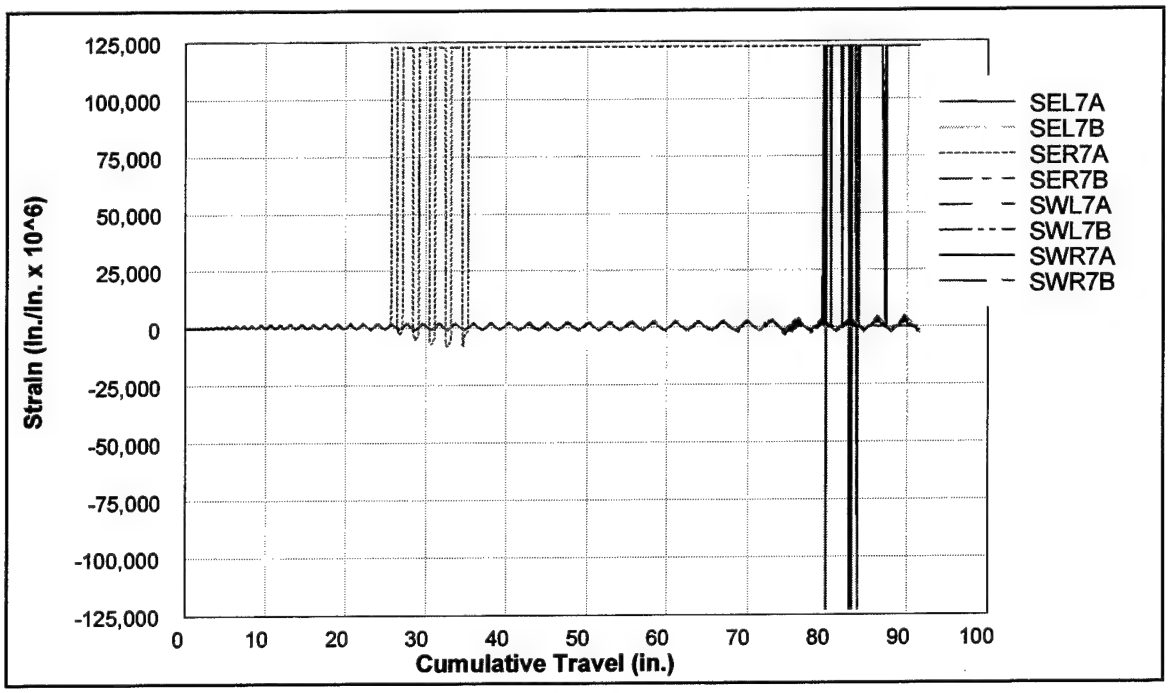

Figure C50. Strains measured 8.5 in. above and below cold joint, 5SHCL

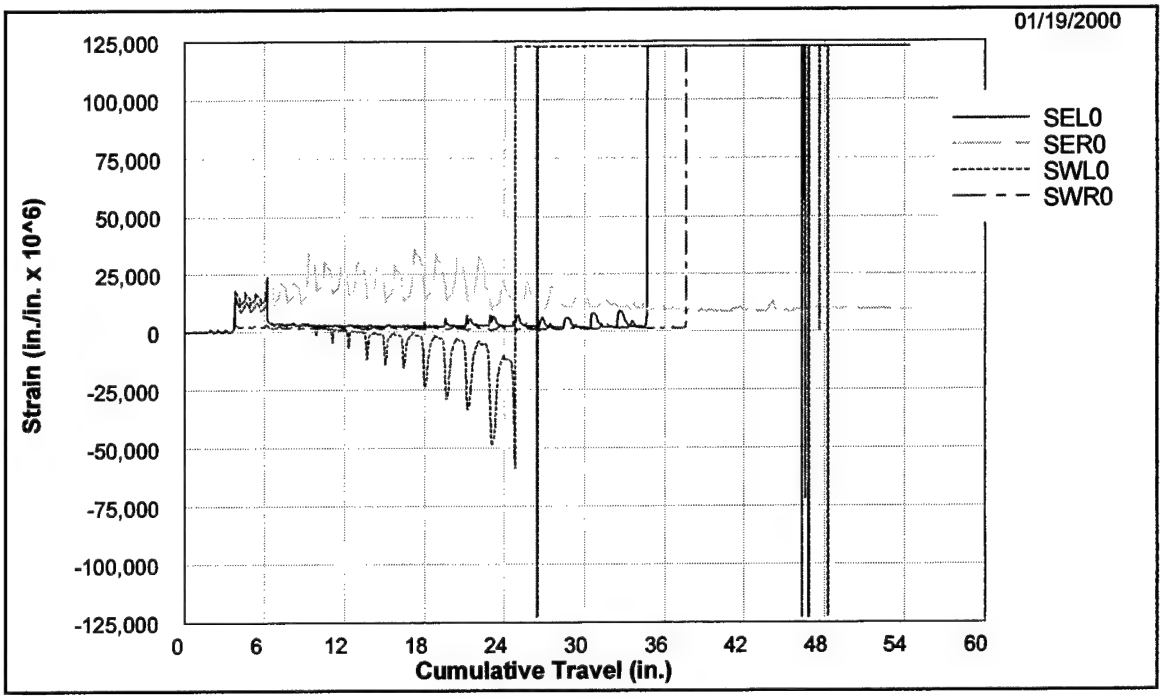

Figure C51. Strains measured at cold joint, 5SLCH

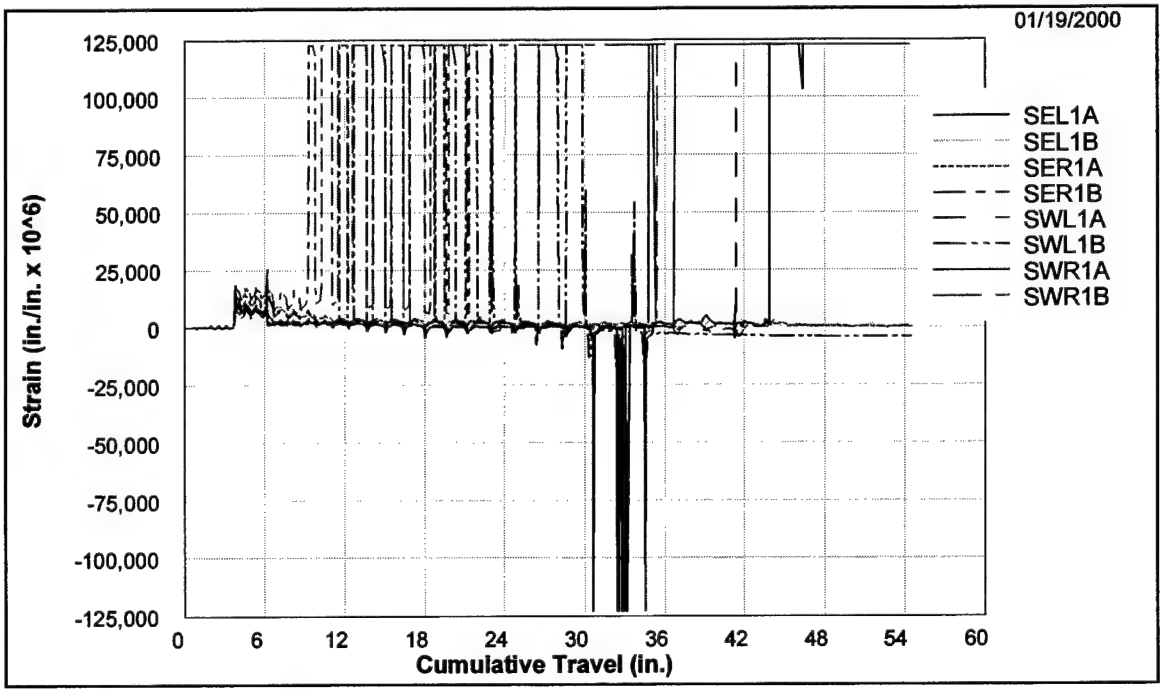

Figure C52. Strains measured 0.5 in. above and below cold joint, 5SLCH

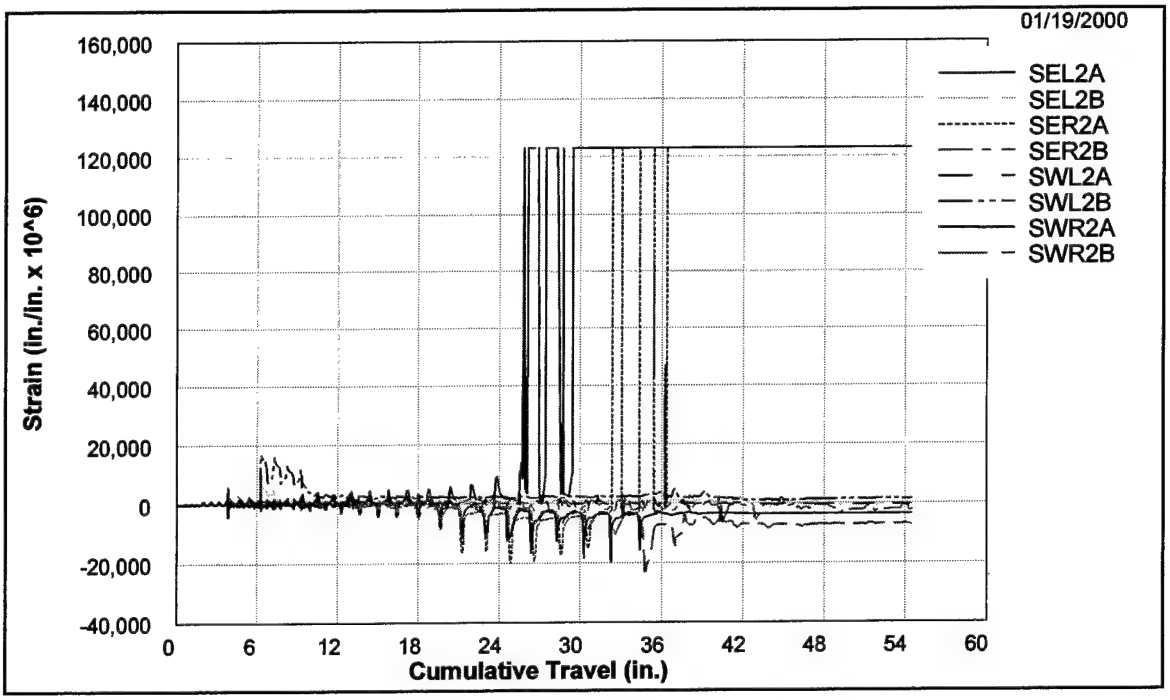

Figure C53. Strains measured 1.5 in. above and below cold joint, 5SLCH

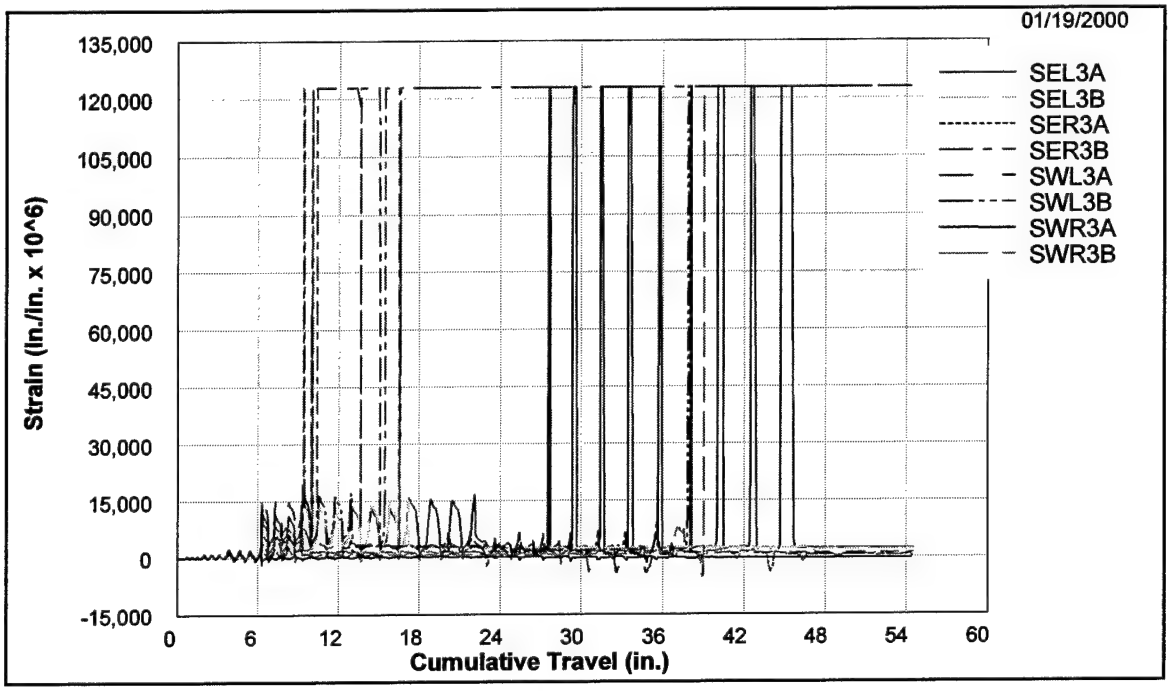

Figure C54. Strains measured 2.5 in. above and below cold joint, 5SLCH

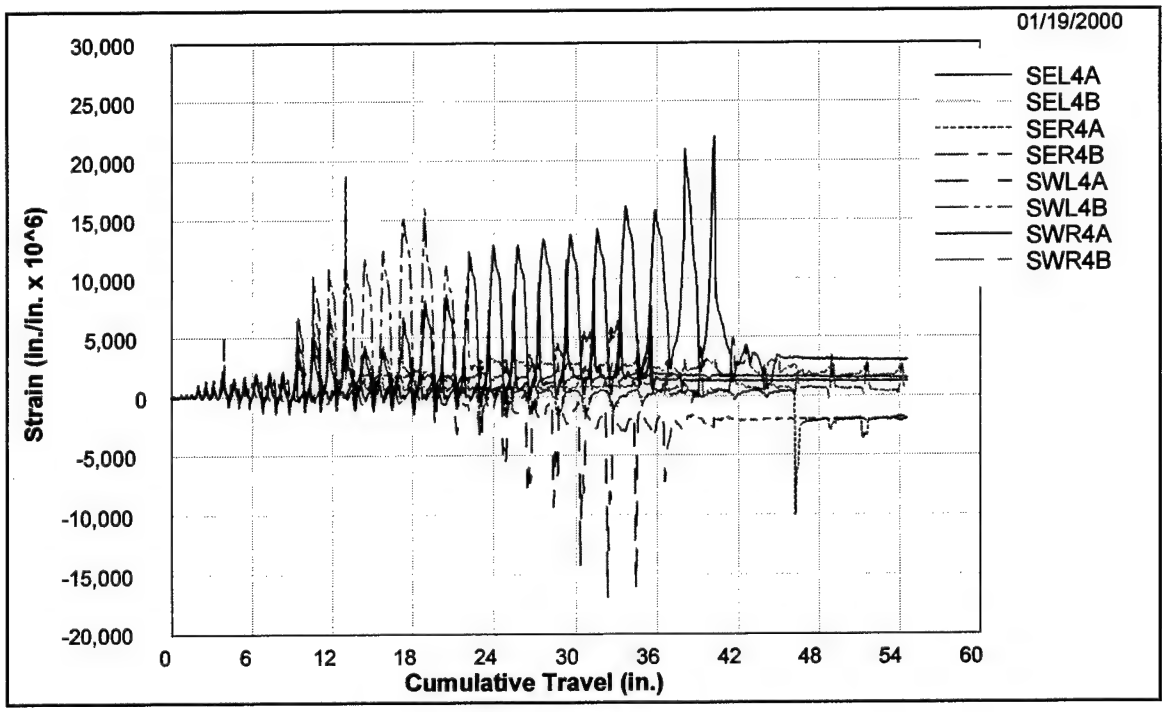

Figure C55. Strains measured 3.5 in. above and below cold joint, 5SLCH

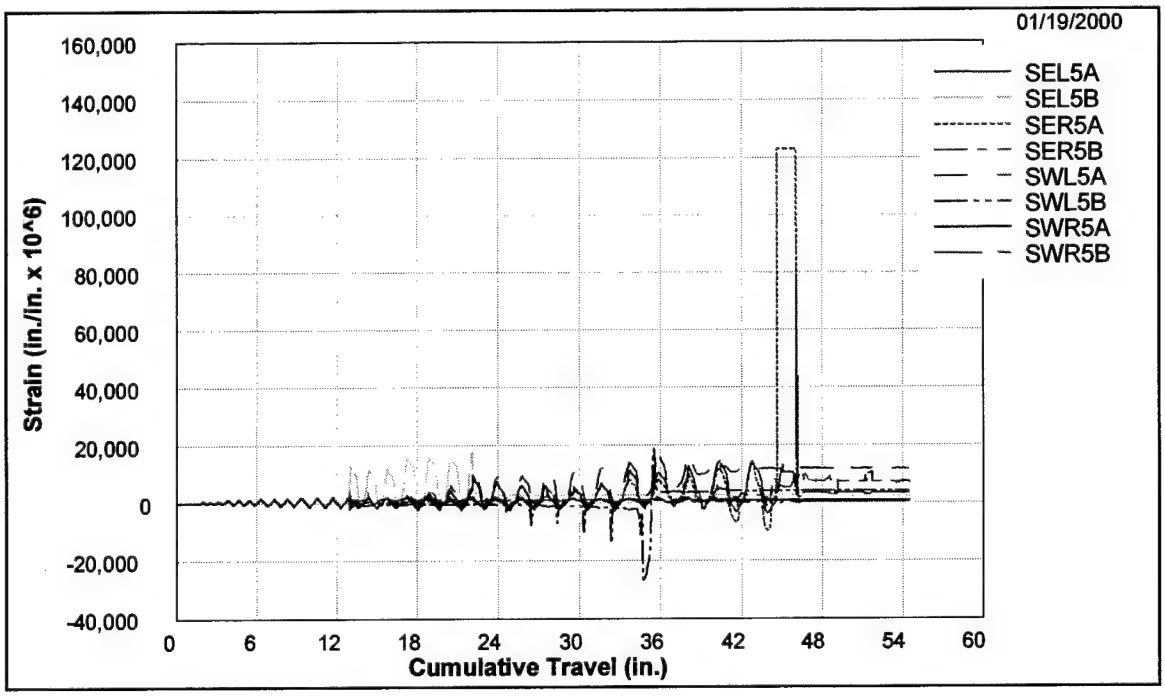

Figure C56. Strains measured 4.5 in. above and below cold joint, 5SLCH

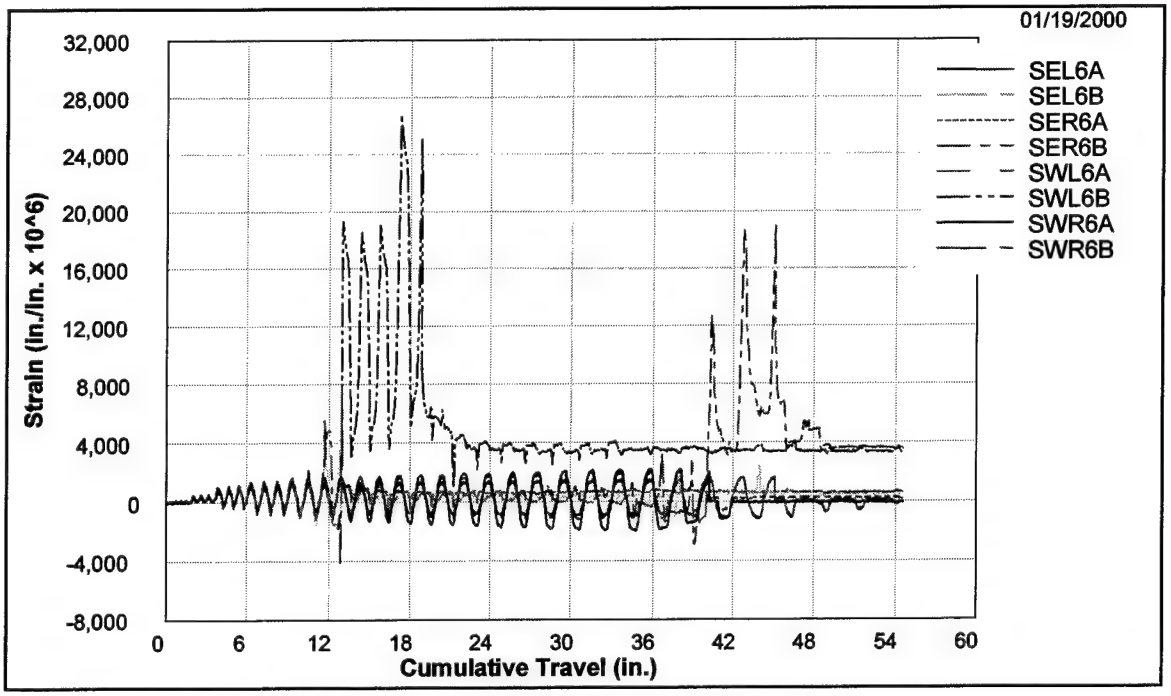

Figure C57. Strains measured 6.5 in. above and below cold joint, 5SLCH

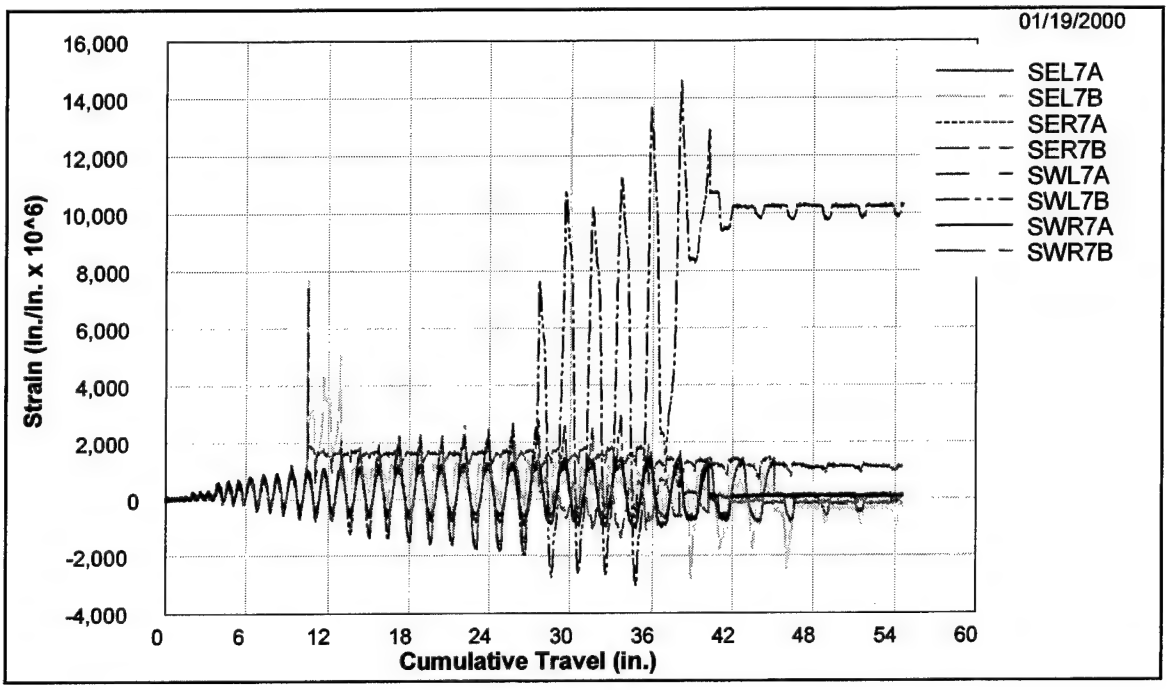

Figure C58. Strains measured 8.5 in. above and below cold joint, SLCH5

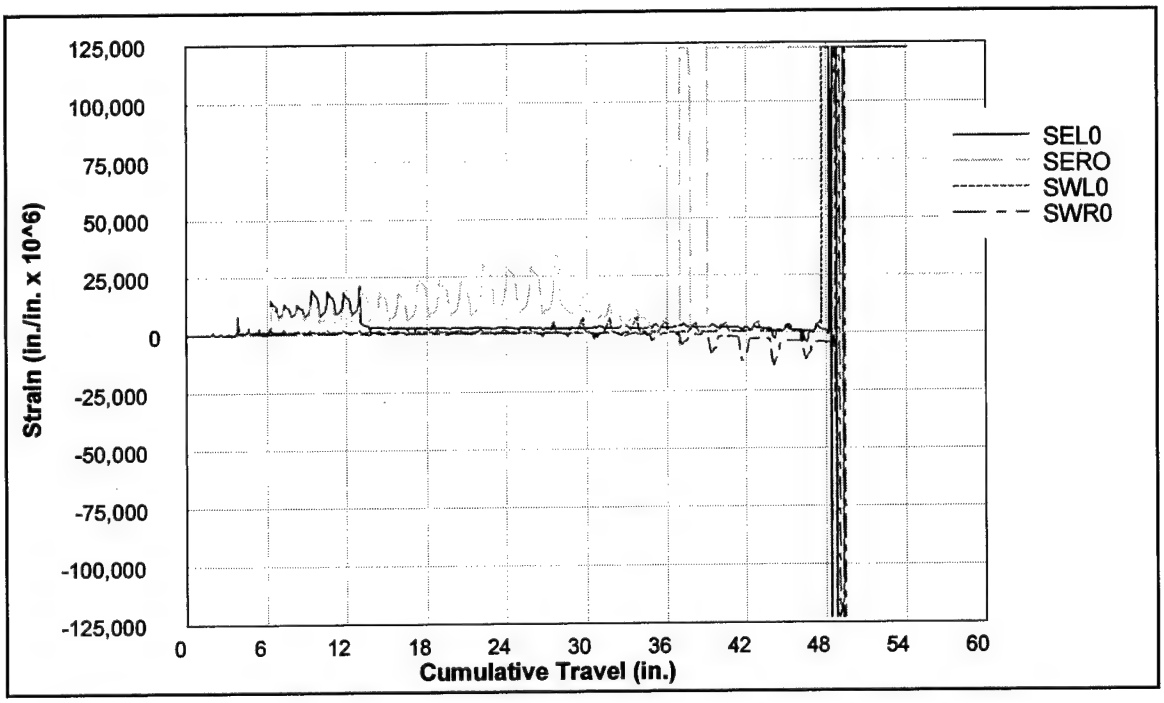

Figure C59. Strains measured at cold joint, 5SLCL

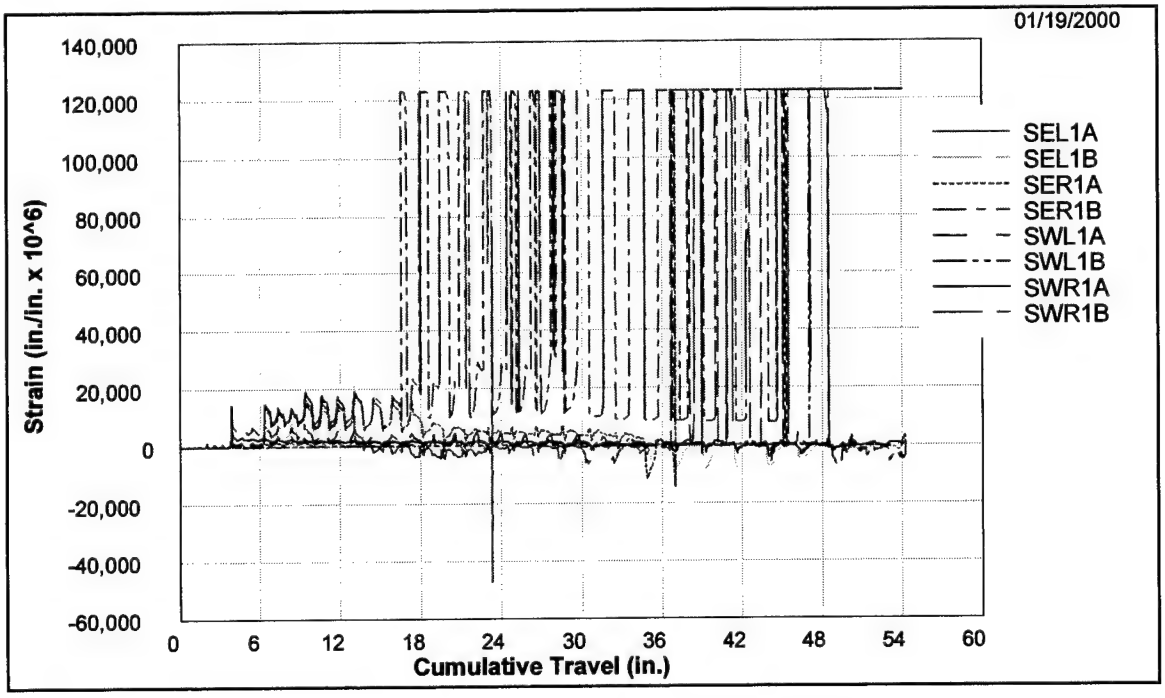

Figure C60. Strains measured 0.5 in. above and below cold joint, 5SLCL

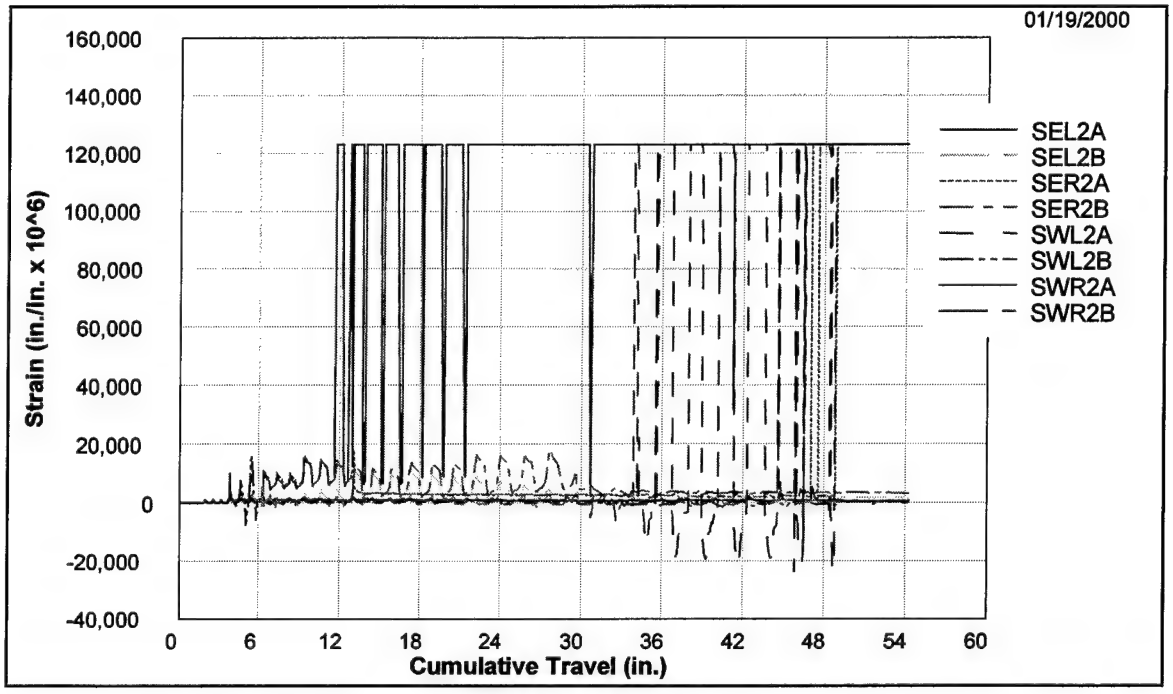

Figure C61. Strains measured 1.5 in. above and below cold joint, 5SLCL

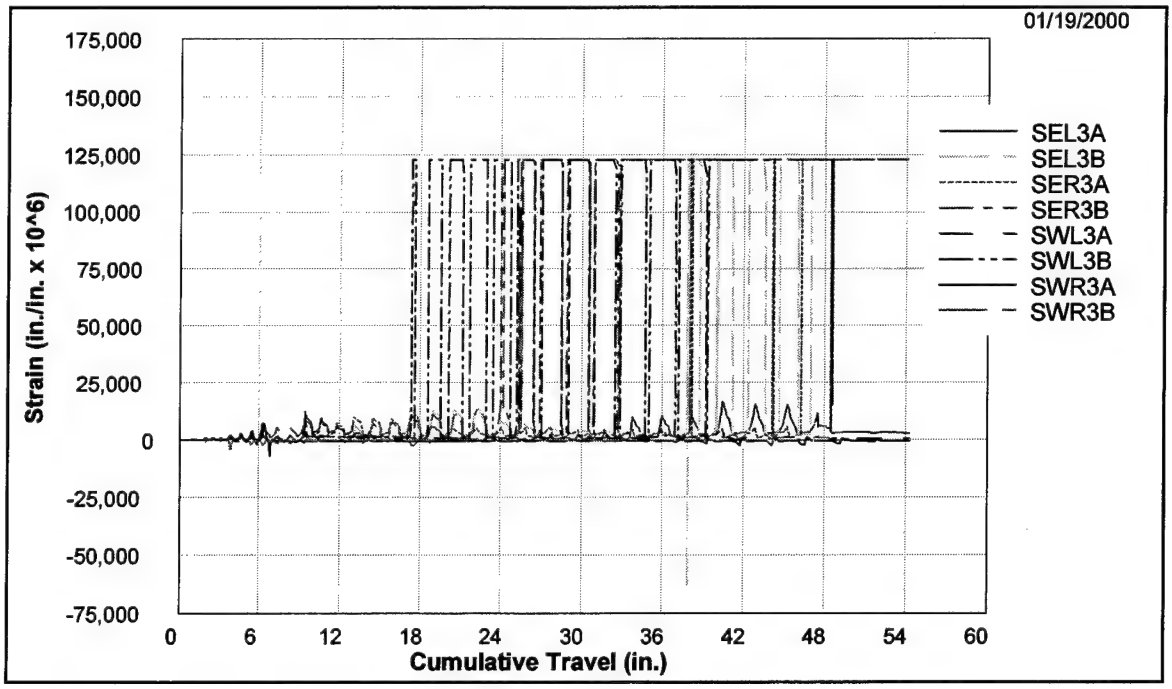

Figure C62. Strains measured 2.5 in. above and below cold joint, 5SLCL

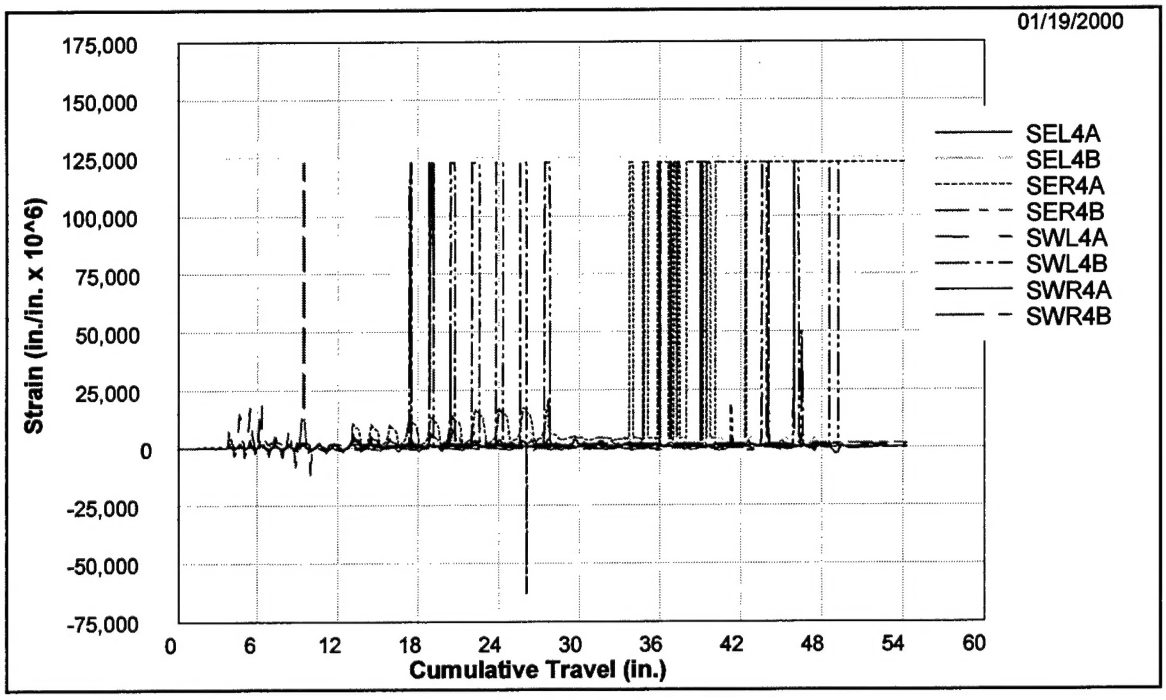

Figure C63. Strains measured 3.5 in. above and below cold joint, 5SLCL

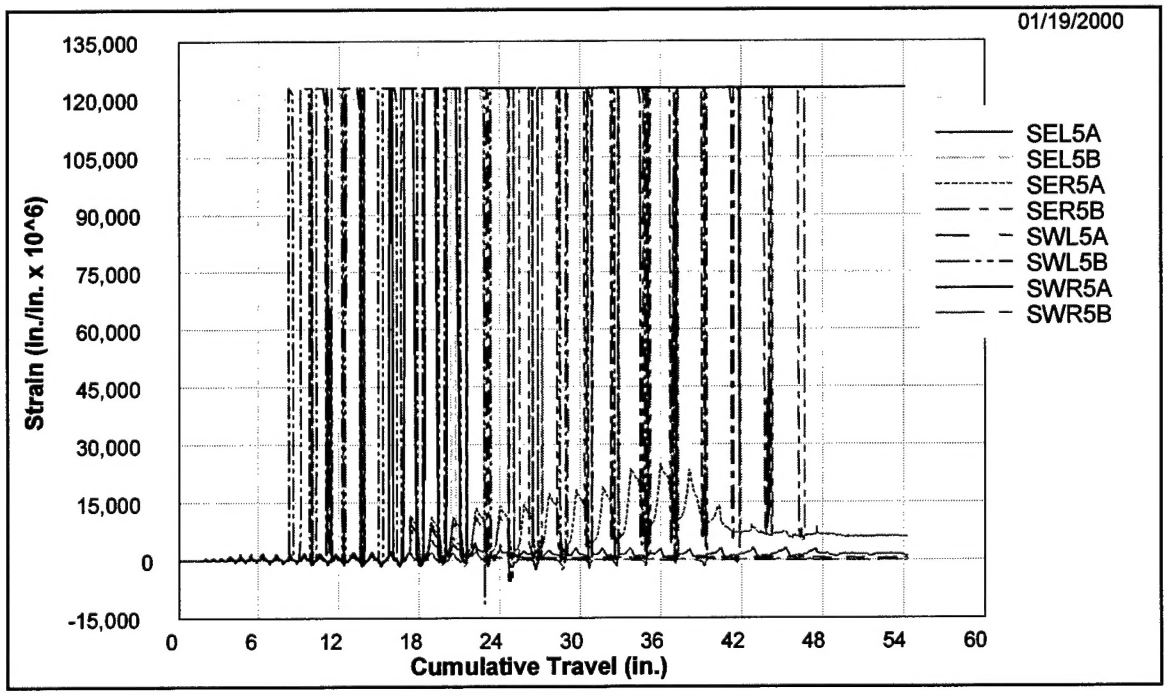

Figure C64. Strains measured 4.5 in. above and below cold joint, 5SLCL

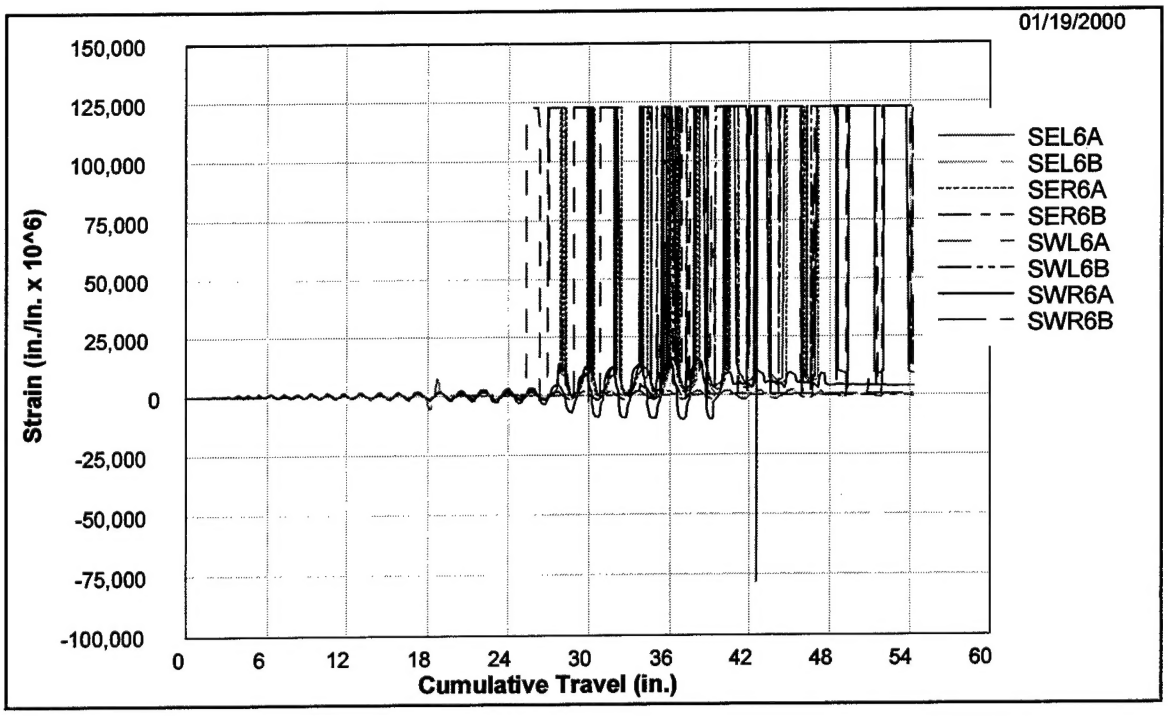

Figure C65. Strains measured 6.5 in. above and below cold joint, 5SLCL

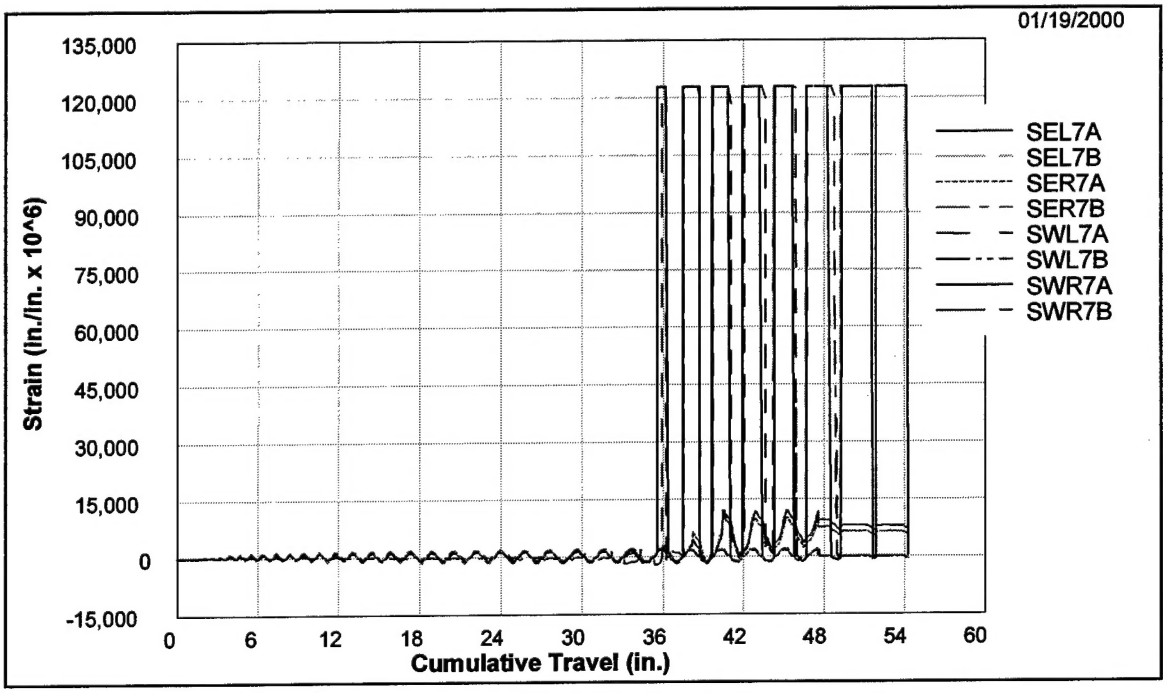

Figure C66. Strains measured 8.5 in. above and below cold joint, 5SLCL

REPORT DOCUMENTATION PAGE

Form Approved
OMB No. 0704-0188

1. REPORT DATE *(DD-MM-YYYY)*	2. REPORT TYPE	3. DATES COVERED *(From - To)*
August 2000	Final report	

4. TITLE AND SUBTITLE

Ultimate Deflection Response of Lightly Reinforced Concrete Intake Towers

5a. CONTRACT NUMBER

5b. GRANT NUMBER

5c. PROGRAM ELEMENT NUMBER

6. AUTHOR(S)

Richard C. Dove

5d. PROJECT NUMBER

5e. TASK NUMBER

5f. WORK UNIT NUMBER
Work Unit 32911

7. PERFORMING ORGANIZATION NAME(S) AND ADDRESS(ES)

U.S. Army Engineer Research and Development Center
Waterways Experiment Station
3909 Halls Ferry Road
Vicksburg, MS 39180-6199

8. PERFORMING ORGANIZATION REPORT NUMBER

ERDC/SL TR-00-6

9. SPONSORING / MONITORING AGENCY NAME(S) AND ADDRESS(ES)

Headquarters, U.S. Army Corps of Engineers
Washington, DC 20314-1000

10. SPONSOR/MONITOR'S ACRONYM(S)

11. SPONSOR/MONITOR'S REPORT NUMBER(S)

12. DISTRIBUTION / AVAILABILITY STATEMENT

Approved for public release; distribution is unlimited.

13. SUPPLEMENTARY NOTES

14. ABSTRACT

The overall objective of this research is to understand the nonlinear response of existing, lightly reinforced intake towers. The ultimate objective is the evaluation and/or development of approximate or simplified analysis procedures for the evaluation of the ductility of existing intake towers.

There were three phases in the fulfillment of this ultimate objective. The first phase was a statistical analysis of the inventory of existing intake towers. The specific objective of this tower inventory analysis was to quantify the distribution and variation of the structural characteristics of the U.S. Army Corps of Engineers' inventory of existing intake towers as relating to their earthquake location hazard. This analysis was used to assist in the identification of possible failure mechanisms to help quantify the extent of the problem of the seismic response of existing towers. The information generated was used in planning the second phase of this research effort, the Intake Tower Substructure (ITS) experimentation series conducted in 1996 and 1997. The objectives of these experiments were to observe the response of scale models of typical intake towers, quantify the ductility available, and use the information generated for the development of approximate and/or simplified analysis procedures for the evaluation of the ductility of existing intake towers.

(Continued)

15. SUBJECT TERMS

Deflection response
Earthquake
Intake towers
Seismic response
Strain penetration

16. SECURITY CLASSIFICATION OF:			17. LIMITATION OF ABSTRACT	18. NUMBER OF PAGES	19a. NAME OF RESPONSIBLE PERSON
a. REPORT	b. ABSTRACT	c. THIS PAGE			19b. TELEPHONE NUMBER *(include area code)*
UNCLASSIFIED		UNCLASSIFIED		125	

13. (Concluded).

The most important finding was that the crack width in the failure zone is largely controlled by the steel rupture strain. Steel rupture strain is well understood and usually easy to obtain.

In summary, we now have a deflection-based analysis procedure. However, the rotational spring model needs further development and the procedure must be verified for dynamic response and perhaps for larger bar sizes. It is recommended that further experimental and analytical work address these concerns.

This experimental effort successfully generated a substantial amount of data on the strain penetration/failure deflection characteristics of the reinforcing steel in the failure zone of lightly reinforced intake towers. The subsequent analysis of the data provided information on the rotational capacity of the critical section at the base of the tower and hence to an estimation of the ultimate deflection capacity of existing intake towers. An empirical equation was generated for the estimation of the parameters required for this calculation, and the method was successfully applied to an example problem. This fulfills the objectives as initially stated in this report.